Ionic Liquid Supported Thermal Dehydrogenation of Amine Borane Derivatives

A thesis submitted
in partial fulfillment of the requirements
for the degree of

Doctor of Philosophy
by

Basudhrity Banerjee

Department of Chemical Engineering
Indian Institute of Technology Guwahati, Guwahati, India
January 2018

Department of Chemical Engineering

Indian Institute of Technology Guwahati, Guwahati, India

CERTIFICATE

It is certified that the work contained in this thesis entitled "**Ionic Liquid Supported Thermal Dehydrogenation of Amine Borane Derivatives",** by Basudhrity Banerjee, has been carried out under our supervision and that this work has not been submitted elsewhere for a degree.

Prof. Tamal Banerjee
Professor
Department of Chemical Engineering
Indian Institute of Technology Guwahati

Prof. G. Pugazhenthi
Professor
Department of Chemical Engineering
Indian Institute of Technology Guwahati

TH-1791_136107007

Department of Chemical Engineering

Indian Institute of Technology Guwahati, Guwahati, India

STATEMENT

I hereby declare that the matter embodied in this thesis is the result of investigations carried out by me in the Department of Chemical Engineering, Indian Institute of Technology Guwahati, Assam, India under the supervision of **Dr. Tamal Banerjee** and **Dr. G. Pugazhenthi**.

In keeping with the general practice of reporting scientific observations, due acknowledgement has been made wherever the work described is based on the findings of other investigations.

Guwahati — Basudhrity Banerjee

January 2018

TH-1791_136107007

ACKNOWLEDGEMENT

It is my great privilege to sincerely thank several people who have supported me to complete my Doctoral Dissertation.

First and foremost, with the deepest sense of gratitude, I would like to express my sincere thanks to my supervisors **Prof. Tamal Banerjee** and **Prof. G. Pugazhenthi**, who have been a constant source of inspiration for me. Their timely help during the crucial phases of my Ph.D. career has made it possible for me to achieve my target. My special thanks to them for their valuable guidance, encouragement, inspiration, creative, and scientific ideas which helped me to enhance my knowledge. I am also fortunate enough to have their guidelines to cultivate scientific thought. I would like to thank them for their wonderful and friendly nature that encouraged me to have many scientific discussions and also for teachings of life, for which I will remain indebted to them.

I would like to acknowledge my sincere gratitude to my doctoral committee members, **Dr. Vairakannu Prabu** and **Dr. Venkatesh R. Prasanna**, Department of Chemical Engineering and **Dr. Aditya Narayan Panda**, Department of Chemistry. Their intuitive revision of my work, valuable advice, and constructive suggestions during my research progress kept the flow of my research work in the right direction.

I am indebted to **Prof. Aloke Kumar Ghoshal, Prof. Kaustubha Mohanty, Dr. Vaibhav V. Goud and Dr. Chandan Das** for their research oriented teaching during my course of work. I also thank **Prof. Bishnupada Mandal**, Head, and Department of Chemical Engineering for his administrative support. Furthermore, I would like to thank all the other Faculties and Staff members of the Department of Chemical Engineering for their invaluable support during my research.

I express my sincere gratitude and acknowledgment to IIT Guwahati for all the facilities that were made available to me. I am grateful to the Analytical Laboratory of the **Department of Chemical Engineering** and **Department of Chemistry, Central Instruments Facility**, **IIT Guwahati** for providing me with the necessary support for Sample Analysis.

I would also like to thank **Indian Institute of Science Education and Research Bhopal (IISER-Bhopal) India** and **Indian Association for the Cultivation of Science (Kolkata)** for letting us use their analytical instrument facilities.

I wish to thank our lab seniors **Dr. Santhi Raju Pilli**, **Dr. Dharamashibhai V. Rabari**, **Dr. Sanjukta Bhoi**, **and Dr. Anand Bharti** for lending their hands of support whenever needed. I thank all my lab members **Mr. Pyarimohan Dehury**, **Ms. Upasana**

TH-1791_136107007

Mahanta, Mr. Dhirendra Mishra, Ms. Rima Biswas, Mr. Debasish Kundu, **Mr. Papu Nayak**, **Mr. Rupesh Verma, Mr. Mood Mohan, Mr. Janardhan Singh, Mr. Suman Mahato, Mr. Debanjan Dey**, **Mr. Ankit Bishnoi**, **Mr. Sarvesh Namdeo and Mr. Paritosh Dayma** for providing a co-operative research environment.

My sincere thanks to IIT Guwahati friends **Mr. Rahul Saha, Ms. Geeta Kumari, Mr. Suman Saha**, **Mr. Ranjit Mishra**, **Mr. Nirmal Mullick**, **Mr. Atanu Kumar Paul, Mr. Gourhari Chakraborty and Ms. Tanushree Ray** for all the laughs, joyful moments, support and suggestions. I am thankful to the other research scholars of Chemical Engineering Department and all my IITG friends, who have shared their thoughts and views with me.

Words of motivation and encouragement from some of my friends and relatives were only a call away. They always appreciated my efforts and outcomes of my research work. My sincere gratitude to **Mr. Subhankar Bhadra.** My friends who always stood beside me, giving me hope and courage **Ms. Pinkey Sarkar, Mrs. Madhuparna Dey, Ms. Sudeepta Mukherjee, Mrs. Mismi Basu, Mr. Sayantan Biswas, Mr. Anupam Mukherjee** and many more. And I would like to take this opportunity to thanks each and every relatives of mine for their constant encouragement.

My whole hearted gratitude goes to my parents, **Mr. Badal Chandra Bandyopadhaya** and **Mrs. Gongotri Banerjee,** whose blessings, wise advice and boundless patience kept my morale high during the course of study.

Finally, for the financial support of this research, I would sincerely like to thank **the Science and Engineering Research Board (SERB), Department of Science and Technology (DST), Government of India** for the research grant **(SB/S3/CE/063/2013)**.

Sincerely,

Basudhrity Banerjee

TH-1791_136107007

Synopsis

Currently, finding an economic way for hydrogen storage is a daunting challenge. The necessity of hydrogen storage is mainly due to ever-growing demand of energy. The use of hydrogen in fuel cell technology and petroleum sector has definitely brought interest all over the world. Hydrogen is considered a 'green' source of energy as it does not produce greenhouse gases upon burning which makes it as an alternative for fossil fuel. However, substantial challenges involving storage and on-board generation of hydrogen have to be addressed before its use as a potential energy source. There are two main pathways for storing of hydrogen, namely: physical storage and chemical storage.

Amine boranes are chemical hydrogen storage materials consisting of hydride B-H and protic N-H bonds and thus are exceptional candidates for hydrogen release [1]. Ammonia borane (AB) is the simplest compound in amine borane family having hydrogen content of 19.6 wt. %. However, limitations such as longer induction period and production of borazine have led this thesis to concentrate on other substituted amine borane such as Ethylene DiAmine *bis* Borane (EDAB). It is known to have a hydrogen content of ~10 wt. % [2]. Unlike AB, which shows an induction period of ~3 hours at 85 ℃ [3], EDAB shows no induction period upon heating. This makes EDAB a natural choice for potential hydrogen storage material. Here the thermal dehydrogenation of EDAB is known to occur between 100 - 200 ℃ in two moderately exothermic steps [2, 4].

However, on a standalone basis, the release of hydrogen from EDAB is limited. To improve this, the use of Ionic Liquid (IL) as solvent cum catalyst medium is recommended. In such a scenario, IL's are known to play a dominant role for dehydrogenation. IL are molten salts, but most are liquids at room temperature due to the structure of two asymmetric ion i.e. large organic structure of the cation and a small inorganic structure of the anion .Some of the interesting features of incorporating IL are (a) it helps in reducing

TH-1791_136107007

both the induction period of EDAB and the working temperature of thermal dehydrogenation. This invariably leads to higher production of hydrogen (Figure 1).

The increase in reaction rate and lowering of the required temperature by IL's are due to the stabilization of the ionic intermediate by a more Bronsted basic environment provided by certain ILs. The β values of Kamlet-Taft parameters relate the hydrogen release to the basicity of Ionic Liquids. A short period of time suggests that the activating effect of the ionic liquid may be related to its ability to induce formation of such ionic species. However, the selection of Ionic Liquid in literature has been random without taking into account of other cation families. With the help of quantum chemical calculation, especially COSMO-SAC (COnductor like Screening MOdel Segment Activity Coefficient), will guide us selecting the proper cation and anion combination. Figure 1 and the ensuing subsections summarizes the work carried out in the thesis.

TH-1791_136107007

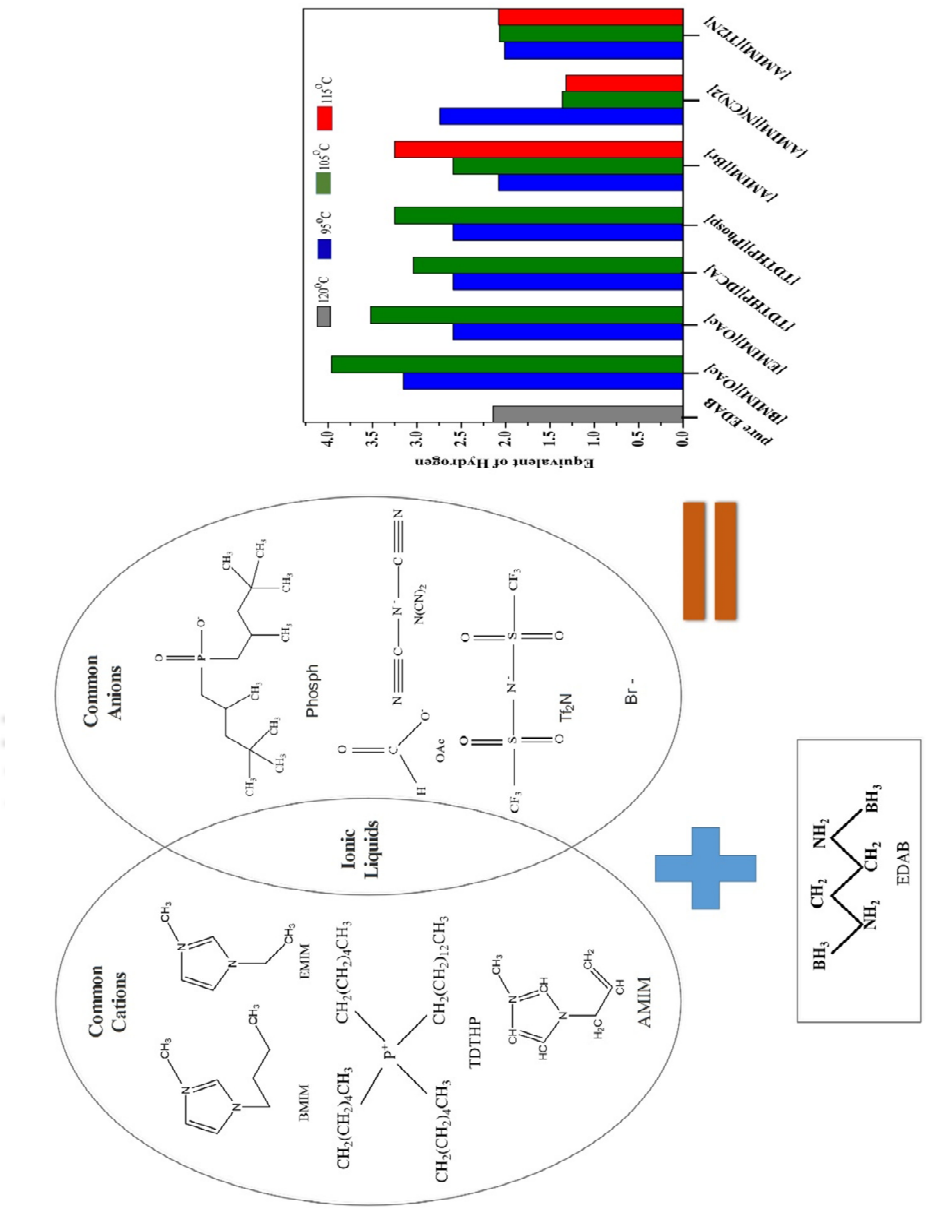

Figure 1 Outline of the thesis

TH-1791_136107007

1. COSMO-SAC Screening and Dehydrogenation Kinetics of Ammonia Borane - Ionic Liquid Mixtures

The chapter attempts to predict the reaction kinetics of two different hydrogen storage pathways namely Ammonia Borane (AB) and Ionic Liquid (IL) assisted AB. The reaction kinetics has been predicted for six reported ILs at 85 °C with AB using the GA toolbox. In addition, solid state AB thermal decomposition at 85 ºC has been also studied. It was found that the Avrami Erofeyev model [5] which is known to be useful for AB – IL mixtures, however, fails when applied to predict reaction kinetics for solid state AB decomposition. To overcome this challenge we have used logistic growth model for solid state decomposition. Thus we propose a logistic growth model for solid AB decomposition while an Avrami Erofeyev model for AB-IL mixtures. The logistic growth model was characterized by a single step reaction for the solid state decomposition of AB, while the Avrami Erofeyev model for AB-IL mixtures successfully predicted two single step reactions. Rate constants for decomposition of EDAB in [AMIM][Br] using Avrami-Erofeyev model was studied in this thesis. In order to explain the effects of dehydrogenation, we regressed the experimental kinetic data using the Avrami Erofeyev model in order to obtain the activation energy, rate constant and reaction order [6].

We have also attempted to correlate the Infinite Dilution Activity Coefficient (IDAC) value of AB and EDAB in IL with the activation energies of the mixture using the quantum chemical based COSMO-SAC theory. All the IDAC values being close to unity indicated a high solubility with IL. A general trend of increase in hydrogen release with decreasing IDAC values was observed for both AB-IL and EDAB-IL mixtures. From the IDAC study the best ILs selected were 1-ethyl-3-methyl imidazolium acetate ([EMIM][OAc]), 1-butyl-3-methyl imidazolium acetate ([BMIM][OAc]), Trihexyl (tetradecyl) phosphonium bis(2,4,4-trimethylpentyl) phosphinate, Trihexyl (tetradecyl)

TH-1791_136107007

phosphonium dicyanamide ([TDTHP][DCA]), 1-allyl-3-methylimidazolium dicyanamide ([AMIM][$N(CN)_2$]), 1-allyl-3-methylimidazolium bis(trifluoromethylsulfonyl) imide ([AMIM][Tf_2N]), and 1-allyl-3-methylimidazolium bromide ([AMIM][Br]).

2. Dehydrogenation Studies using Acetate Based IL

Chemical hydrides like Ethylene diamine bisborane (EDAB) are of great interest as they can liberate 14% hydrogen on thermal dehydrogenation [7]. In this chapter, we followed a systematic approach for the selection of these ILs for the dehydrogenation of EDAB on the basis of solubility. The solubility of EDAB in ILs was predicted by the coupling of a quantum chemical and a statistical mechanical framework, namely the COSMO-SAC model. Furthermore, the stability of the selected EDAB/IL complexes were then analyzed by HOMO-LUMO energies. The IL with the highest solubility of EDAB was then selected for experiments. In this chapter, the dehydrogenation of EDAB facilitated by imidazolium cation and acetate anion based ILs was investigated in vacuum. The molecular modeling studies converged on the two ILs, namely 1-ethyl-3-methyl imidazolium acetate ([EMIM][OAc]) and 1-butyl-3-methyl imidazolium acetate ([BMIM][OAc]), which were subsequently chosen for the dehydrogenation experiments. The thermal dehydrogenation of EDAB was carried out at 95 ºC and 105ºC under vacuum so as to prevent generation of oxygen moieties. A total of 3.96 and 3.52 equivalents of hydrogen were released from the desorption of EDAB/[BMIM][OAc] and EDAB/[EMIM][OAc], respectively, at 105°C . The same set of EDAB/IL produced 3.15 and 2.59 equivalents of hydrogen respectively at 95°C.

The purity of released gas was confirmed by gas chromatographic analysis, while the catalytic activity of ILs was confirmed by ^{1}H NMR characterization of pure EDAB, ILs and EDAB/IL complexes both before and after the reaction. ^{11}B NMR analysis confirms the presence of trigonal boron (sp_2) BH_2 group as the only hydrogen containing

TH-1791_136107007

boron moiety in dehydrogenated EDAB. High resolution mass spectrometry was able to detect the mass of cyclic repeat units in the polymeric chain containing a sp^2 BH_2 group**.**

3. Dehydrogenation Studies using a Phosphonium Based IL

Central cationic heteroatoms like phosphorous and nitrogen based ILs are relatively less explored in comparison with nitrogen based imidazolium based ILs. Phosphonium based ILs are another class of cations, which are relatively inexpensive compared to imidazolium based ILs. The phosphonium based cations are known to possess superior physio-chemical properties such as thermal stability, viscosity, electrochemical stability, ionic conductivity over its ammonium counterparts.

In this chapter, we have reported the selective dehydrogenation scheme of EDAB by Trihexyl (tetradecyl) phosphonium based ILs. The thermal dehydrogenation of EDAB with Trihexyl (tetradecyl) phosphonium bis(2,4,4-trimethylpentyl) phosphinate ([TDTHP][Phosph]) and Trihexyl (tetradecyl) phosphonium dicyanamide ([TDTHP][DCA]) was carried out separately at high vacuum. The dehydrogenation experiments of EDAB/phosphonium ILs were carried out at 95 and 105 °C at a gauge pressure of 4×10^{-2} mbar. At 105 ºC, total equivalents hydrogen released from EDAB/ [TDTHP][Phosph] is 3.25, which is higher than 3.04 equivalent of hydrogen as obtained from EDAB/[TDTHP][DCA]. At 95 °C, both the systems produce 2.59 and 2.45 equivalent of hydrogen. The IL facilitated hydrogen release is higher than the 2.14 equivalent hydrogen release of pure EDAB at 120 °C.

Development of milder dehydrogenation environment is important since dehydrogenation of amine boranes is fairly exothermic, which limits direct dehydrogenation path. Since phosphonium based ILs have different characteristics than the acidic imidazolium based ILs we presumed the formation of different oligomeric

TH-1791_136107007

amine-borane products after dehydrogenation. Based on the ^{1}H Nuclear Magnetic Resonance (NMR) and High Resolution Mass Spectrometry (HR-MS) studies, a detailed reaction mechanism of IL facilitated dehydrogenation of EDAB is proposed. The identification of exact mass of dehydrogenated EDAB through HR-MS characterization has also revealed the extent of polymerization reaction which has been attributed to the reaction environment provided by different classes of ILs. A comparative reaction mechanism of imidazolium assisted dehydrogenation of EDAB to that of phosphonium based IL assisted dehydrogenation is also presented to have a detailed picture on selective dehydrogenation.

4. Dehydrogenation Studies using Allyl Based Ionic Liquids

1-Allyl-3-methylimidazolium halides based Ionic Liquids are known to possess higher thermal stability and lower viscosity when compared to the imidazolium and phosphonium based cations. It is found to exhibit a good thermo stability despite its unsaturated chemical structure. The relatively lower melting point and viscosity for 1-allyl-3-methylimidazolium halides Ionic Liquids have prompted us to explore these as potential media for thermal dehydrogenation.

This concluding chapter reports the use of allyl-based imidazolium cations for dehydrogenation of ethylene diamine bis borane (EDAB) at three different temperatures, namely, 95, 105, and 115 °C, under vacuum. The allyl-based ionic liquid (IL) was selected by using the infinite dilution activity coefficient (IDAC) as predicted from the COSMO-SAC (COnductor-like Screening MOdel−Segment Activity Coefficient) model. Based on the results of the COSMO-SAC model, the following allyl based ILs were used for experimentation: 1-allyl-3-methylimidazolium dicyanamide ([AMIM][$N(CN)_2$]), 1-allyl-3-methylimidazolium bis(trifluoromethylsulfonyl)imide ([AMIM][Tf_2N]), and 1-allyl-3-

TH-1791_136107007

methylimidazolium bromide ([AMIM][Br]). The highest amount of hydrogen (3.25 equiv) was measured from the EDAB/[AMIM][Br] system at 115 °C.

The equivalent of hydrogen released for following ILs at three different temperatures (95,105 and 115 °C) are as follows: EDAB/[AMIM][Br] : 2.08, 2.59 and 3.25 respectively; EDAB/[AMIM][$N(CN)_2$] : 2.74, 1.36 and 1.32 respectively ; EDAB/[AMIM][Tf_2N] : 2.01,2.07, 2.08 respectively. For all the dehydrogenation process, it was observed that two ILs, namely [AMIM][Br] and [AMIM][Tf_2N] have accelerated the catalytic effect of the dehydrogenation process. However, a contrary was observed for the remaining IL, namely [AMIM][$N(CN)_2$]. Further no induction time was observed in each of the three cases as opposed to a non-zero induction time for the neat EDAB. Gas chromatography was conducted to confirm that the gas released was pure hydrogen. To better understand the reaction mechanism of EDAB dehydrogenation, the Reactive Force Field (ReaxFF) method was employed [8, 9]. The ReaxFF study confirmed the intramolecular pathway of Hydrogen liberation from the EDAB entity.

Further analyses with ^{1}H and ^{11}B NMR were performed on pure IL and IL/EDAB complexes to reassert the role of IL as a catalyst. ^{1}H NMR spectra was recorded to study and characterize the pure EDAB, IL and EDAB/IL mixture before and after reactions. A comparative discussion of ^{1}H NMR plots of pure EDAB, IL , EDAB/IL complexes will determine the possible formation of any product after dehydrogenation and further elucidate the role of IL in dehydrogenation. Here the peaks from referred literature [10] were used to locate the peak of our compounds. Thermo gravimetric analysis was also conducted on pure EDAB, pure IL, and EDAB/IL complexes to understand the weight loss phenomenon with respect to rising temperature.

TH-1791_136107007

References:

1. Hoffmann. R. Extended Hückel Theory. III. Compounds of Boron and Nitrogen, *J. Chem. Phys*. **1964**, 40, 2474-2480.

2. Neiner, D.; Karkamkar, A; Bowden, M.; Choi, Y. J.; Luedtke, A.; Holladay, J.; Fisher, A.; Szymezak N.; Autrey, T. Kinetic and thermodynamic investigation of hydrogen release from ethane 1,2-di-amineborane. *Energy Environ. Sci.* **2011**, 4, 4187–4193.

3. Himmelberger, D. W.; Alden, L. R.; Bluhm, M.E.; Sneddon, L.R. Ammonia Borane Hydrogen Release in Ionic Liquids. *Inorg. Chem.* **2009**, 48, 9883–9889.

4. Leardini, F.; Valero-Pedraza, M. J.; Perez-Mayoral, E.; Cantelli, R.; Bañares, M. A. Thermolytic Decomposition of Ethane 1,2-Diamineborane Investigated by Thermoanalytical Methods and in Situ Vibrational Spectroscopy. *J. Phys. Chem. C.* **2014**, 118, 17221−17230.

5. Ahluwalia, R.K.; Peng, J.K.: Hua, T.Q. Hydrogen Release from Ammonia Borane Dissolved in an Ionic Liquid. *Int. J. Hydrogen Energy*, **2011,** 36, 15689-15697.

6. Mahato. S.; Banerjee. B.; Pugazhenthi. G.; Banerjee. T. Optimization and quantum chemical predictions for the dehydrogenation kinetics of Ammonia Borane-Ionic Liquid mixtures. *Int. J. Hydrogen Energy*, **2015**, 40, 10390-10400.

7. Sahler, S.; Konnerth, H.; Knoblauch, N.; Prechtl, M.H.G. Hydrogen storage in amine boranes: Ionic liquid supported thermal dehydrogenation of ethylene diamine bisborane. *Int. J. Hydrogen Energy*, **2013**, 38, 3283-3290.

8. van Duin. A.C.T.; Dasgupta. S.; Lorant. F.; Goddard. W.A. ReaxFF: A Reactive Force Field for Hydrocarbons. *J. Phys. Chem. A.* **2001**, 105, 9396– 9409.

9. Furukawa, S.; Inoue, N.; Ishioka, T.; Furuya K.; Harata, H. Rapid Decomposition of Cellulose Dissolved in Ionic Liquid Using Gas–Liquid Interface Discharge. *Jpn. J. Appl. Phys.* **2012**, 51, 070205-1-3.

10. Banerjee, B.; Kundu, D.; Pugazhenthi, G.; Banerjee, T. Quantum chemical and experimental insights for the ionic liquid facilitated thermal dehydrogenation of ethylene diamine bisborane. *RSC. Adv.* **2015**, 5, 85280-85290.

TH-1791_136107007

Table of Contents

Name	Page No.
List of Figures	i
List of Tables	v
Nomenclature	vii
Chapter 1. Introduction	1
1.1 Hydrogen as Source of Energy	3
1.2 Hydrogen Storage Materials	4
1.2.1 Chemical Hydrides	5
1.2.2 Ethylene DiAmine bis Borane (EDAB)	7
1.3 Ionic Liquids	9
1.4 Objectives	12
1.5 Structure of Thesis	13
References	15
Chapter 2. Experimental Details	17
2.1 Dehydrogenation Set up	19
2.2 Chemicals Used	22
2.3 Characterization Studies	25
2.4 Computational Studies	25
2.4.1 Kinetic Data Regression	26
2.4.2 COSMO-SAC Model	27
2.4.3 Stability Analysis through HOMO-LUMO Energy Gaps	28
References	30

TH-1791_136107007

Chapter 3. Results and Discussions 33

3.1 Introduction 35

3.2 Solid State AB Dehydrogenation 35

3.3 Avrami-Erofeyev Model for Thermal dehydrogenation of Ionic Liquid Ammonia Borane 43

3.4 Predictions of Activation Energies and Infinite Dilution Activity Coefficient 55

3.5 EDAB as the Chemical Hydride 60

3.6 Screening of potential Ionic Liquid Combination using COSMO-SAC Model 61

3.7 Stability Analysis using HOMO-LUMO Analysis 64

3.8 Dehydrogenation Experiments with Acetate based Ionic Liquids 67

3.8.1 Thermal Dehydrogenation of EDAB/[BMIM][OAc] and [EMIM][OAc] 67

3.8.2 TGA profile of EDAB with acetate based Ionic Liquids 70

3.8.3 ^{1}H NMR analysis of EDAB along with acetate based Ionic Liquids 71

3.8.4 ^{11}B NMR analysis of EDAB along with acetate based Ionic Liquids 77

3.8.5 HR-MS of EDAB along with acetate based Ionic Liquids 80

3.9 Dehydrogenation Experiments of EDAB/Phosphonium Ionic Liquids 82

3.9.1 ^{1}H NMR analysis of EDAB along with Phosphonium based Ionic Liquids 84

3.9.2 High Resolution-Mass Spectrometry (HR-MS) Analysis 89

3.9.3 Experimentally Facilitated Reaction Mechanism 92

3.10 Dehydrogenation Experiments with 1-Allyl-3-Methylimidazolium cation based IL 105

3.10.1 Thermal Dehydrogenation Experimental Results 105

TH-1791_136107007

3.10.2 Kinetic Regression using Avrami-Erofeyev model for Allyl based Ionic Liquids 110

3.10.3 ^{1}H NMR Spectra of EDAB with 1-Allyl-3-Methylimidazolium cation based Ionic Liquids 113

3.10.4 ^{11}B NMR Spectra of EDAB with 1-Allyl-3-Methylimidazolium Bromide based Ionic Liquids 119

3.10.5 TGA Analysis of EDAB with 1-Allyl-3-Methylimidazolium cation based IL 122

3.11 Reactive Force Field (ReaxFF) 126

3.11.1 Pyrolysis Study of EDAB 132

3.11.2 Reaction mechanism as proposed by using ReaxFF Force Field 135

References 138

Chapter 4. Conclusions and Future Work 141

4.1 Conclusions 143

4.2 Future Scope 147

Research Outputs 149

TH-1791_136107007

List of Figures

Figure No.	Captions	Page No.
2.1	Schematic experimental setup	21
2.2	Description of the actual setup	21
2.3	Structures of AB and EDAB.	23
2.4	Anion and cation structure of ILs used	24
3.1	Comparison of experimental and predicted hydrogen release at T = 85 °C using (a) Growth Propagation Model and (b) Avrami-Erofeyev model.	41
3.2	Predicted hydrogen release at 95 °C using (a) Avrami-Erofeyev model and (b) Growth Propagation Model.	42
3.3(a)	Experimental and predicted kinetic data for the release of equivalents of hydrogen from AB and [BMIM][PF_6] mixture.	49
3.3(b)	Experimental and predicted kinetic data for the release of equivalents of hydrogen from AB and [EMIM][OTf] mixture.	49
3.3(c)	Experimental and predicted kinetic data for the release of equivalents of hydrogen from AB and [BMIM][OTf] mixture.	50
3.3(d)	Experimental and predicted kinetic data for the release of equivalents of hydrogen from AB and [MMIM][$MeSO_4$] mixture.	50
3.3(e)	Experimental and predicted kinetic data for the release of equivalents of hydrogen from AB and [BMIM][Cl] mixture.	51
3.3(f)	Experimental and predicted kinetic data for the release of equivalents of hydrogen from AB and [BMMIM][Cl] mixture.	51
3.4(a)	Experimental and predicted kinetic data for the release of equivalents of hydrogen from AB and [BMIM][Cl] (80:20) mixture at 85°C.	53
3.4(b)	Experimental and predicted kinetic data for the release of equivalents of hydrogen from AB and [BMIM][Cl] (80:20) mixture at 105°C.	53

TH-1791_136107007

3.4(c)	Experimental and predicted kinetic data for the release of equivalents of hydrogen from AB and [BMIM][Cl] (80:20) mixture at 120°C.	54
3.4(d)	Experimental and predicted kinetic data for the release of equivalents of hydrogen from AB and [BMIM][Cl] (50:50) mixture at RT	54
3.5	Reaction pathway of IL ([BMIM][X]) mediated Ammonia Borane Dehydrogenation at T = 85 °C.	58
3.6	Optimized structures of DADB (units in Å)	59
3.7	Optimized structure of [BMIM][Cl]-DADB complex (units in Å)	59
3.8	Frequency of ILs. Frequency represents the number of times an anion has shown a capacity of $\geq 10^5$	63
3.9	Logarithmic value of infinite dilution activity coefficient [*ln (IDAC)*] of 7 ILs. System 1: 1-ethyl-3-methylimidazolium Acetate, System 2: 1-butyl-3-methylimidazolium Acetate, System 3: 1-allyl,3-methylimidazolium bromide, System 4: 1-allyl, 3-methylimidazolium dicyanamide, System 5: 1-allyl,3-methylimidazolium bis (trifluoromethylsulfonyl) imide, System 6: Trihexyltetradecylphosphonium bis (2,4,4-trimethylpentyl) phosphinate: System 7: Trihexyltetradecylphosphonium dicyanamide	64
3.10	HOMO-LUMO energy gap of EDAB/IL complex. (a) EDAB/[EMIM][OAc], (b) EDAB/[BMIM][OAc].	66
3.11	Time resolved equivalent hydrogen release from EDAB/[EMIM][OAc] and EDAB/[BMIM][OAc] complexes at 95 °C and 105 °C. (■) EDAB/[EMIM][OAc] at 95 °C, (●) EDAB/[BMIM][OAc] at 95 °C, (▲) EDAB/[EMIM][OAc] at 105 °C, (▼) EDAB/[BMIM][OAc] at 105 °C.	69
3.12	Cumulative hydrogen generation from EDAB facilitated by ILs at 95 °C and 105 °C.	70
3.13	TGA profile of EDAB/[BMIM][OAc] and EDAB/[EMIM][OAc]	71
3.14	Plot for ^{1}H NMR. (a) pure EDAB, (b) pure [EMIM][OAc], (c) EDAB/[EMIM][OAc] before reaction, (d) EDAB/[EMIM][OAc] after reaction, (e) pure [BMIM][OAc], (f) EDAB / [BMIM][OAc] before reaction, (g) EDAB/[BMIM][OAc] after reaction	77
3.15	Plots for ^{11}B NMR: (a) EDAB/[BMIM][OAc] before reaction (b) EDAB/[BMIM][OAc] after reaction	79

TH-1791_136107007

3.16	APCI-HR-MS plot of EDAB/[BMIM][OAc] after reaction	81
3.17	Time resolved equivalent hydrogen release from EDAB/[TDTHP][Phosph] and EDAB/[TDTHP][DCA] complexes at 95 °C and 105 °C (●) EDAB/[TDTHP][Phosph] at 95 °C, (▼) EDAB/[TDTHP][DCA] at 95 °C (■) EDAB/[TDTHP][Phosph] at 105 °C (▲) EDAB/[TDTHP][DCA] at 105 °C.	83
3.18	Plot for ^{1}H NMR. (a) pure [TDTHP][DCA], (b) EDAB/[TDTHP][DCA] before reaction, (c) EDAB/[TDTHP][DCA] after reaction, (d) pure [TDTHP][Phosph], (e) EDAB/[TDTHP][Phosph] before reaction, (f) EDAB/[TDTHP][Phosph] after reaction	88
3.19	Structure of intermediates and residual products as observed in HR-MS	90
3.20	APCI-HR-MS plot of EDAB/Phosphonium IL systems after reaction. (a) EDAB/[TDTHP][Phosph], (b) EDAB/[TDTHP][DCA]	91
3.21	Dehydrogenation mechanism proposed by Leardini et al.	93
3.22	Common initiation pathway for dehydrogenation of pure EDAB	96
3.22(a)	Scheme 3.22.1 Dehydrogenation pathway of EDAB/Phosphonium ILs	98
3.22(b)	Scheme 3.22.2.a Dehydrogenation pathway of oligomer EDAB/Phosphonium ILs for possessing four units	99
3.22(c)	Scheme 3.22.2.b Dehydrogenation pathway of oligomer EDAB/Phosphonium ILs for possessing five units.	100
3.22(d)	Scheme 3.22.3 Dehydrogenation pathway of EDAB/Imidazolium-acetate ILs	101
3.22(e)	Scheme 3.22.4.a Dehydrogenation pathway of oligomer EDAB/ Imidazolium acetate ILs for possessing two units.	102
3.22(f)	Scheme 3.22.4.b Dehydrogenation pathway of oligomer EDAB/ Imidazolium acetate ILs for possessing three units	103
3.23(a)	Equivalent release of hydrogen from EDAB/1-Allyl-3-methylimidazolium Bromide at 95 °C, 105 °C and 115 °C.	108
3.23(b)	Equivalent release of hydrogen from EDAB/1-Allyl-3-methylimidazolium bis (trifluoromethylsulfonyl) imide at 95 °C, 105 °C and 115 °C.	109

TH-1791_136107007

3.23(c)	Equivalent release of hydrogen from EDAB/1-Allyl-3-methylimidazolium dicyanamide at 95 °C, 105 °C and 115 °C.	110
3.24	Plot for ^{1}H NMR**:**(a) pure [AMIM][Br] (b) EDAB/[AMIM][Br] (before reaction) (c) EDAB/[AMIM][Br] (after reaction),(d) pure [AMIM][Tf_2N], (e) EDAB/ [AMIM][Tf_2N] (before Reaction) and (f) EDAB/ [AMIM][Tf_2N] (after Reaction), (g) pure [AMIM][$N(CN)_2$] , (h)EDAB/ [AMIM][$N(CN)_2$] (before reaction) , (i) EDAB/ [AMIM][$N(CN)_2$] (after reaction).	119
3.25	Plots for ^{11}B NMR: (a) EDAB/[AMIM][Br] (before reaction), and (b) EDAB/[AMIM][Br] (after reaction)	121
3.26	(a) TGA profile of pure EDAB, EDAB/ [AMIM][Br], EDAB/[AMIM][Tf_2N] and EDAB/ [AMIM][$N(CN)_2$], (b) TGA profile of pure ILs : [AMIM][Br], [AMIM][Tf_2N] and [AMIM][$N(CN)_2$].	125
3.27	Overview of total energy of the system in ReaxFF reactive force field	131
3.28	The release of H_2 at different temperature ranging from 2500 K to 5000 K	134
3.29	Detailed pyrolysis study of EDAB at 2500 K.	135
3.30	Proposed reaction mechanism of EDAB dehydrogenation using ReaxFF	137
4.1	Overall thermal dehydrogenation EDAB with selected ILs	146

TH-1791_136107007

List of Tables

Table No.	Captions	Page No.
1.1	Conventional storage device and the method of release	5
1.2	Physical properties of Ethylene DiAmine *bis*-Borane (EDAB)	8
3.1	Optimized parameters for logistic growth model and Avrami-Erofeyev model for solid state AB.	40
3.2	Optimized parameters for logistic growth model and Avrami-Erofeyev model for [BMIM][Cl] mediated AB.	47
3.3	Rate constants for decomposition of 50-wt% AB in ILs at 85 °C using Avrami Erofeyev model	48
3.4	Comparison of regressed and predicted activation energies of AB in IL	55
3.5	IDAC value and capacity of EDAB in selected IL	62
3.6	HOMO, LUMO energies and HOMO-LUMO energy gap	67
3.7	Cumulative equivalent of hydrogen released by EDAB/IL complexes at two different temperatures of 95 °C and 105 °C (Acetate)	68
3.8	Cumulative equivalent of hydrogen released by EDAB/IL complexes at two different temperatures of 95 °C and 105 °C (Phosphonium).	83
3.9	Cumulative equivalent of hydrogen released by EDAB/IL complexes at three different temperatures of 95 °C, 105 °C and 115 °C (1-Allyl-3-Methylimidazolium)	108
3.10	Rate constants for decomposition of EDAB in [AMIM][Br] using Avrami-Erofeyev model.	112
3.11	Major byproduct gases released	134

TH-1791_136107007

TH-1791_136107007

Nomenclature

Abbreviations

AAD	Absolute Average Deviation
AB	Ammonia Borane
B3LYP	Becke, Three-Parameter, Lee-Yang-Parr
COSMO-RS	COnductor Like Screening MOdel For Real Solvent
COSMO-SAC	COnductor Like Screening MOdel For Segment Activity Coefficient
DES	Deep Eutectic Solvents
DFT	Density Functional Theory
EDAB	Ethylene Di Amine bis Borane
EA	Electron Affinity
GA	Genetic Algorithm
GC TCD	Gas Chromatography Thermal Conductivity Detector
HB	Hydrazine Borane
HOMO	Higher Occupied Molecular Orbital
HR MS	High Resonance Mass Spectrometry
IDAC	Infinite Dilution Activity Coefficient
IP	Ionization Potential
IL	Ionic Liquids
LUMO	Lower Unoccupied Molecular Orbital
MD	Molecular Dynamic
NPT	Fixed Number of atoms, at a constant Pressure and Temperature

TH-1791_136107007

NVT	Fixed Number of atoms, at fixed Volume, and Temperature
NVE	Fixed Number of atoms, fixed Volume, and a total Energy
NRTL	Non Random Two Liquids
NMR	Nuclear Magnetic Resonance
QC	Quantum Chemistry
QM	Quantum Mechanics
ReaxFF	Reactive Force Field
RT	Room Temperature
SLE	Solid Liquid Equilibrium
TGA	Thermogravimetric Analysis
UNIQUAC	UNIversal QUAsi Chemical
UNIFAC	UNIversal Functional Group Activity Coefficient

Ionic Liquids

[AMIM][Br]	1-Allyl-3-Methylimidazolium bromide
[AMIM][$(D(CN)_2$]	1- Allyl-3-methylimidazolium dicyanamide
[AMIM][Tf_2N]	1- Allyl-3-methylimidazolium bis (trifluoromethylsulfonyl) imide
[BMIM] [AOc]	1-Butyl-3-methylimidazolium acetate
[BMIM][Cl]	1-Butyl-3-methylimidazolium chloride
[BMIM][PF_6]	1-Butyl-3-methylimidazolium hexafluorophosphate
[BMIM][OTf]	1-Butyl-3-methylimidazolium trifluoromethanesulfonate
[BMMIM][Cl]	1-Butyl-2,3-dimethylimidazolium Chloride
[EMIM] [AOc]	1-Ethyl-3-methylimidazolium Acetate

TH-1791_136107007

[EMIM][OTf]	1-Ethyl-3-methylimidazolium trifluoromethanesulfonate
[MMIM][$MeSO_4$]	1,3-dimethylimidazolium methylsulfate
[TDTHP][Phosph]	Trihexyltetradecylphosphonium bis (2,4,4-trimethylpentyl) phosphinate
[TDTHP][DCA]	Trihexyltetradecylphosphonium dicyanamide

TH-1791_136107007

Chapter 1: Introduction

TH-1791_136107007

TH-1791_136107007

1.1 Hydrogen as Source of Energy

Till date fossil fuel have served as the primary supplier of energy with coal and petroleum products being the primary source of energy. Being non-renewable in nature, a need for alternative source of energy is getting much attention. Some of them are water, wind and solar and recently to a higher extent, hydrogen. Technically, carbon can be stated as the most feasible and workable carrier of energy because of its unique nature. The archetypal storage capabilities [1] of the carbon atoms enhances the release of energy when hydrogen is burned along with it. However, one of the major cause of concern of using carbon based fuel is its by-products. The exhausts such as greenhouse gases released by carbon based fuels are extremely threatening as it contributes to global warming. Moreover several other harmful byproducts of carbon fuel have also forced the scientists and environmentalist to incline towards a better and cleaner hydrogen energy system.

Hydrogen can be found in enormous quantities in water, hydrocarbons, and other organic matter, but extracting hydrogen from these compounds to use it as a fuel is a challenge. It can be produced by different processes such as steam reforming with natural gas [2]. Another popular method involves electrolysis of water to produce hydrogen, but it is limited to the requirement of higher processing costs. Hydrogen energy from any of the sources can be stored in fuel cell for its later usage such as generation of electricity and heat or even to run combustion engines [3]. Energy wise, hydrogen fuel is a wise choice as it can produce a significant amount of fuel after burning. For example 2.2 pounds (1 kilogram) of hydrogen gas is about the same as the energy in 1 gallon (6.2 pounds, 2.8 kilograms) of gasoline. The efficiency of hydrogen fuel is far better than a gasoline based internal combustion engine especially when hydrogen energy is used in forms of fuel cell coupled with electric motors. Hydrogen also possess a low volumetric energy density.

TH-1791_136107007

However, on the downside, pure hydrogen being the smallest and lightest element, its transportation and storage is a difficult step. Though pipes are considered as classic and efficient way for gaseous or liquid hydrogen transportation, it fails for hydrogen as it causes metal to become brittle. Current applications use high-pressure tanks capable of storing hydrogen at either 5,000 or 10,000 psi. [4]. Other storage technologies are under development, including bonding hydrogen chemically with a material such as metal hydride, or low-temperature sorbent materials.

1.2 Hydrogen Storage Materials

Among the hydrogen liberating materials available are metal hydrides (MgH_2, Mg_2NiH_4), chemical hydride ($NaAlH_4$, $LiBH_4$, $Mg(BH_4)_2$), carbon based materials (carbon nanotubes, active carbons, carbon derived carbon) and metal organic hydride (metal organic framework (MOF)). Table 1.1 represents the conventional storage device and the method of release. Among all of the options, the best bet has been placed on chemical hydrides as they possess very high capacity and liberate hydrogen at moderate temperatures

TH-1791_136107007

Table 1.1 Conventional storage device and the method of release

Storage device	**Example**	**Bonding with Hydrogen**	**Desorption Temperature**	**Kinetics**	**Advantages**
Metal Hydrides	MgH_2,Mg_2NiH_4	Chemical	Very High	Slow	High capacity
Chemical Hydrides	$NaAlH_4$,$LiBH_4$, Mg $(BH_4)_2$	Chemical	High	Moderate	Very high capacity
Carbon Based Materials	CNT, Active carbons, Carbon derived carbon	Physical	Too Low	Fast	Reversible
Metal Organic Hydrides	Metal organic framework (MOF)	Physical	Too Low	Fast	Large surface area

1.2.1 Chemical Hydrides

Among the chemical hydride, Amine Borane is known to release a substantial amount of hydrogen gas at temperatures below 200 ºC and atmospheric pressure. The simplest of these compounds is NH_3BH_3 (Ammonia Borane, or AB), which contains 19.6 % hydrogen by weight. Boron hydrides having high hydrogen content are notable mention in the complex hydride family because of its use as a reversible storage material in rigorous conditions. Still they suffer from releasing volatile borane during dehydrogenation. Amine Borane prototype such as Ammonia Borane (NH_3BH_3) , Methyl Amine Borane (MeAB) [5], sec-butyl borane (SBAB) [6], hydrazine borane (HB) and Ethylene Diammine *bis*-Borane (EDAB) [7] are more volatile and hence reduce the contamination of the released hydrogen. Among these Ammonia Borane (AB) with a high hydrogen-storage capacity (19.6 wt. %) and low molecular weights has been investigated intensively. AB complexes contain high amount of hydrogen and it is the stability which makes them a suitable choice

TH-1791_136107007

for fuel cell applications. For example, AB contains around 19.6 % hydrogen which is almost higher than any metal hydrides except $Be(BH_4)$ [8]. AB hydrides further have potential to provide a safe, efficient and economical way for the development of hydrogen storage medium. As stated above, Ammonia Borane is the best candidate when it comes to dehydrogenation. It has the highest hydrogen gravimetric capacity among all amine borane adducts.

But on the downside, the decomposition also produces Borazine (highly toxic) and ammonia [9-11]. Furthermore, the dehydrogenation of AB also has certain limitations such as its incomplete decomposition at high temperature of 500 ºC and virtually impossible in regenerating the end products such as hydrazine borane. Efforts to overcome this problem were made by making chemical modifications to AB molecules, such as using carbon derivatives of AB molecules. Methyl amine borane (MeAB), sec-butyl amine borane (SBAB) and ethylene diamine *bis* borane (EDAB) are amongst some of the prominent carbon substituted amine boranes which are being investigated currently. Where on the other hand, these derivatives generate lesser amount of hydrogen after heating; on the other hand there is no formation of volatile compounds such as borazine as side products in dehydrogenation reactions.

The above disadvantages of AB have paved the way for Ethylene DiAmine bisBorane (EDAB), although they possess lower hydrogen content compared to AB. However, formation of volatile compound such as borazine is not observed in the dehydrogenation. The most attractive feature of EDAB is the absence of induction period during dehydrogenation process. The rate of dehydrogenation of EDAB is also known to be faster than AB at higher temperatures.

TH-1791_136107007

1.2.2 Ethylene DiAmine *bis*- Borane (EDAB)

Ethylene diamine bis-borane (EDAB) was first synthesized by Kelly and Edward [12] by reacting ethylene diamine with diborane under vacuum. The release of two equivalents of hydrogen at 110 ºC was reported and with prolonged heating no volatile impurities were found. The same authors then reported an easier approach of producing EDAB by reacting ethylene diamine dihydrochloride and sodium borohydride in tetrahydrofuran using high vacuum apparatus [13]. Some of the physical properties of EDAB is given in Table 1.2. Neiner and coworkers [7] reported a hydrogen release of 10% at a temperature less than 200 ºC involving a two-step thermal dehydrogenation process. At a temperature range of 100 – 200 ºC, an intra and intermolecular dehydrogenation process of EDAB was also reported by the same group. Though the release of hydrogen content is less in comparison to AB, still EDAB evolved lesser amount of impurities. The absence of an induction period during the dehydrogenation process was also recorded by them.

Leardini and co-workers [14] studied the dehydrogenation mechanism of EDAB in vacuum as well as under inert gas flow and reported four equivalent hydrogen release during first and second desorption stages. It was followed up by Carpenter and co-workers [15] where an intensive study about the infrared matrix of amino borane and its related compounds was studied. Sebastian Sahler et al. [16] also conducted experiments with a variety of IL's for its catalytic effect on the dehydrogenation of ethylene diaminebisborane (EDAB). The catalytic activity of IL's, such as 1-butyl-2, 3-dimethylimidazolium chloride ([BMMIM][Cl]), 1-butyl-2, 3-dimethylimidazolium acetate ([BMMIM][OAc]), 1-butyl-3-methylimidazolium acetate ([BMIM][OAc]) and 1-butyl-3-methylimidazolium methylsulfonate ([BMIM][OMs]) were studied and the mixture ratio namely [BMMIM][Cl] /EDAB was investigated. This system was able to deliver about 6.5 wt. %

TH-1791_136107007

of hydrogen at 140 °C which prompted them to compare with conventional hydrogen storage pressure tanks.

The correlation between polarity of the ILs and hydrogen yield was investigated and the suitability for hydrogen storage systems was evaluated and discussed by Sahler et al. [17]. In the same study EDAB with suitable catalyst such as Pd- and Ru-NPs (NPs: nanoparticles) were used for thermal dehydrogenation [17]. They reported the use of the hydrogenation catalyst for the unsaturated C-C bond reduction and also for chemo-selective hydrogenation of carbonyl functionalities. They have further concluded that EDAB can be also utilized as a reducing agent for carbonyl functionalities in water under metal-free conditions. Functional groups like alkenes, aromatic double bonds, nitro groups, lactames, esters, ethers, and acids was found to remain inert which implies that EDAB is highly selective for aldehydes and ketones . In another review by Ting et al. [18] solid state EDAB was examined and was found to be an open-chain molecule which exists in the *trans* conformation. Some of the physical properties of EDAB have been summarized in Table 1.2.

Table 1.2 Physical properties of Ethylene DiAmine *bis*-Borane (EDAB)

Molecular Formula	$C_2H_{14}B_2N_2$
Appearance	White crystalline solids
Density	0.82 g cm^{-3}
Melting point	114 - 130 °C
Molecular weight	87.77 g/mol
Hydrogen content	9.2 wt.% H_2

TH-1791_136107007

1.3 Ionic Liquids (ILs)

Ionic liquids are combination of organic cations and inorganic/organic anions which are basically solvents that are liquid at a temperature below 100°C or even in room temperature. Based on the cation-anion combination, a huge number of ILs are possible. Ionic liquids are quickly gaining popularity because of certain advantages such as dissolving both neutral and ionic species and promoting polar transition states. It exhibits negligible vapor pressures and is also known to lower induction period and temperature for hydrogen release. Because of its non-coordinating anions and cations, it provides a polar, inert reaction medium for catalytic reactions. It was also found that the presence of IL's catalyzes the dehydrogenation reaction at a faster rate. They decrease the induction period of the reaction and also account for faster release of hydrogen. In the presence of IL, the dehydrogenation rate is found to be faster when compared to only EDAB as chemical storage media. This is primarily because of the formation of the more reactive diammoniate of diborane (DADB) intermediate which gets stabilized under the influence of IL as solvent media.

Himmelberger et al. [19] used AB-1-butyl-3-methylimidazolium chloride (BMIMCl) (50:50-wt %) which on reaction exhibited no induction period. A comparative study on solid state AB and AB-IL showed a release of 1.0 H_2 equivalent in 67 min and 2.2 H_2 equivalent in 330 min at 85 ºC, whereas solid-state AB at 85 °C exhibited an induction period of 3 hours and on further heating released ~0.8 H_2 equiv. The change in AB-IL ratio also proved to be better than in comparison to neat AB. A dehydrogenation pathway was also proposed which showed IL helps in formation of diammoniate of diborane (DADB).The very stabilization effects contributes to the enhancement of hydrogen release and suppression of induction time.

TH-1791_136107007

The most prominent among the IL's are the imidazolium based ILs, which have been explored to facilitate milder condition for dehydrogenation of amine borane compounds [19, 16, 20-22]. Banerjee et al. [20] reported a total of 3.96 and 3.52 equivalents of hydrogen from the desorption of EDAB/[BMIM][OAc] and EDAB/[EMIM][OAc], respectively, at 105 ºC. Bluhm and co-workers [21] carried out a study of the release of hydrogen using borane complexes in the presence of IL, 1-butyl-3-methylimidazolium chloride and compared the same to analogous solid-state reactions. The presence of acidic proton in imidazolium ring does not make it entirely inert and thus is known to form intermediate carbenes in certain reactions [22]. In a detailed study about the nature of AB-IL mixture by Nakagawa et al. [23], the dehydrogenation and structural properties was investigated. They concluded that ILs are favorable for thermal dehydrogenation of AB as they provide stability to the reactive intermediate species. Imidazolium ILs with 1-alkyl-2,3-dimethylimidazolium chloride were selected for the study. The IL helped in the liberation of ammonia and other impurity. Further ^{1}H, ^{11}B ^{13}C NMR spectra were then used in the understanding the reaction of AB-IL dehydrogenation.

As the selection of cations and anions influence the IL facilitated reactions, hence a judicial choice of ILs is required so as to influence the formation of dehydrogenated products. In this regard, the phosphonium-based cations poses an alternative option for thermal dehydrogenation of amine boranes due to its higher thermal stability, which makes them an efficient energy carrier for boranes. Phosphonium based ionic liquids when treated with borane can be used for carbonyl compound reduction [24]. Absence of acidic protons in cation is known to enhance the thermal stability of these phosphonium ILs in basic and nucleophilic conditions [25, 26]. Additionally, these ILs are produced in industrial scale and offer superior physio-chemical properties than ammonium based ILs [27].

TH-1791_136107007

The effect of allyl group on the imidazolium cation was also studied. The allyl substituted imidazolium salts were found to possess moderate viscosity. The TGA curve of 1-allyl-3-methylimidazolium chloride gave an onset temperature of degradation of about 273 °C, which was slightly higher than 1-butyl-3-methylimidazolium chloride [Bmim][Cl] (254 °C). It also gave a lower melting point at 17°C and a considerably lower viscosity of 685 mPa s at 30 °C, in contrast with [Bmim][Cl] which gave a melting point of 65 °C and a viscosity of 11,000 mPa s at 30 °C [28]. It was also reported that N-allylcarbazole, which had a similar chemical structure to the allyl based IL does not get homopolymerized even after heating at 228 °C [28]. Thus a lower viscosity gives a strong plasticizing effect so as to introduce amorphous nature within the ionic liquids but at the same time retain its polarity. The relatively lower melting point and viscosity for 1-allyl-3-methylimidazolium halides Ionic Liquids are attributed to the suppressed crystallization of the IL effectively by an allyl group on the N-position [29]. The IL, 1-allyl-3-methylimidazolium bromide is known to be stable at a very high range of temperature (>230 °C).

From the above stated literature we can see that various studies of AB-IL mixtures have already been reported. However, thermal dehydrogenation of EDAB-IL mixtures are scarce. This thesis hence attempts to explore and compare both EDAB and AB as hydrogen storage materials with IL as potential media for thermal dehydrogenation reactions.

TH-1791_136107007

1.4 Objectives

Based on the literature survey, the objectives of this thesis are:

(a) ***Selection of Potential Ionic Liquid using COnductor like Screening MOdel-Segment Activity Coefficient model (COSMO–SAC)***

COSMO-SAC model shall predict the a-priori liquid phase non-ideal activity coefficient of EDAB in a mixture of EDAB and IL. The selection of ILs will be thereafter be performed based on the values of Infinite Dilution Activity Coefficients (IDAC) i.e. of EDAB in IL's.

(b) ***Reaction Kinetics for the Thermolysis of Amine Boranes complexes***

In order to explain the effects of dehydrogenation, a regression analysis with the experimental kinetic data is required. This will be attempted using the Avrami Erofeyev model in order to obtain the activation energy, rate constant and reaction order of EDAB/AB-IL mixtures.

(c) ***Thermal Dehydrogenation of Ethylene Diammine bis-Borane (EDAB) with Ionic Liquids***

Ionic Liquids selected for thermal dehydrogenation will be primarily from objective (a) and (b). It is also envisaged to carry out the characterization of residual product after thermal dehydrogenation. Overall based on the screening criteria three classes of cations namely imidazolium, phosphonium and allyl based cations have been adopted.

(d) ***ReaxFF Reactive Force Field Simulations on EDAB Dehydrogenation***

In the penultimate stage, a reactive MD simulation shall be adopted to study the dehydrogenation reactions of EDAB within a computational affordable time especially for Ethylene Diammine *bis*-Borane (EDAB). In this present thesis, ReaxFF force field simulations will be used to perform the initiation mechanism of Ethylene Diammine bis-Borane (EDAB) dehydrogenation.

TH-1791_136107007

1.5 Structure of Thesis

The thesis is organized within the following chapters:

Chapter 2 describes the experimental details such experimental set up, materials used and several analytical instruments so as to have a better understanding for the thermal dehydrogenation of EDAB with ILs. This chapter also includes the details of materials used. The residue of the experiments were further characterized and reported so as to find the nature of residual products and thereafter formulate a reaction mechanism. It also discusses computational details of EDAB and EDAB/IL system. The choice of IL is quite cumbersome owing to its infinite cation and anion combination. This chapter discusses the computational screening methodology which is the Continuum Solvation Model or COSMO-SAC model for the IL selection in dehydrogenation. Stability analysis through HOMO LUMO gap is also discussed briefly in this chapter. In order to explain the effects of dehydrogenation, a regression using the experimental kinetic data using the Avrami Erofeyev model [5] has been performed so as to obtain the activation energy, rate constant and reaction order.

Chapter 3 discusses the experimental studies of thermal dehydrogenation of EDAB using COSMO-SAC predictions. Initially benchmarking studies are reported for data available in literature for Ammonia Borane and Ionic Liquids as solvent. Kinetic regression using the single step logistic growth model and the two step Avrami Erofeyev model for AB/IL and EDAB/IL is also included. It then initiates the screening on the potential Ionic Liquids using COSMO-SAC model followed by the stability analysis with the HOMO-LUMO orbital energy gaps. IL's with the highest solubility or lower values of IDAC were chosen as a potential solvent for the dehydrogenation process. Here 1-ethyl-3-methyl imidazolium acetate ([EMIM][OAc]) and 1-butyl-3-methyl imidazolium

TH-1791_136107007

acetate ([BMIM][OAc]) were selected as the solvent for dehydrogenation studies of EDAB. Further characterization experiments on the residual products were conducted to have a better understanding about the nature of IL-EDAB mixtures.

It further focuses on the next best IL within the COSMO-SAC framework i.e. the phosphonium based Ionic Liquids. It then discusses the effect of Trihexyl (tetradecyl) phosphonium bis(2,4,4- trimethylpentyl) phosphinate and Trihexyl (tetradecyl) phosphonium dicyanamide ([TDTHP][DCA]) on EDAB for dehydrogenation studies. The previous literature proposed two possible pathways of EDAB dehydrogenation based on either an intramolecular or intermolecular approach. In this chapter we have proposed an intermolecular dehydrogenation which is initiated by the formation of EDAB dimer. The penultimate section reports the Allyl-Based Ionic Liquids for thermal dehydrogenation of EDAB. The three Allyl based ILs chosen are 1-allyl-3-methylimidazolium dicyanamide ([AMIM][$N(CN)_2$]), 1-allyl-3-methylimidazolium bis(trifluoromethylsulfonyl) imide ([AMIM][Tf_2N]), and 1-allyl-3-methylimidazolium bromide ([AMIM][Br]). Rate Constants for decomposition of EDAB in [AMIM][Br] using the Avrami–Erofeyev Model was also deduced so as to confirm the two step dehydrogenation process of EDAB-IL mixture. The concluding section reports the Reactive Force Field (ReaxFF) method which was employed to have a better understanding about intramolecular reaction mechanism of EDAB. Pyrolysis study of EDAB at high temperatures which is usually not measured experimentally have also been reported**.**

Chapter 4 summarizes the key results obtained from the present studies and also the future scope for dehydrogenation of EDAB and other amine borane complexes using IL's and Deep Eutectic Solvents (DES).

TH-1791_136107007

References:

1. Judson. H.F. The Search for Solutions, *Holt Rinehart & Winston press,* **1980**.

2. Martavaltzi, C.S.; Pampaka, E. P.; Korkakaki,E. S.; Lemonidou, A. A. Hydrogen Production via Steam Reforming of Methane with Simultaneous CO_2 Capture over CaO $Ca_{12}Al_{14}O_{33}$. *Energy Fuels*. **2010**, 24, 2589–2595.

3. Ono, K. Fundamental Theories on a Combined Energy Cycle of an Electrostatic Induction Hydrogen Electrolytic Cell and Fuel Cell to Produce Fully Sustainable Hydrogen Energy. *Electrical Engineering in Japan.* **2015**,190, 1–9.

4. "Alternative Fuels Data Center: Hydrogen Basics". www.afdc.energy.gov. (Retrieved 2016-02-27).

5. Jaska, C.A.; Temple, K.; Lough A. J. Manners,I. Transition Metal-Catalyzed Formation of Boron-Nitrogen Bonds: Catalytic Dehydrocoupling of Amine-Borane Adducts to Form Aminoboranes and Borazines. *J.Am.Chem.Soc.* **2003**, 125, 9424-9434.

6. Mal, S.S.; Stephens, F.H.; Tom Baker, R. Transition metal catalysed dehydrogenation of amine-borane fuel blends. *Chem. Comm.* **2011**, 47, 2922–2924.

7. Neiner, D.; Karkamkar, A; Bowden, M.; Choi, Y. J.; Luedtke, A.; Holladay, J.; Fisher, A.; Szymezak N.; Autrey, T. Kinetic and thermodynamic investigation of hydrogen release from ethane 1,2-di-amineborane. *Energy Environ. Sci.* **2011**, 4, 4187–4193.

8. http://www.sigmaaldrich.com/content/dam/sigma-aldrich/articles/material-matters/pdf/metal-borohydrides.pdf (accessed 10.06.14)

9. Stephens, F.H.; Pons V.; Tom Baker, R. Ammonia–borane: the hydrogen source par excellence?. *Dalton Trans.* **2007**, 2613–2626.

10. Al-Kukhum, A.; Hwang, H.T.; Varma, A. A Comparison of Ammonia Borane Dehydrogenation Methods for Proton-Exchange-Membrane Fuel Cell Vehicles: Hydrogen Yield and Ammonia Formation and Its Removal. *Ind. Eng. Chem. Res*. **2011**, 50, 8824–8835.

11. Halseid, R.; Vie, P.J.S.; Tunold, R. Effect of ammonia on the performance of polymer electrolyte membrane fuel cells. *Journal of Power Sources*. **2006**, 154, 343–350.

12. Kelly, H.C.; Edwards J. O. Ethane 1,2-Diamineborane. *J. Am. Chem. Soc.* **1960**, 82, 4842-4846.

13. Kelly, H.C.; Edwards J. O. Evidence for the Open Chain Structure of Ethane 1,2-Diamineborane. *Inorg. Chem.* **1963**, 2, 226-227.

14. Leardini, F.; Valero-Pedraza, M. J.; Perez-Mayoral, E.; Cantelli, R.; Bañares, M. A. Thermolytic Decomposition of Ethane 1,2-Diamineborane Investigated by Thermoanalytical Methods and in Situ Vibrational Spectroscopy. *J. Phys. Chem. C.* **2014**, 118, 17221−17230.

TH-1791_136107007

15. Carpenter, J.D.; Ault, B.S. Infrared Matrix Isolation Characterization of Aminoborane and Related Compounds. *J.Phys.Chem.* **1991**, 95, 3502-3506.

16. Sahler, S.; Konnerth, H.; Knoblauch, N.; Prechtl, M.H.G. Hydrogen storage in amine boranes: Ionic liquid supported thermal dehydrogenation of Ethylene DiAmine bisBorane. *Int. J. Hydrogen Energy*. **2013**, 38, 3283-3290.

17. Sahler, S.; Scott, M.; Gedig, C; Prechtl, M.H.G. Transfer Hydrogenation Employing Ethylene DiAmine bisBorane in Water and Pd- and Ru-Nanoparticles in Ionic Liquids. *Molecules.* **2015**, 20, 1758-17069

18. Ting, H.Y.; Watson, W. H.; Kelly, H. C. The Molecular and Crystal Structure of Ethylene diamine-bisborane $C_2H_{14}B_2N_2$. *Inorganic Chemistry.* **1972**, 11, 374-377

19. Himmelberger, D. W.; Alden, L. R.; Bluhm, M.E.; Sneddon, L.R. Ammonia Borane Hydrogen Release in Ionic Liquids. *Inorg. Chem.* **2009**, 48, 9883–9889.

20. Banerjee, B.; Kundu, D.; Pugazhenthi, G.; Banerjee, T. Quantum chemical and experimental insights for the ionic liquid facilitated thermal dehydrogenation of Ethylene DiAmine bisBorane . *RSC. Adv.* **2015**, 5, 85280-85290.

21. Bluhm, M.E.; Bradley, M.G.: Butterick, R.,III; Kusari, U.; Sneddon, L.G. Amineborane-Based Chemical Hydrogen Storage: Enhanced Ammonia Borane Dehydrogenation in Ionic Liquids. *J.Am.Chem.Soc.* **2006**, 128, 7748-7749.

22. Scholten, J. D.; Ebeling, G,; Dupont, J. On the involvement of NHC carbenes in catalytic reactions by iridium complexes, nanoparticle and bulk metal dispersed in imidazolium ionic liquids. *Dalton Trans.* **2007**, 47, 5554-5560.

23. Nakagawa, T.; Burrell, A. K.; Del Sesto, R. E.; Janicke, M. T.; Nekimken, A. L.; Purdy,; B. Paik, G. M.; Zhong, R.-Q.; Semelsberger, T. A.; Davis, B. L.; Physical, structural, and dehydrogenation properties of borane in ionic liquids. *RSC Adv*. **2014**, 4, 21681-21687.

24. Ramnial, T.; Hauser, M. K.; Clyburne, J. A. C. Phosphonium-Based Ionic Liquids as Efficient Borane Carriers. *Aust. J. Chem.* **2006**, 59, 298-301.

25. Atefi, F.; Garcia, M. T.; Singer, R. D.; Scammells, P. J. Phosphonium ionic liquids: design, synthesis and evaluation of biodegradability. *Green Chem.* **2009**, 11, 1595-1604.

26. Del Sesto, R. E.; Corley, C.; Robertson, A.; Wilkes, J. S. Tetraalkylphosphonium-based ionic liquids. *J. Organomet. Chem.* **2005**, 690, 2536-2542.

27. Bradaric, C. J.; Downard, A.; Kennedy, C.; Robertson, A. J.; Zhou,Y. Industrial Preparation of Phosphonium Ionic Liquids, *Green Chem.* **2003**, 5, 143-152.

28. Zhang, H.; Wu, J.; Zhang, J.; He, J. 1-Allyl-3-Methylimidazolium Chloride Room Temperature Ionic Liquid: A New and Powerful Non derivatizing Solvent for Cellulose. *Macromolecules*. **2005**, 38, 8272–8277.

29. Mizumo, T.; Marwanta, E.; Matsumi, N.; Ohno, H. Allyl imidazolium Halides as Novel Room Temperature Ionic Liquids. *Chem. Lett*. **2004**, 33, 1360-1361.

TH-1791_136107007

Chapter 2: Experimental Details

TH-1791_136107007

TH-1791_136107007

The selection of the ILs to be used in the experiment will be discussed in the upcoming chapter. The selection of IL through its IDAC value is a crucial step in determining the solubility of EDAB in IL. The need for experiments to confirm the amount of hydrogen released from EDAB using different ILs is however required so as to obtain the kinetic data. The experimental insights not only throws light about the equivalent of hydrogen released but also gives us the nature of the residual products. The mixture of EDAB/IL and the residue collected after the experiment were collected and characterization techniques such as ^{1}H NMR, ^{11}B NMR and HR-MS were conducted on the residual products.

2.1 Dehydrogenation Setup

The entire experimental set up is made up of glass and high quality plastic ware and is completely detachable. Special care has been taken so that once assembled, everything remains fixed except the reactor which can be detached for the next batch of reaction. Schematic of experimental set up is given in Figure 2.1 while the actual setup is given in Figure 2.2. The whole set up can be divided into two distinct parts. The right side of the set up included the liquid nitrogen condenser (with stopper) and reservoir which collectively is known as 'GAS CHAMBER SIDE'. The left side of the set up constituting the reactor with ports for input and thermowell is labeled as "REACTOR SIDE". All the dehydrogenation studies were done under vacuum at around 4.5×10^{-2} mbar. The mixture of EDAB along with IL (15 mg of EDAB and 0.5 mL of IL) was kept in the reactor port and heated at different temperatures for various time intervals on the oil bath. The condenser (GC) was then filled with liquid nitrogen. After every time interval of 20 minutes, the "REACTOR SIDE" was opened and the gas was allowed to pass to the other side of the set up. The main reason for which liquid nitrogen was used as condensing agent

TH-1791_136107007

is to condense the undesirable gas such that it gets accumulated in the collecting flask (MV) (right under the liquid nitrogen condenser). Only hydrogen being the lightest element travels to the gas chamber via the gas valve.

After a certain predetermined time, the gas valve was closed resulting in the separation of the collected gas from rest of the set up. The amount of hydrogen gas released was then determined by compressing the gas into the marked gas burette (GB). This was done by rising the mercury from the mercury vessel (MV) by allowing atmospheric air to enter the system through air valve (AV). The atmospheric air through AV forces the collected gas to rise up which is then compressed in the GB. The rise in mercury level was noted down for computing the equivalents of hydrogen by using a mercury leveler (ML). In order to negate water as an impurity, an operating temperature close to the boiling point of water was adopted. Further vacuum ensures that no atmospheric air enters the set up as the Vacuum Valves (VV) are kept closed throughout the whole experiment. The working temperature have varied between 95 ℃ to 115 °C as dehydrogenation below 95 ℃ did not show appreciable release. Moreover the melting point of EDAB is 115 °C which is just above our prescribed range.

The confirmatory test for hydrogen gas was performed by collecting the gas from the marked Gas Burette using a HAMILTON 5.0 ml (22/2'/2) GAS SYRINGE. The gas chromatography was conducted in BRUKER 450 GC with Thermal Conductivity Detector or GC-TCD technique. This was being used to analyze inorganic gases such as Argon, Nitrogen, Hydrogen and Ammonia. The peak location and detection of evolved gas was further checked by the GC analysis of pure hydrogen (99.8%) so as to confirm the presence of hydrogen by obtaining a similar peak location.

TH-1791_136107007

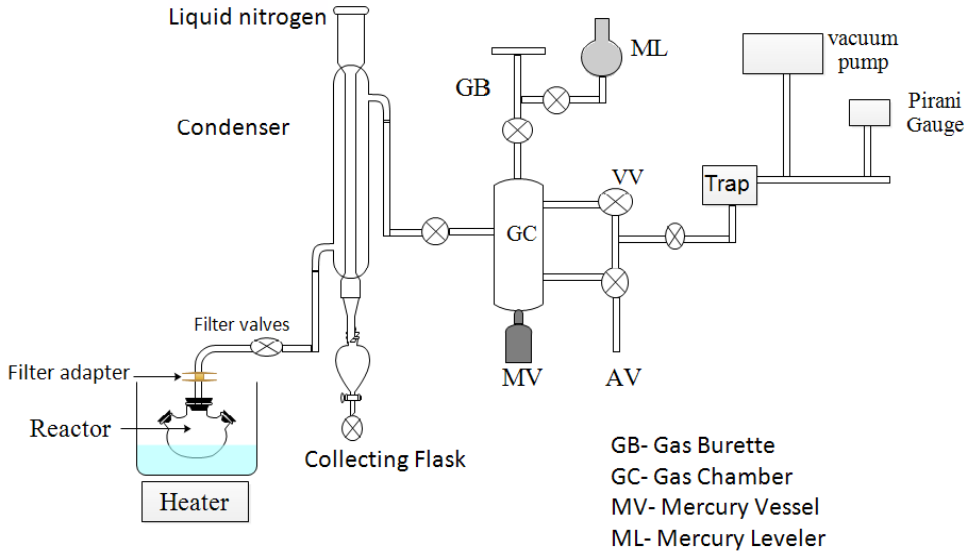

Figure 2.1 Schematic experimental setup

1. PID Controller**;** **2.** Vacuum pump; **3.** Pirani gauge**; 4.** Oil bath**;** **5.** Heater**; 6.** Reactor; **7.** Condenser**; 8.** Collector flask**; 9.** Gas Chamber**; 10.** Mercury vessel**; 11.** Air valve**; 12.** Gas burette

Figure 2.2 Description of the actual setup

TH-1791_136107007

2.2 Chemicals Used

All commercially available chemicals were used of analytical reagent grade. Ammonia Borane (AB) (97%) (CAS Number 13774-81-7) and Ethylene DiAmine *bis* Borane (EDAB) (96%) (CAS Number 15165-88-5) were bought from Sigma Aldrich where no further purification was performed. Figure 2.3 represent the structure of AB and EDAB.

Ionic Liquids were also obtained from Sigma Aldrich. The structures are given in Figure 2.4. The IL's procured were 1-ethyl-3-methyl imidazolium acetate ([EMIM][OAc]) (97%) (CAS Number 143314-17-4), 1-butyl-3-methyl imidazolium acetate ([BMIM][OAc]) (≥95%) (CAS Number 284049-75-8), Trihexyl (tetradecyl) phosphonium bis (2,4,4-trimethylpentyl) phosphinate ([TDTHP][Phosph]) (≥95%) (CAS Number 465527-59-7), Trihexyl (tetradecyl) phosphonium dicyanamide ([TDTHP][DCA]) (≥95%) (CAS Number 701921-71-3), 1-Allyl-3-methylimidazolium bromide ([AMIM][Br]) (≥97%) CAS Number 31410-07-8, 1-Allyl-3-methylimidazolium dicyanamide ([AMIM][$N(CN)_2$]) (≥98.5%) (CAS Number 917956-73-1) and 1-Allyl-3-methylimidazolium bis (trifluoromethylsulfonyl) imide ([AMIM][Tf_2N]) (≥98.5%) (CAS Number 655249-87-9). Impurities like water vapor are removed by keeping the ILs in an oil bath (Borosil mm 150 x 75) for 48 hours at 80°C. Other chemicals such as Dimethyl sulfoxide-d6 (deuteration degree min 99.8%, DMSO) was used as a solvent for NMR spectroscopy, while methanol (HPLC grade) was used for HR-MS characterization.

TH-1791_136107007

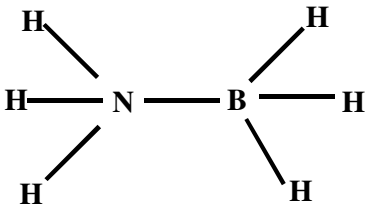

Ammonia Borane (AB)

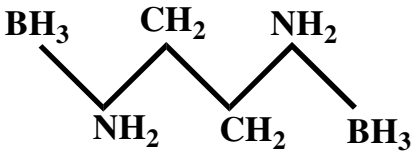

Ethylene Di Amine *bis*-Borane (EDAB)

Figure 2.3 Structures of AB and EDAB.

Name of IL	Structures
1. 1-Ethyl-3-methyl imidazolium acetate [EMIM][OAc]	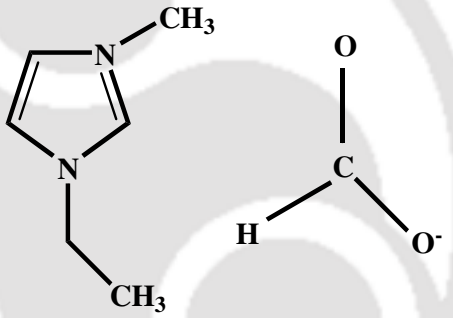
2. 1-Butyl-3-methyl imidazolium acetate [BMIM][OAc]	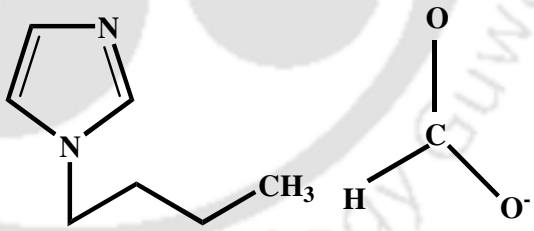
3. Trihexyl(tetradecyl) phosphonium dicyanamide [TDTHP][DCA]	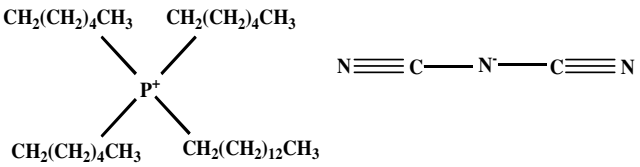

TH-1791_136107007

4. Trihexyl(tetradecyl) phosphonium bis (2,4,4-trimethylpentyl) phosphinate [TDTHP][Phosph]

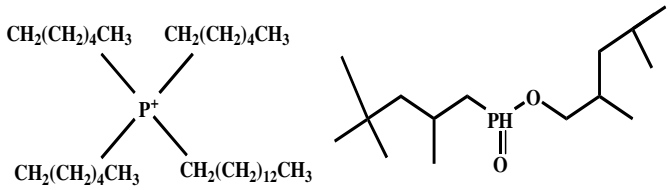

5. 1-Allyl-3-methylimidazolium bromide [AMIM][Br]

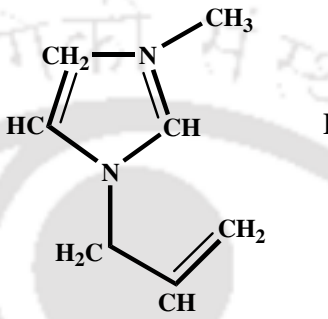

6. 1-Allyl-3-methylimidazolium dicyanamide [AMIM][N(CN)$_2$]

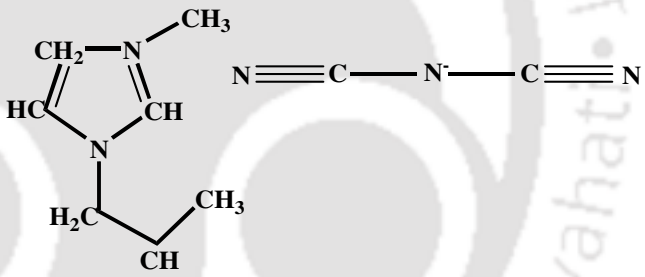

7. 1-Allyl-3-methylimidazolium bis(trifluoromethylsulfonyl) imide [AMIM][Tf$_2$N]

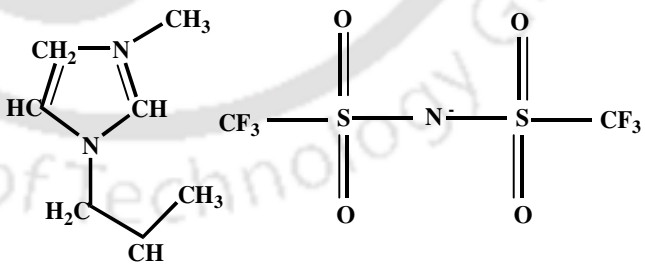

Figure 2.4 Anion and cation structure of ILs used in this work.

TH-1791_136107007

2.3 Characterization Studies

For each experiment, the samples of EDAB-IL were collected for further analysis. Solution ^{1}H NMR and ^{11}B NMR spectra were recorded in DMSO-d6 at room temperature on a 600 MHz nuclear magnetic resonance spectrometer (Bruker). Thermogravimetric analysis of EDAB, EDAB-IL mixtures were performed on a Mettler Toledo Thermogravimetric analyzer (TGA/SDTA model 851). Samples were heated from 30 to 500°C in a 60 mL/min flow of N_2 at a heating rate of 10°C/min. TGA of pure ILs were performed using a Netzsch Thermogravimetric analyzer (TGA/STA 449 F3 Jupiter) from 25 to 500°C in a 60 mL/min flow of Ar at heating rate of 10 °C/min. High resolution mass spectra of EDAB-IL after reaction were recorded in +APCI mode on an Agilent Accurate-Mass Q-TOF LC/MS 6520 where the peaks are given in m/z (% of basis peak).

2.4 Computational Studies

Our emphasis in the future chapters is also to discuss the synergy between computational studies and experimental validation. Keeping in mind the cost of Ionic Liquids, a random selection of cation and anion for dehydrogenation needs to be avoided. This can be performed by the COSMO-SAC (COnductor like Screening MOdel Segment Activity Coefficient) model which a- priori predicts the Infinite dilution activity coefficient (IDAC) values. The ILs with the lowest Infinite dilution activity coefficient (IDAC) can then be selected; as lower the IDAC, higher the solubility of EDAB in IL.

Further we have also proposed a single step logistic growth model for solid AB decomposition while an Avrami Erofeyev model for two step release which is usually seen for AB-IL and EDAB-IL mixtures. The logistic growth model is thus characterized by a single step reaction for the solid state decomposition of AB, while the Avrami

TH-1791_136107007

Erofeyev model for AB/EDAB-IL mixtures can predict two single step reactions. In order to explain the effects of dehydrogenation, we shall attempt to regress the experimental kinetic data using the Avrami Erofeyev model in order to obtain the activation energy, rate constant and reaction order. In the subsequent chapters the predictions using IDAC and kinetic regression using Avrami Erofeyev model has been performed and validated. Let us explore them briefly. The detailed methodology shall be discussed in the next chapter.

2.4.1 Kinetic Data Regression

In both domains i.e. AB, EDAB and IL mediated AB/EDAB, the study of reaction kinetics has not been comprehensive as it requires different modeling strategies. In an earlier work, Ahluwalia et al. [1] adopted the Avrami Erofeyev type model for two step reaction to adequately describe reaction kinetics for dehydrogenation of AB. By regression using least square analysis, they had estimated rate constants for mixtures for AB-IL mixtures. However, such a scheme failed for solid AB decomposition. Further the deviation for AB-IL mixture was particularly high while using a least square analysis. Thus our strategy in future chapter is to model the reaction kinetics using (a) single growth propagation model and (b) Avrami Erofeyev type model for two step reaction. The activation energies computed from these strategies will give us insight into the extent of dehydrogenation reactions which can further be validated with COSMO-SAC predicted IDAC values for AB/EDAB-IL mixtures. The detailed study about growth propagation model and Avrami Erofeyev type model for two step reaction has been discussed in Chapter 3.

TH-1791_136107007

2.4.2 COSMO-SAC Model

From the thermodynamic point of view, infinite dilution activity coefficient (IDAC) predicts the deviation from ideal behavior in a mixture. Heintz et al. [2] first laid down the concept of IDAC of solute in ILs. Excess Gibbs free energy models such as NRTL, UNIQUAC and UNIFAC can predict IDAC but these models are dependent on parameters generated from experiments and hence are not much useful. Interaction parameters involving ILs are scarce in literature, which makes the UNIFAC model redundant for IL's. Therefore, a predictive model for IDAC on a-priori basis was necessitated. Quantum chemical based **CO**nductor like **S**creening **MO**del –**S**egment **A**ctivity **C**oefficient (COSMO-SAC) [3], a variant of COSMO-RS [4] model is a novel and efficient model, which predict IDAC and other thermodynamic properties of mixture on a-priori basis. Screening of solvents by COSMO-RS method and prediction of IDAC is already successfully adopted in extraction studies [5-6].

The most challenging and difficult part are in removing the last traces of AB or EDAB species from Ionic Liquid. The infinite dilution activity coefficient (IDAC) is an important indicator which quantifies this very phenomenon. Further, the activity coefficient at infinite dilution can be measured via gas –liquid chromatography and gives us an important descriptor for the effectiveness of a solvent to remove or reversibly attract the last trace of impurity (Ammonia Borane). Lesser the IDAC values from unity, greater are the tendency for the IL to remove AB ore EDAB species.

The COnductor like Screening MOdel (COSMO) was proposed by Klamt [4]. In such a model the surface properties are calculated from the induced screening charge densities which are developed when a molecule is placed in a perfect conductor. This ensures a complete polarization. Due to the perfect screening or polarization by the

TH-1791_136107007

conductor, charge densities are placed over the interface of solute and conductor. The solution of the charge densities or screening charge densities leads to the generation of what we call a COSMO file. Thereafter a statistical mechanical framework is created so as to develop an expression of chemical potential of these segment. Further the summation of chemical potential of the entire molecular segments leads us to derivation of activity coefficient in a mixture or solution. The derivations and methodology of such a calculation can be obtained from Lin and Sandler [3] and also from our previous work [7-9] of COSMO-RS with Ionic Liquids. In our work, we have assumed the ILs as combination of cation and anions with equimolar ratio. The COSMO-RS parameters are the same as used in our earlier work [7]. In this thesis we have predicted the IDAC of solutes i.e. Ammonia Borane in IL. This essentially becomes a Solid Liquid Equilibria (SLE) problem as AB is solid in nature. It requires the pure component properties namely the heat of fusion (H_f) and melting temperature (T_m), which are easily available [10] for AB or EDAB.

2.4.3 Stability Analysis through HOMO-LUMO Energy Gap

The reactivity and stability of a chemical complex such as for AB-IL and EDAB-IL can be explained by its excitation gaps. There are two different excitation gaps, which are important from a theoretical and practical point of view. The difference between the first ionization potential (*IP*) and the first electron affinity (*EA*) is defined as the fundamental gap, E_g, whereas the optical gap, E_{opt} is the difference between the energy of the lowest dipole allowed excited state and the ground state. Donor–acceptor complexes such as dehydrogenation of amine–borane complexes in the presence of ILs can give insight to these gaps. The HOMO-LUMO [11-13] energy can be written as in the context of Density Functional Theory (DFT) as:

$$EA = -E_{LUMO} \qquad (2.1)$$

TH-1791_136107007

$$IP = -E_{HOMO} \qquad (2.2)$$

where E_{LUMO} and E_{HOMO} is Kohn-Sham [14] Eigen values associated with frontier molecular orbitals.

The application of many body perturbation theory gives us a solid theoretical and reliable estimate of these excitation gaps at the expense of high computational cost. The computation using Density Functional Theory (DFT) can give us an estimation of excitation gaps prevalent in the complex. The fundamental condition within the Kohn–Sham DFT formalism states that the negative of the HOMO energy is equal to the *IP* of the *N* electron system ,while the LUMO energy can be indirectly tuned by considering the (*N* + 1) electron system of the *N* electron system [15]. *EA* characterizes the susceptibility of a molecule toward attack by nucleophiles whereas *IP* characterizes the susceptibility of molecules toward attack by electrophiles. Hard electrophiles have a high LUMO energy whereas hard nucleophiles have a low HOMO energy [16].

The LUMO–HOMO energy gap is another descriptor which is used as in establishing the stability and extent of charge transfer in IL containing systems [17-18]. The high stability of molecules is implied by a large LUMO–HOMO gap because of the lower charge transfer in the complexes. A part of chapter 3 attempts to predict the stability of EDAB/IL complexes in dehydrogenation experiments. Thus with the experimental details mentioned in section 2.1 and an abridged form of the computational details, we shall now move on discussing the results obtained using these techniques.

TH-1791_136107007

References:

1. Ahluwalia, R.K.; Peng, J.K.: Hua, T.Q. Hydrogen Release from Ammonia Borane Dissolved in an Ionic Liquid. *Int. J. Hydrogen Energy*, **2011,** 36, 15689-15697.

2. Heintz. A.; Kulikov. D. V.; Verevkin. S. P. Thermodynamic Properties of Mixtures Containing Ionic Liquids. 1. Activity Coefficients at Infinite Dilution of Alkanes, Alkenes, and Alkylbenzenes in 4-Methyl-*n*-butylpyridinium Tetrafluoroborate Using Gas-Liquid Chromatography. *J. Chem. Eng. Data*, **2001**, 46, 1526-1529.

3. Lin, S. T.; Sandler, S. I. A Priori Phase Equilibrium Prediction from a Segment Contribution Solvation Model. *Ind. Eng. Chem. Res.* **2002**, 41, 899-913.

4. Klamt, A. Conductor-like Screening Model for Real Solvents: A New Approach to the Quantitative Calculation of Solvation Phenomena. *J. Phys. Chem.* **1995**, 99, 2224-2235.

5. Eckert. F.; Klamt. A. Fast Solvent Screening via Quantum Chemistry: COSMO-RS Approach, *AIChE J*., **2002**, 48, 369-385.

6. Banerjee. T.; Khanna. A. Infinite Dilution Activity Coefficients for Trihexyltetradecyl Phosphonium Ionic Liquids: Measurements and COSMO-RS Prediction, *J. Chem. Eng. Data*, **2006**, 51, 2170-2177.

7. Kundu, D.; Banerjee. T. Multicomponent vapor-liquid-liquid equilibrium prediction using an a-priori segment based model. *Ind Eng Chem Res.* **2011**, 50, 14090-14096.

8. Ramalingam. A.; Banerjee. T. Quantum chemical studies on the simultaneous interaction of thiophene and pyridine with ionic liquid. *AIChE J.* **2011**, 57,749-764.

9. Banerjee. T.; Khanna. A. Liquid liquid equilibria for ionic liquid based systems using COSMO-RS: effect of cation and anion combination. *AIChE J.* **2008,** 54, 1874-1885.

10. Bai. L.; Zhu. J.; Chen. B. Quantitative structure property relationship study on heat of fusion for ionic liquids. *Fluid Ph. Equlib.* **2011**, 312, 7-13.

11. Pauling. L. The nature of the chemical bond and the structure of molecules and crystals: an introduction to modern structural chemistry, *Cornell University Press*, **1960**.

12. Pearson. R. G.; Palke. W. E. Support for a principle of maximum hardness, *J. Phys. Chem.* **1992**, 96, 3283-3285.

13. Parr. R. G.; Szentpaly. L. v.; Liu. S. Electrophilicity index, *J. Am.Chem.Soc.* **1999**, 121, 1922-1924.

14. Kohn. W.; Sham. L. J. Self-consistent equations including exchange and correlation effects, *Phys. Rev.*, **1965**, 140, A1133-A1138.

15. Foster. M. E.; Wong. B. M. Nonempirically Tuned Range-Separated DFT Accurately Predicts Both Fundamental and Excitation Gaps in DNA and RNA Nucleobases. *J.Chem.Theory Comput*. **2012**, 8, 2682 – 2687.

TH-1791_136107007

16. Karelson M.; Lobanov. V. S.; Katritzky. A. R. Quantum-Chemical Descriptors in QSAR/QSPR Studies. *Chem. Rev.* **1996**, 96, 1027 – 1043.

17. Anantharaj. R.; Banerjee. T. Evaluation and comparison of global scalar properties for the simultaneous interaction of ionic liquids with thiophene and pyridine. *Fluid Phase Equilib.* **2010,** 293, 22-31.

18. Pilli. S. R.; Banerjee. T.; Mohanty. K. HOMO-LUMO Energy Interactions between Endocrine Disrupting Chemicals and Ionic Liquids using Density Functional Theory: Evaluation and Comparison. *J. Mol. Liq.* **2015**, 207, 112-124.

TH-1791_136107007

TH-1791_136107007

Chapter 3: Result and Discussions

TH-1791_136107007

TH-1791_136107007

3.1 Introduction

The current chapter discusses the thermal dehydrogenation studies of IL-Amine Borane complexes in their order of COSMO-SAC selectivity with the experimental details as provided in chapter 2. It has three subgroups, the first subgroup discusses the kinetic regression using the single step logistic growth model and the two step Avrami Erofeyev model. It then initiates the screening on the potential Ionic Liquids using COSMO-SAC model followed by the stability analysis with the HOMO-LUMO orbital energy gaps. The dehydrogenation of EDAB with acetate based ILs is then reported. The second and third subgroup reports the thermal dehydrogenation with the phosphonium and allyl based IL's respectively. We shall now first focus our attention to the acetate based Ionic Liquids. Before we discuss the presence of Ionic Liquids, the dehydrogenation of Amine Boranes especially Ammonia Borane (AB) deserves attention, so that we can know the nature of the reaction mechanism. This is explained by the regression of kinetic data for pure chemical hydride such as Ammonia Borane (AB) when undergoing thermolysis.

3.2 Solid state AB Dehydrogenation

It has been reported that solid state AB [1] had shown an induction period of 3 hours at 85 °C, whereas at 95 °C, it reduces to 1 hour. After 17 hours heating at 95 °C, 0.9 equivalent of hydrogen have been found to be released. Thereafter even heating for 67 hours at 85 °C produced merely 0.9 equivalent hydrogen. At 95 °C, a similar resemblance has been found with a shorter induction period. Previous authors [1] have also obtained 0.84 equivalent hydrogen after heating for 7 hours at 85 °C. Thereafter only 0.04 equivalent amount of hydrogen has been found after 3 hours. However, a drastic increase in growth rate has been seen for the next few hours. Though at the end, after the generation of 0.85 equivalent hydrogen, the growth rate fell off gradually (Figure 3.1).

TH-1791_136107007

Thus the whole dehydrogenation process irrespective of temperature can be described as following: an induction period, followed by a sharp increase in hydrogen release and then a slow decrease as time progresses. We have proposed a logistic growth model to represent the kinetic reaction data for solid AB dehydrogenation. In order to account for the three domains, we represent reaction mechanism for solid state AB decomposition at 85°C through a single step reaction assuming the contribution due to the last domain insignificant (Eqs. 3.1a-3.3).

$$S_1 \rightarrow S_2 + \beta_1 H_2 \qquad (3.1a)$$

$$\frac{d\alpha_i}{dt} = \alpha_i k_i \left(1 - \frac{\alpha_i}{K}\right) \qquad (i = \text{no of step reactions}) \qquad (3.2)$$

$$k_i = k_{i0} e^{-\frac{E_i}{RT}} \qquad (3.3)$$

Here S_1 represents NH_3BH_3, whereas S_2 denotes final products which are most likely to be unreacted AB, DADB, borazine ($B_3N_3H_6$), cycloborazanes and polyaminoborane $(BH_2NH_2)_n$. In eq. (3.2), the expression $\frac{d\alpha_i}{dt}$ represents the rate of change of mole numbers of Ammonia Borane or simply the rate of decomposition. Here, t is the time and α_i stands for the decomposition amount at time t. K and k_i are the maximum decomposition amount and reaction rate constant, respectively. It is obvious that K can have maximum value of unity because it is the maximum possible value of fraction for decomposition. In the model, we have accounted the initial growth rate by including a factor of $(1-\frac{\alpha_i}{K})$ which is close to unity. This implies that this term is smaller when $\alpha_i << K$, and is close to zero when $\alpha_i \sim K$. The resulting model is known as logistic growth model or Verhulst model

TH-1791_136107007

[2]. The logistic growth model is a simple first-order non-linear differential equation. Which is a convenient way to represent the AB decomposition data by the following alternate form of logistic growth model eq. (3.2). Hence in this model, the values of rate constant (k_{i0}), activation energy (E_i) and total hydrogen equivalent (β_i) are thus predicted. For the generation of parameters, we have performed a nonlinear regression using the Genetic Algorithm Toolbox as available in MATLAB 8.3 (R2014a), to regenerate the experimental data of solid state AB decomposition at 85°C.

The Avrami Erofeyev Model can be represented as follows:

$$S_1 \rightarrow S_2 + \beta_1 H_2 \tag{3.4}$$

As mentioned in the literature [3], S_1 represents NH_3BH_3, whereas S_2 denotes final products which are most likely to be mixture of DADB, AB, polyaminoborane and borazine [4] which is exactly the same as eq. (3.1a). The equations take the form:

$$\frac{d\alpha_i}{dt} = n_i k_i (1-\alpha_i)[-\ln(1-\alpha_i)]^{\frac{n_i-1}{n_1}} \tag{3.5}$$

$$k_i = k_{i0} e^{-\frac{E_i}{RT}} \tag{3.6}$$

Here α_i is the extent of decomposition for S_1 (eq. 3.4) which corresponds to the release of β_1 equivalents of hydrogen. Here $n_i\,(i = 1)$ and $k_i\,(i = 1)$ represents the order of reaction as in eq. (3.5) and rate constant as per equation 3.6. In eq 3.7, α_i is defined as below where subscript *1, 2* represents compound AB and final product respectively. Here *N* refers to the number of moles.

$$\alpha_1 = \frac{N_2}{N_1 + N_2} \tag{3.7}$$

The equations thus formed below describe the change in composition of the condensed-phase reactant (DADB and Final Products) and the product gas (subscript *g*).

TH-1791_136107007

$$\frac{dN_1}{dt} = -\frac{dR_1}{dt}$$

$$\frac{dN_g}{dt} = \beta_1 \frac{dR_1}{dt} \tag{3.8}$$

$$\frac{dR_1}{dt} = (N_1 + N_2)\frac{d\alpha_1}{dt}$$

The equations are then integrated using Adam Moulton's method with the help of GA toolbox. For running the simulation using GA, initial bound for the parameters namely rate constant (k_{i0}), activation energy (E_i) and total hydrogen equivalent (β_i) were given. Thereafter GA was invoked to compute the objective function (eq. 3.9). Along with the objective function, the following properties were also calculated namely decomposition rate $\frac{d\alpha_i}{dt}$ for every second or every minute by incorporating either logistic growth model or Avrami-Erofeyev model. The objective function comprises the difference between experimental result and the cumulative hydrogen production data which is given below:

$$\text{Obj} = \sum_{k=1}^{T}\sum_{i=1}^{N}\left| func^{\exp t} - func^{pred} \right| \tag{3.9}$$

Here indices *k* and *i* refers to the values of temperature and the corresponding data point respectively.

$$func = \beta_1\left[(N_1 + N_2)\times\frac{d\alpha_1}{dt}\right]$$

func = cumulative H_2 generation at a fixed temperature (3.10)

Where,

$$\frac{d\alpha_1}{dt} = n_1 k_1(1-\alpha_1)[-\ln(1-\alpha_1)]^{\frac{n_1-1}{n_1}} \tag{3.11}$$

$$k_1 = k_{10}e^{-\frac{E_1}{RT}} \tag{3.12}$$

TH-1791_136107007

While eq. (3.5) represents a general form of i^{th} single step reaction, eq. (3.11) refers to the single step reaction for decomposition of solid AB. To obtain the parameters from each iteration, '*ode*' solver using Adam Bashford method is used. As we know that at one second, decomposition of any compound is not zero but very close to zero so it is logical to use 0.00001 as an initial guess of decomposition. Further a check was performed such that the initial guess of decomposition does not have any influence in the solution. A detailed description for the GA toolbox is given in Section 3.3. In this process, the thermal decomposition at every second (or every minute) is calculated. In the concluding step, the cumulative H_2 at each experimental time were calculated and errors computed by comparing it with experimental data (eq. 3.9). A suitable tolerance was given and the GA solver was run accordingly. The final parameter values are tabulated in Table 3.1 and the comparison with the experimental data is given in Figure 3.1a (growth propagation model) and Figure 3.1b (Avrami Erofeyev Model). With these generated parameters, we have predicted the hydrogen evaluation at 95°C and have found excellent result when compared with the experimental data (Figure 3.2b).

We have also tried to incorporate the Avrami Erofeyev model to predict the solid state reaction kinetics, however, the predictions are worse as compared to growth propagation model (Figures. 3.1 and 3.2). From previous work [5] we have witnessed that Avrami Erofeyev model is useful for those reactions which has a reaction order of more than unity. It should be noted that solid AB simply follows a first order reaction with ample amount of time as induction period. So, it is clearly noticeable that Avrami Erofeyev model is not helpful in this particular case. Moreover the capacity factor (K) is also non-existent in the equation. So, it is reasonable to use logistic growth model to obtain the reaction kinetics of solid state AB.

TH-1791_136107007

Table 3.1 Optimized parameters for logistic growth model and Avrami-Erofeyev model for solid state AB.

Logistic growth Model (Equation 3.2)					
	α	β	n	$k_0(sec^{-1})\times10^{-17}$	E (kJ $mol^{-1})\times 10^5$
$R_1\rightarrow R_2+\beta_1H_2$	$N_2/(N_1+N_2)$	0.85077	0.998	2.8155	1.41688
Avrami-Erofeyev model ((Equation 3.5)					
	α	β	n	$k_0(sec^{-1})\times 10^{-17}$	E (kJ $mol^{-1})\times 10^5$
$R_2\rightarrow R_3+\beta_2 H_2$	$N_2/(N_1+N_2)$	0.89833	1.45	1.6890	1.47526

TH-1791_136107007

(a)

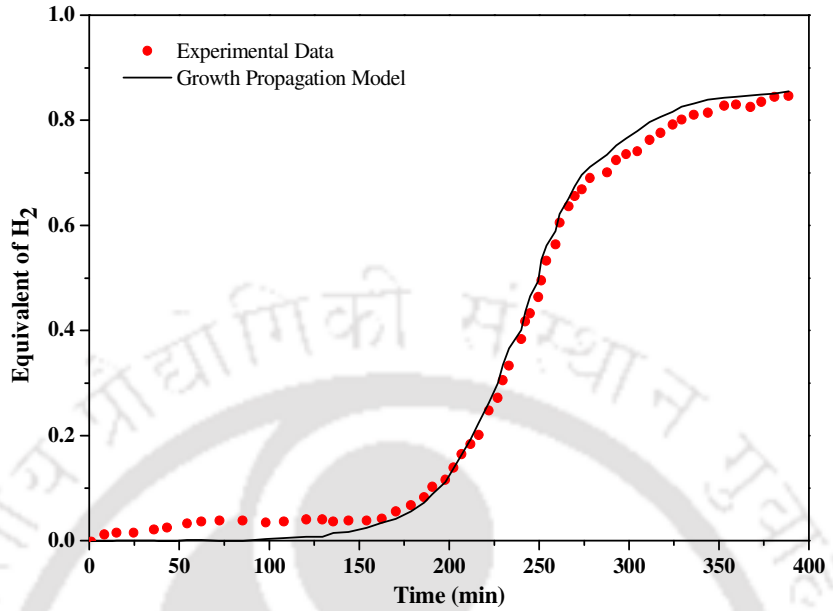

(b)

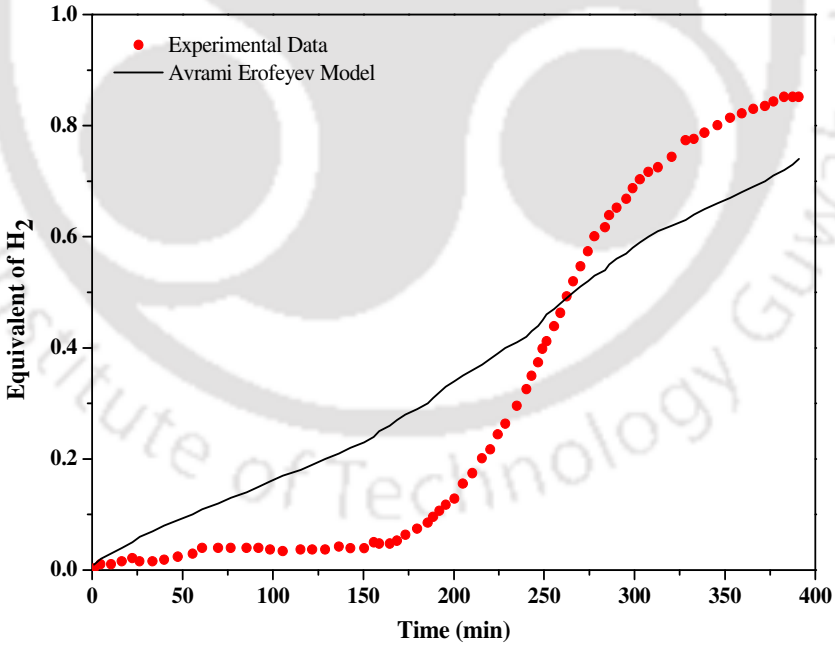

Figure 3.1 Comparison of experimental and predicted hydrogen release at *T*=85 °C using (a) Growth Propagation Model and (b) Avrami-Erofeyev model.

TH-1791_136107007

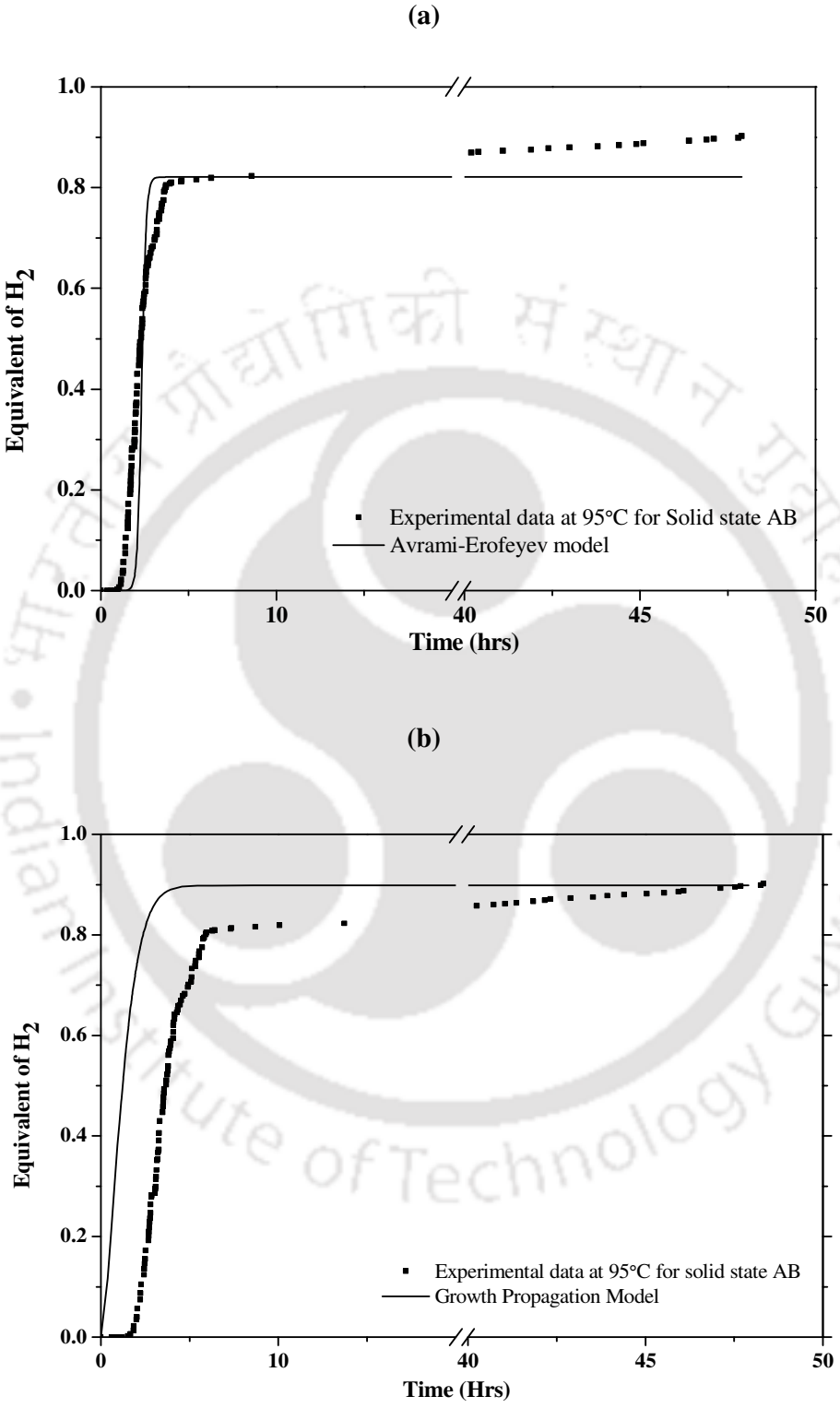

Figure 3.2 Predicted hydrogen release at 95 °C using (a) Avrami-Erofeyev model and (b) Growth Propagation Model.

TH-1791_136107007

3.3 Avrami-Erofeyev Model for Thermal dehydrogenation of Ionic Liquid - Ammonia Borane

A similar procedure has been used to replicate the entire reaction mechanism for AB-IL mixtures using two step reactions as given by Avrami-Erofeyev equations (eqs. 3.13-3.16). In an isothermal system, it appears that the IL assisted AB decomposition shows a sigmoid *α-t* curve of an auto accelerated reaction process [5]. Thus Avrami Erofeyev reaction mechanism is suitable for describing these type of reactions. As discussed earlier in Section 3.2, here again we take an initial bound for all parameters. We then invoke the *gamultiobj* solver for nonlinear regression and evaluate the multiple objective function. So at each iteration whereby a suitable tolerance is given, the following quantities are computed namely (a) cumulative hydrogen production from AB+[BMIM][Cl] mixtures, and (b) corresponding decomposition rate for every second. By using Adams-Bashford-Molton method, we then solve ODE (eq. 3.15) to find the decomposition rate at every second. The ODE which is used to describe the reaction mechanism for AB+[BMIM][Cl] mixture is then represented by the Avrami Erofeyev model. After determining the cumulative H_2 at experimental time [1], we compute the error with experimental data. Overall the Avrami Erofeyev model can be represented for AB-IL mixture as follows:

$$S_1 \rightarrow S_2 + \beta_1 H_2 \tag{3.13}$$

$$S_2 \rightarrow S_3 + \beta_2 H_2 \tag{3.14}$$

As mentioned in the literature [3], S_1 represents NH_3BH_3, whereas S_2 denotes intermediate product dominated by the composition of DADB. It should be noted that although eqs. (3.1), (3.4) and (3.13) are similar, previous ^{11}B NMR [4, 6] confirmed the presence of predominately DADB as S_2 when IL is used as a medium for eq. (3.13). For solid state AB i.e. eqs. (3.1) and (3.4), a similar NMR predicted DADB along with Poly

TH-1791_136107007

Amino Borane (PAB), Borazine and unreacted AB as the intermediate product S_2 [4]. S_3 the final product after releasing total equivalents of hydrogen i.e. $\beta_1 + \beta_2$. Thus the total equivalent of H_2 is greater than β_1 but less than $\beta_1 + \beta_2$. In summary, the final product is a mixture of S_2 and S_3. At 95 °C, 105 °C and 110 °C, the total released H_2 is around 2.35 equivalents of H_2. The Avrami Erofeyev equations then takes the form as below:

$$\frac{d\alpha_1}{dt} = n_1 k_1 (1-\alpha_1)[-\ln(1-\alpha_1)]^{\frac{n_1-1}{n_1}} \quad (3.15a)$$

$$\frac{d\alpha_2}{dt} = n_2 k_2 (1-\alpha_2)[-\ln(1-\alpha_2)]^{\frac{n_2-1}{n_2}} \quad (3.15b)$$

$$k_1 = k_{10} e^{-\frac{E_1}{RT}} \quad (3.16a)$$

$$k_2 = k_{20} e^{-\frac{E_2}{RT}} \quad (3.16b)$$

Here α_i is the extent of decomposition for S_1 eqs. (3.13 and 3.15a) and S_2 (eqs. 3.14 and 3.15b) respectively which corresponds to the release of β_1 and β_2 equivalents of hydrogen. Here n_i (i = 1, 2) and k_i (i = 1, 2) represents the order of reaction and rate constants (eq. 3.16 a,b) for (eq 3.15 a, b), respectively. In eq. 3.17, α_i is defined as below where subscript 1, 2 and 3 represents compound AB, DADB and final product respectively. Here N refers to the number of moles.

$$\alpha_1 = \frac{N_2}{N_1 + N_2}$$
$$\alpha_2 = \frac{N_3}{N_2 + N_3} \quad (3.17)$$

The equations thus formed describe the change in composition of the condensed-phase reactant (DADB and Final Products) and the product gas (subscript g).

TH-1791_136107007

$$\frac{dN_1}{dt} = -\frac{dR_1}{dt}$$
$$\frac{dN_2}{dt} = \frac{dR_1}{dt} - \frac{dR_2}{dt}$$
$$\frac{dN_3}{dt} = \frac{dR_2}{dt}$$
$$\frac{dN_g}{dt} = \beta_1 \frac{dR_1}{dt} + \beta_2 \frac{dR_2}{dt} \qquad (3.18)$$
$$\frac{dR_1}{dt} = (N_1 + N_2)\frac{d\alpha_1}{dt}$$
$$\frac{dR_2}{dt} = (N_2 + N_3)\frac{d\alpha_2}{dt}$$

In a similar manner as for Ammonia Borane, the equations are integrated using Adam Moulton's method with the help of GA toolbox.

It is customary that every solver needs either an objective function or a set of objective functions to find the optimized parameters. With three different temperatures, we have a sum of three different objective functions as represented by one generalized eq. 3.19. For the GA Multiple objective Function *gamultiobj*, the following seven variables were used, namely reaction orders (n_1 and n_2), activation energies (E_{01} and E_{02}), the temperature independent rate constants (k_{01} and k_{02}) for reaction and β_1, β_2 which are the equivalents of hydrogen released in eqs. (3.13) and (3.14) respectively. The bounds for these variables were set to [1.01; 1.6] for n_1 and [2.01; 3] for n_2; [12,000; 16,000] for E_{01} and E_{02}; [0.01 x 10^{17}; 10 x 10^{17}] for k_{01}, k_{02}; and [0.9; 1.2] for β_1. Based on the previous literature [3] the sum i.e. $\beta_1 + \beta_2 = 2.35$ is used as total hydrogen production. Hence the values of β_2 for other IL's were obtained from the subtraction of β_1 from total equivalents (Table 3.3). The values of Population Size and Population type have been kept to 50 and double vector, respectively. Further the selection function has been kept as tournament with a size of 2. For the reproduction, the crossover function of 0.8 has been used while the mutation function was kept as constraint independent. The objective function used is given below:

TH-1791_136107007

$$Obj = \sum_{l=1}^{N_T} \sum_{i=1}^{N_{exp}} \left| func^{expt} - func^{pred} \right| \tag{3.19}$$

Here indices *l* and *i* refers to the number of temperature and the corresponding data point, respectively. The *func* (*n,k,T,β*) (eq. 3.20) is the cumulative hydrogen production and is dependent on the reaction kinetic parameters and temperature (*T*) of the reaction. N_{exp} is the total number of experimental data at a specified temperature. N_T represents the number of different temperatures at which experimental data are available. Eq. (3.19) exhibits a dependency of the cumulative hydrogen production on the single step reactions. In our case a two single step reactions (i = 1, 2) are sufficient to characterize the whole mechanism. The details of N_1, N_2, N_3 and $\frac{d\alpha_i}{dt}$ have been mentioned in eqs. (3.15) - (3.18).

$$func = \beta_1 \left[(N_1 + N_2) \times \frac{d\alpha_1}{dt} \right] + \beta_2 \left[(N_2 + N_3) \times \frac{d\alpha_2}{dt} \right] \tag{3.20}$$

$func$ = cumulative H_2 generation data at a fixed temperature.

Here $\frac{d\alpha_1}{dt}$ and $\frac{d\alpha_2}{dt}$ is given as per eqs. (3.15 a, b) respectively. A similar process has been adopted for the solid state AB decomposition as discussed in Section 3.2. Here, experimental result comprises the cumulative H_2 generation data at a fixed temperature. To find the proper decomposition rate, we have use Adams Bashforth method to solve ODE. The estimated parameters for AB+ [BMIM][Cl] mixture by using *gamultiobj* solver are given in Table 3.2. In a similar manner the parameters were also generated for different AB-IL mixtures by using single objective GA solver at 85°C. It has been reported in previous work [6] that there is not much variation of hydrogen production is in the first few hours. Thus from the reaction kinetics, the equivalents of H_2 is taken as a known parameter i.e. β_1, which is simply the result of the first step reaction (eq. 3.13) in which the total H_2 release amount is known beforehand. The parameters have been summarized in Table 3.3. We notice a very small variation in activation energy as well as pre

TH-1791_136107007

exponential factor for the different IL combinations. So it can be concluded from Figure 3.3(a-e) that a proportionate increase in hydrogen equivalent is observed till (β_1+ β_2) equivalents of hydrogen is released.

Table 3.2 Optimized parameters for logistic growth model and Avrami-Erofeyev model for [BMIM][Cl] mediated AB.

Rate constants (eq. 3.15a and 3.15b) for decomposition of 50-wt% AB in [BMIM][Cl] at 95, 105 and 110 °C					
	α	β	N	k_0 (sec^{-1})	E (kJ mol^{-1})
$R_1 \rightarrow R_2+\beta_1 H_2$	$N_2/(N_1+N_2)$	0.99871	1.4864	7.5592	1.4575e+05
$R_2 \rightarrow R_3+\beta_2 H_2$	$N_3/(N_2+N_3)$	1.35129	2.5135	1.0861	1.4604e+05

TH-1791_136107007

Table 3.3 Rate constants for decomposition of 50-wt% AB in ILs at 85 °C using Avrami Erofeyev model (equation 3.15a and 3.15b)

IL	β_1	β_2	n_1	n_2	k_{01} (sec^{-1}) $\times 10^{-17}$	k_{02} (sec^{-1}) $\times 10^{-17}$	E_{01} (kJ mol^{-1})	E_{02} (kJ mol^{-1})	Total H_2 equiv. released*
[BMIM][PF_6]	1.05	0.38	1.5	2	4.85	1.95	145.51	150.9	1.43 (1.46)
[EMIM][OTf]	1	0.64	1.5	2	6.25	2.25	145.51	151.39	1.64 (1.71)
[BMIM][OTf]	1.1	0.79	1.5	2	7.85	2.45	146.01	150.94	1.89 (1.91)
[MMIM][$MeSO_4$]	1.1	0.9	1.5	2	8.25	2.65	146.91	151.4	2.00 (2.04)
[BMIM][Cl]	1.1	1.05	1.5	2	6.75	2.85	146.91	151.7	2.15 (2.20)
[BMIM][Cl] ** (T=85°C)	0.90	0.12	1.02	2.09	6.43	0.04	127.61	165.4	0.90 (1.02)
[BMIM][Cl] ** (T =105°C)	1.29	0.31	1.51	2.15	1.27	0.17	139.29	143.53	1.6 (1.59)
[BMIM][Cl] ** (T =120°C)	1.91	0.26	1.99	2.20	2.31	0.04	144.55	144.26	2.17 (2.16)
[BMIM][Cl] *** (T =25°C)	0.14	-	0.69	-	0.15	-	1046.7	-	0.14 (0.15)
[BMMIM][Cl]	1.15	1.25	1.5	2	9.25	3.05	147.51	151.8	2.30 (2.34)

* in Brackets, experimentally hydrogen release data taken from [1]
** (80:20) AB/[BMIM][Cl] mixture, data obtained from [7]
*** (50:50) AB/[BMIM][Cl] mixture at room temperature (RT or (T =25°C)), data obtained from [8]

TH-1791_136107007

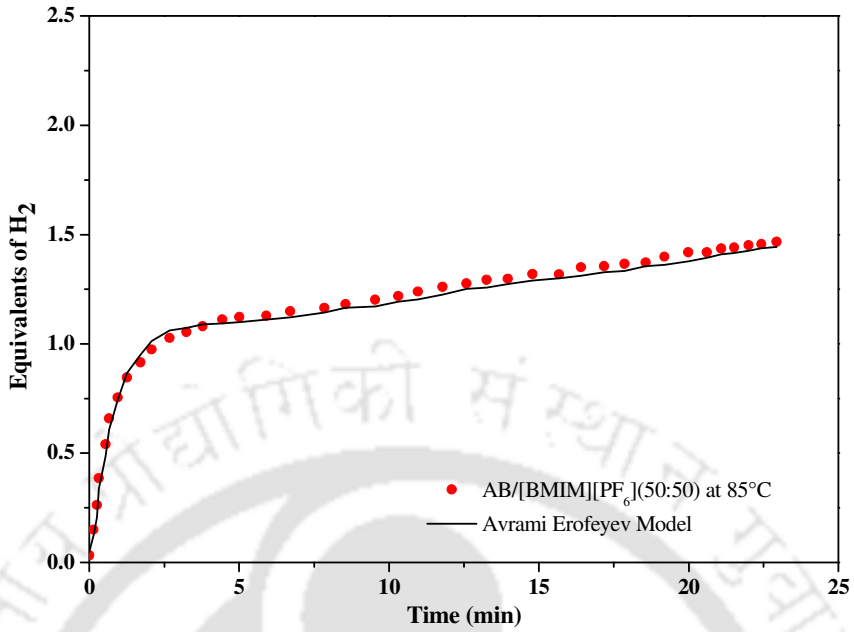

Figure 3.3(a) Experimental and predicted kinetic data for the release of equivalents of hydrogen from AB and [BMIM][PF_6] mixture.

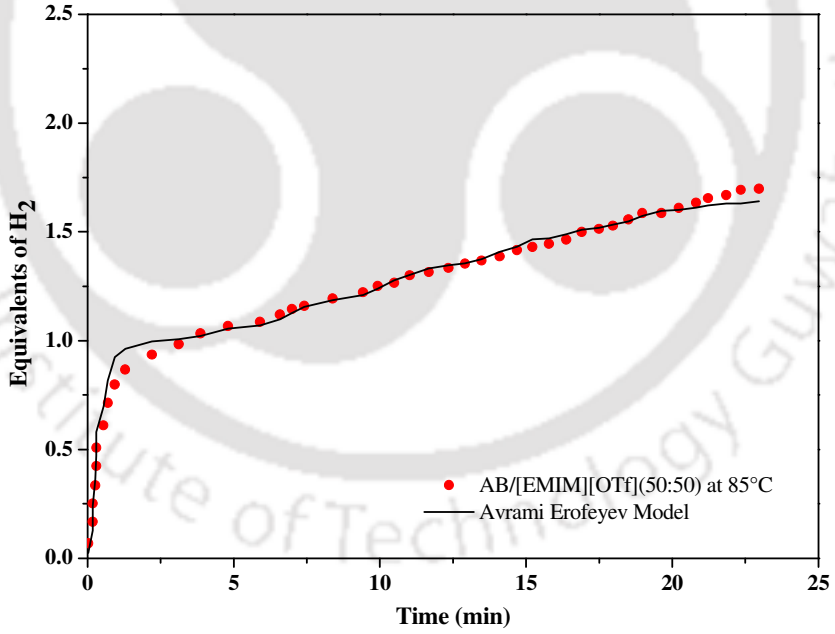

Figure 3.3(b) Experimental and predicted kinetic data for the release of equivalents of hydrogen from AB and [EMIM][OTf] mixture.

TH-1791_136107007

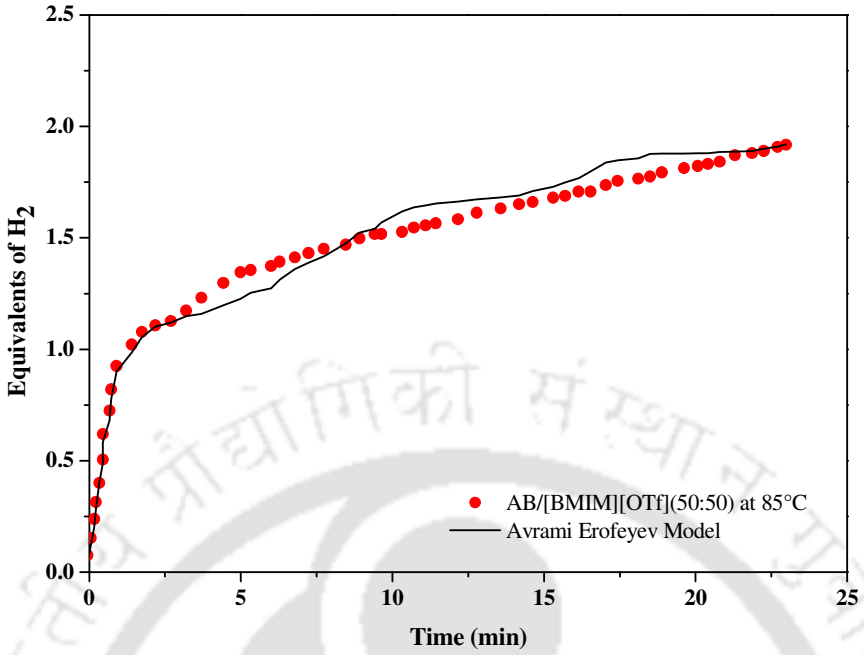

Figure 3.3(c) Experimental and predicted kinetic data for the release of equivalents of hydrogen from AB and [BMIM][OTf] mixture.

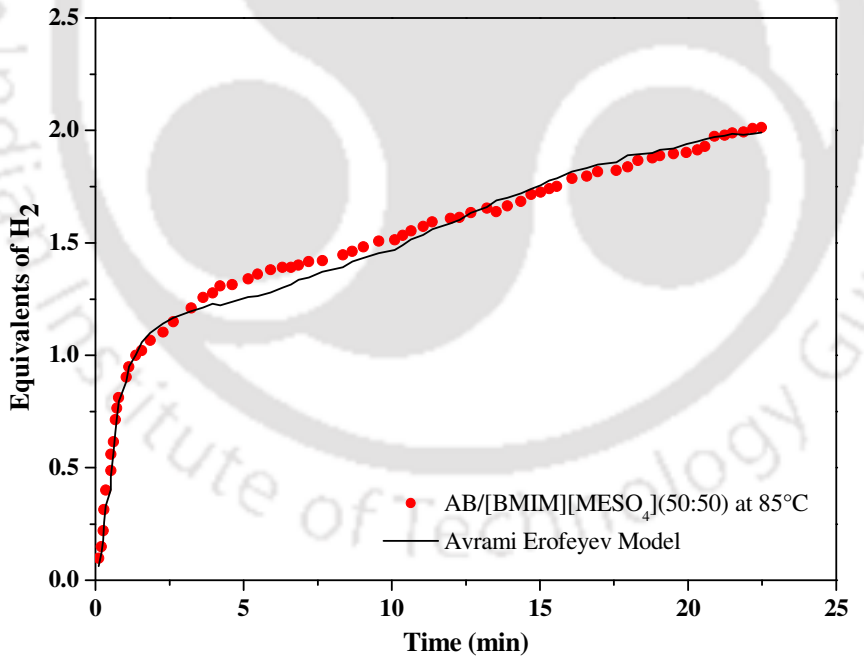

Figure 3.3(d) Experimental and predicted kinetic data for the release of equivalents of hydrogen from AB and [MMIM][$MeSO_4$] mixture.

TH-1791_136107007

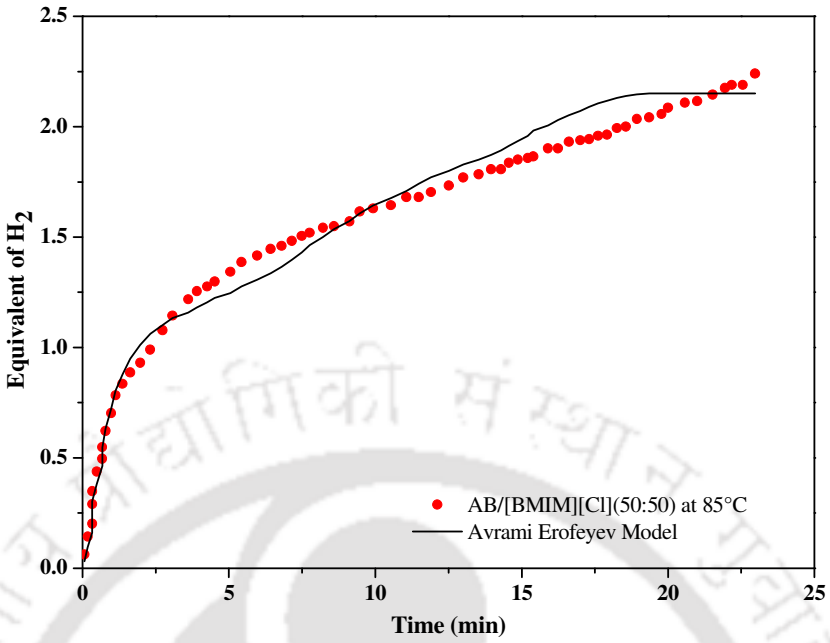

Figure 3.3(e) Experimental and predicted kinetic data for the release of equivalents of hydrogen from AB and [BMIM][Cl] mixture.

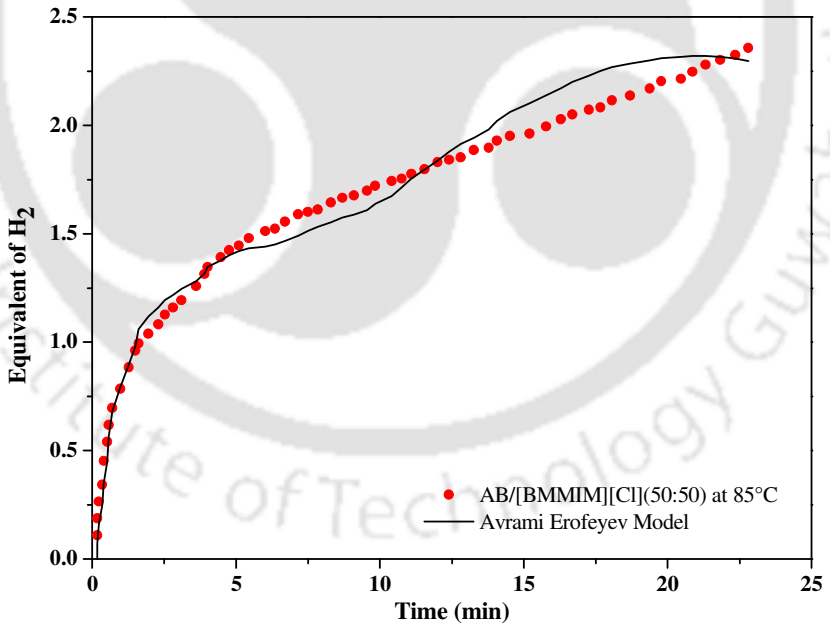

Figure 3.3(f) Experimental and predicted kinetic data for the release of equivalents of hydrogen from AB and [BMMIM][Cl] mixture.

TH-1791_136107007

The predictions till now are on mixtures with 50:50 weight percent of AB and IL. In order to further validate the model we attempted to predict the equivalent of hydrogen at different weight ratios. Basu et al. [7], reported the dehydrogenation of AB using AB/IL mixture at 80:20 ratio for a temperature range of 85°C-120 °C. Figure 3.4(a-c) depicts the prediction of hydrogen equivalents for 80:20 weight ratio of AB-IL at T = 85,105 and 120 °C respectively. It is observed that both the weight ratios gave a similar trend. The activation energies are found to be lower for [BMIM][Cl] (80:20 ratio) as compared to 50:50 ratio. However, the induction time was found to be longer for 80:20 ratio and it decreased with temperature (Table 3.3). This is also confirmed with a higher equivalent of hydrogen for the first step (1.91 at 120 °C). However, the second step release is the lowest among all other IL's, including [BMIM][Cl] at 50:50 ratio. This is primarily due to the lesser amount of [BMIM][Cl], as the stability of the intermediate product namely DADB is directly related to the IL quantity [1,3,6,9]. This indicates that the release is governed by the first step (eq.3.14) as a smaller amount of IL is unable to stabilize the DADB moiety. Due to this reason, we get low values of both rate constant (k_{02}) and equivalent (β_2) for 80:20 ratio. This proves that the amount of IL plays a crucial role, as it helps in lowering the induction period and increases the hydrogen equivalents.

The double step model was also attempted to predict the equivalents of hydrogen for [BMIM][Cl] at room temperature for which experimental data were taken from Nakagawa et al.[8]. As evident from Table 3.3 and Figure 3.4d, the predictions with respect to the induction period are lower for reported data as compared to the predicted one. However, our predictions correctly accounts for the total equivalents (0.14) as compared to 0.15 experimentally. The parameters for the second step (eq. 3.15) are close to zero and thus were not reported in Table 3.3. The activation energy obtained (1046.7 kJ/ mol) is

TH-1791_136107007

around eight orders more than that observed for 120 °C. This is expected because of a very low temperature leading to a redundant second step.

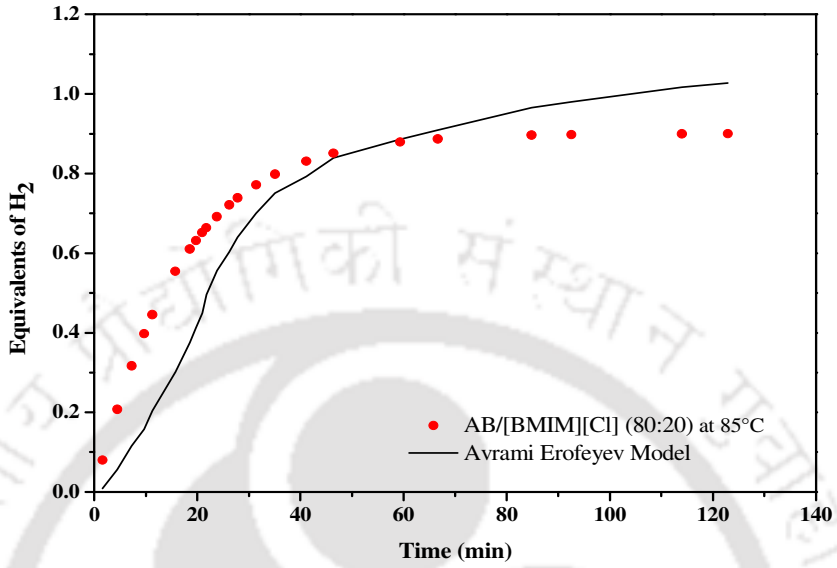

Figure 3.4(a) Experimental and predicted kinetic data for the release of equivalents of hydrogen from AB and [BMIM][Cl] (80:20) mixture at 85°C.

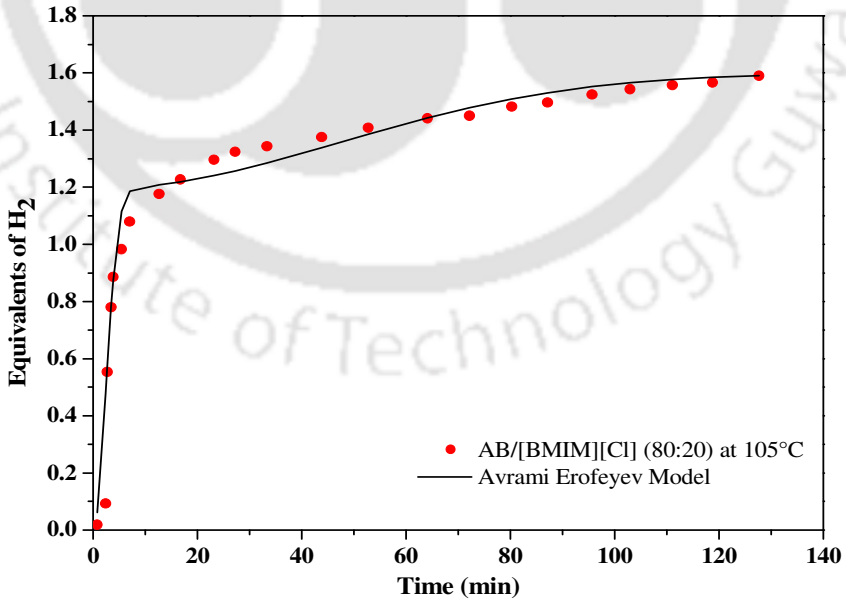

Figure 3.4(b) Experimental and predicted kinetic data for the release of equivalents of hydrogen from AB and [BMIM][Cl] (80:20) mixture at 105°C.

TH-1791_136107007

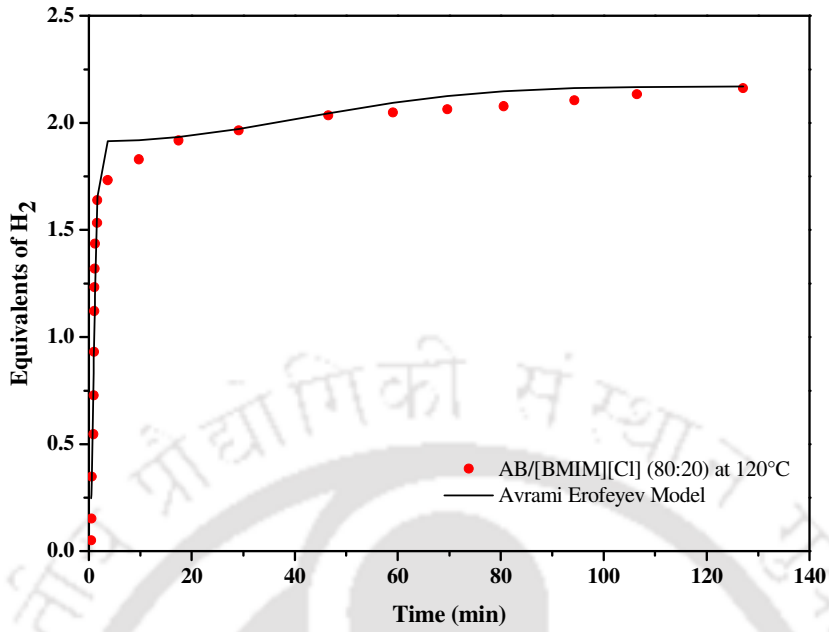

Figure 3.4(c) Experimental and predicted kinetic data for the release of equivalents of hydrogen from AB and [BMIM][Cl] (80:20) mixture at 120°C.

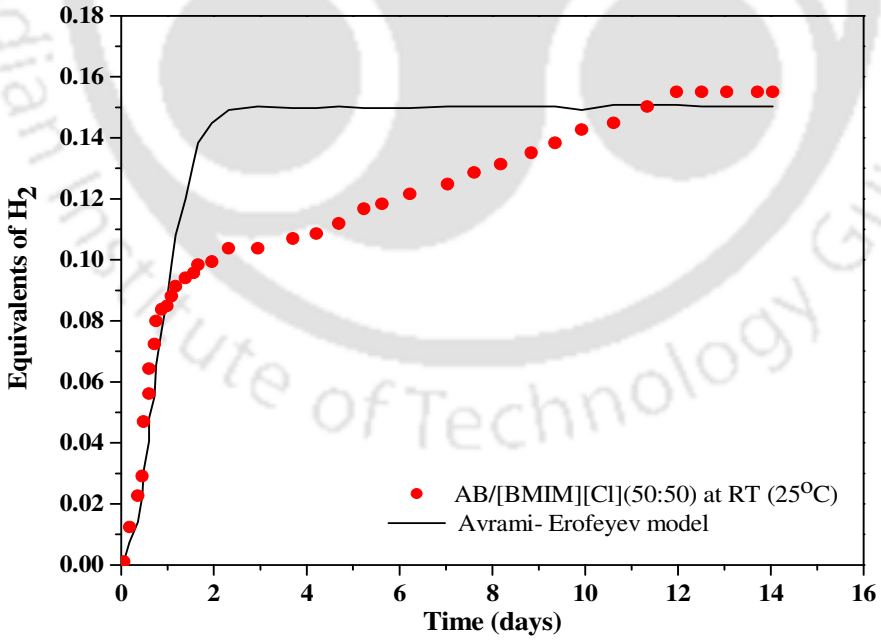

Figure 3.4(d) Experimental and predicted kinetic data for the release of equivalents of hydrogen from AB and [BMIM][Cl] (50:50) mixture at RT.

TH-1791_136107007

Further the parameters value of reaction kinetics for all AB + IL mixtures (Table 3.4), confirms negligible variation in the activation energy and rate constant irrespective of the nature of IL. One of the main reasons is the initial 3-4 hours, where hydrogen production was almost same for every AB + ILs mixture. However, the hydrogen production varied, when the reaction was kept for a longer run at 85 °C. The predictions with Avrami Erofeyev model gave an excellent fit with an Absolute Average Deviation (AAD) of ~2% when compared to experimental results [10].

Table 3.4 Comparison of regressed and predicted activation energies of AB in IL

Name of IL	E_{01} **(kJ mol^{-1})**	**Total H_2 equiv. released***	**IDAC by COSMO-RS**
[BMIM][PF_6]	145.51	1.43(1.46)	1.677
[EMIM][OTf]	145.51	1.64(1.71)	0.851
[BMIM][OTf]	146.01	1.89(1.91)	0.658
[MMIM][$MeSO_4$]	146.91	2.00(2.04)	0.105
[BMIM][Cl]	146.91	2.15(2.20)	0.079
[BMMIM][Cl]	147.51	2.30(2.34)	0.067

* in Brackets, experimentally hydrogen release data is given

3.4 Predictions of Activation Energies and Infinite Dilution Activity Coefficient

Till now we have discussed the activation energies which cannot be measured experimentally. However, an attempt is made where the activation energies can be correlated to experimental measurements. The most challenging and difficult part are in removing the last traces of AB species from Ionic Liquid. The Infinite Dilution Activity

TH-1791_136107007

Coefficient (IDAC) is an important indicator which quantifies this very phenomenon. Further, the activity coefficient at infinite dilution can be measured via gas-liquid chromatography and gives us an important descriptor for the effectiveness of a solvent to remove or reversibly attract the last trace of impurity (Ammonia Borane). Lesser the IDAC values from unity, greater is the tendency for the IL to remove AB species. Due to lack of experimental data of IDAC of AB in IL, we could not perform a benchmarking of IDAC values with COSMO-SAC. However, previous successful benchmarking of IDAC values by our group on other solutes such as thiophene and pyridine are already available [11-13] which led us to the adoption of the COSMO-SAC model.

The result obtained for the IDAC values as predicted by COSMO-SAC and the activation energies (E_{01}) are given in Table 3.4. On comparing both the IDAC values as predicted by COSMO-SAC; and the activation energies values as predicted Multiobjective GA, it can be seen that the activation energies vary inversely with IDAC values. In the case of [BMIM] based cation i.e. [BMIM][PF_6], [BMIM][OTf] and [BMIM][Cl] the E_{01} values are 145.51, 146.01 and 146.91 respectively. The corresponding IDAC values were 1.6779, 0.658 and 0.079 respectively. It indicates that higher activation energies implies a higher solubility of AB in the respective IL. In other words the complex has to go through a higher interaction energy barrier in order to reach the transition state. A similar trend was also obtained by our earlier work [12] on sulfur and nitrogen compound in IL. Thus from the result, it can be concluded that [BMIM][Cl] is the most soluble in IL and will thus evolve the highest moles of hydrogen. This trend is also visible in case of [EMIM][OTf] and [BMIM][OTf]. Here the anion [OTf] plays a crucial role and hence we see that there is a gradual decrease in the E_{01} by regression with an increase in IDAC values. In order to explain the higher hydrogen release of [BMIM][Cl] we have performed a quantum chemical calculation on [BMIM][Cl]-AB mixture.

TH-1791_136107007

Optimized geometry was performed using 6-311+G(d) basis set at BVP86 level of density functional theory in *Gaussian 09*. The diffuse function was added to the basis set to accommodate polarization functions. The same optimized structures were used for COSMO file generation using the BVP86 level of density functional theory. For the COSMO file generation, the SVP [14] basis set was then used in combination with density fitting basis set DGA1 [15]. The Gaussian generated COSMO files displays the induced screening charge and Cartesian coordinates for all the segments in the molecule when it is placed in the midst of medium having infinite dielectric constant. An important output from the COSMO file are the screening charge for the molecules which in turn gives the sigma profile. The sigma profile contains a histogram of all the surface charges within the molecule. This is then summarized in the form of segment activity coefficient using the RS or Real Solvents framework [16]. Thereafter the summation of all the segment activity coefficient gives us the component activity coefficient in either phase. The activity coefficient when computed at infinite dilution gives us the Infinite Dilution Activity Coefficient or simply IDAC. This is a measurable property and gives us the extent of the solubility of s solute (for e.g. AB or EDAB) in IL (solvent) (Table 3.4). Lower values of IDAC represent higher solubility and vice versa. The details of the calculation and methodology are not discussed here as it is given in our earlier work [11-13].

The reaction pathways for IL-mediated Ammonia Borane are given in Figure 3.5. It should be noted that the transition step is the rate determining step for thermal dehydrogenation of Ammonia Borane. The optimized structures of AB/DADB; and AB/DADB + IL are given in Figures. 3.6 and 3.7 respectively.

TH-1791_136107007

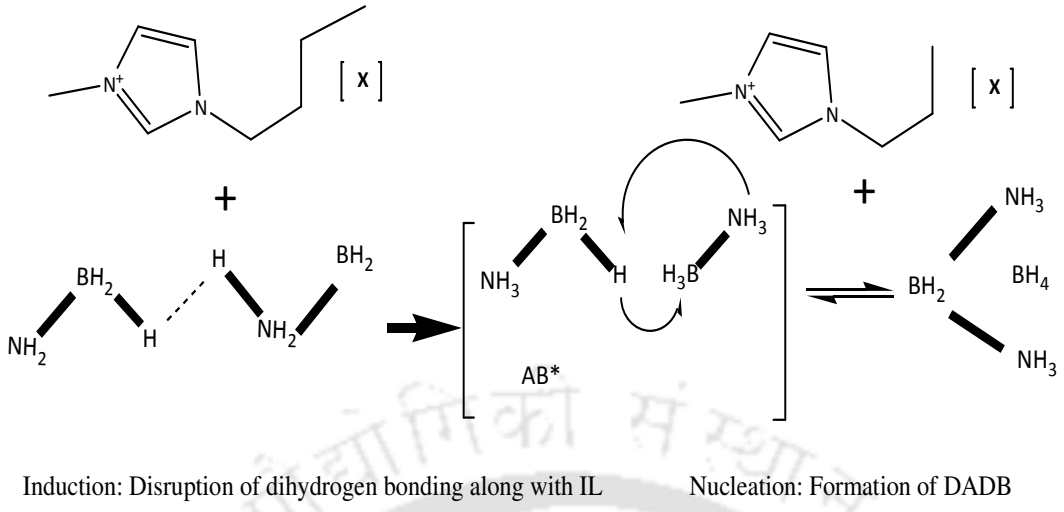

Figure 3.5 Reaction pathway of IL ([BMIM][X]) mediated Ammonia Borane dehydrogenation at T = 85 °C. [1]

We have prepared two structures namely DADB (Figure 3.6) and DADB+ [BMIM][Cl] (Figure 3.7). It can be seen that the hydrogen bond lengths within DADB (2.245 A°) (Figure 3.6) is greater than DADB-IL (2.179 A°) (Figure 3.7), thereby resulting in greater stability of the transition product i.e. DADB. It is also verified that the anion [Cl] controls the solubility of AB in IL. This is evident in the formation of hydrogen bond of length 2.068 A° between H (DADB) with Cl(IL). This is also lower than the intramolecular hydrogen bonding within DADB i.e. 2.245 A° (Figure 3.7).

TH-1791_136107007

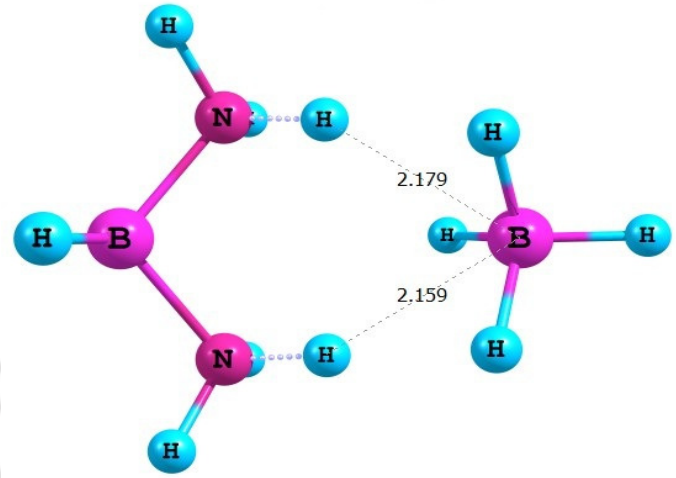

Figure 3.6 Optimized structures of DADB (units in Å)

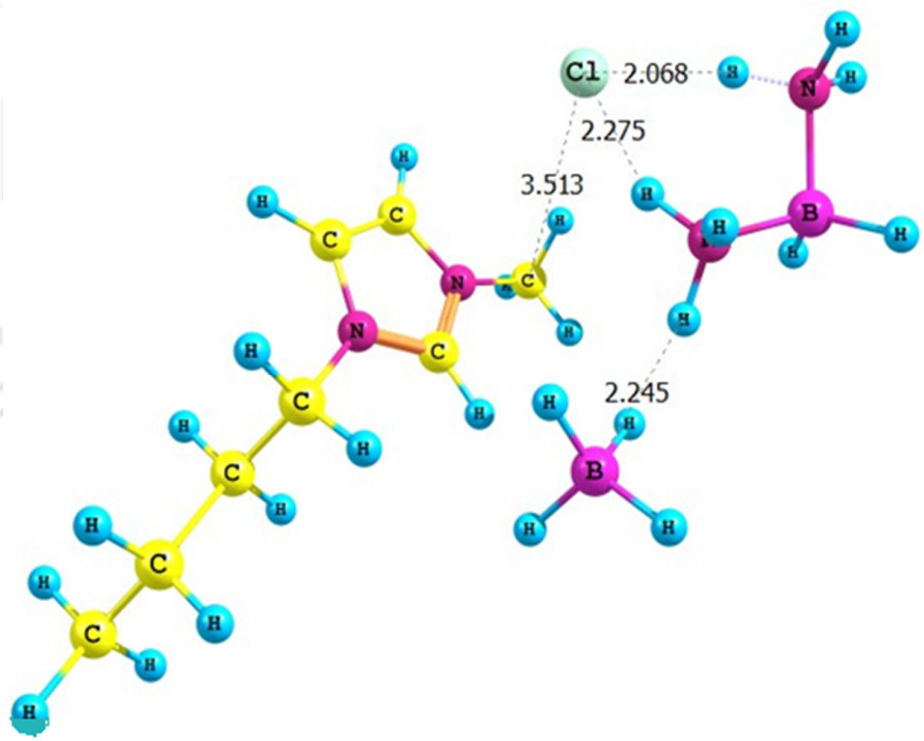

Figure 3.7 Optimized structure of [BMIM][Cl]- DADB complex (units in Å)

TH-1791_136107007

3.5 EDAB as Chemical Hydride

Till now we have successfully discussed the AB thermal dehydrogenation with and without Ionic Liquids. This has been adequately benchmarked through both kinetic studies and quantum chemical interaction. However, as mentioned in chapter 1, the focus of the thesis is on Ethylene Di Amine *bis*Borane (EDAB). This is because of the potential limitation such as the decomposition of AB which produces Borazine (highly toxic) and ammonia [17-19]. Furthermore, the dehydrogenation of AB also has certain other limitations such as its incomplete decomposition at high temperature of 500 °C and virtually impossible in regenerating the end products such as Hydrazine Borane. Efforts to overcome this problem were made by making chemical modifications to AB molecules, such as using carbon derivatives of AB molecules. Methyl Amine Borane (MeAB), Sec-Butyl Amine Borane (SBAB) and Ethylene DiAmine bisBorane (EDAB) are amongst some of the prominent carbon substituted amine boranes which are being investigated currently. Where on the other hand, these derivatives generate lesser amount of hydrogen after heating; on the other hand there is no formation of volatile compounds such as borazine as side products in dehydrogenation reactions.

This disadvantages of AB have paved the way for Ethylene DiAmine bisBorane (EDAB), even though they possess lower hydrogen content as compared to AB. Further the formation of volatile compound such as borazine is not observed in the dehydrogenation studies. The most attractive feature of EDAB is the absence of induction period during dehydrogenation process. The rate of dehydrogenation of EDAB is also known to be faster than AB at higher temperatures. Keeping this in mind we shall move forward for the screening of these hydrides with Ionic Liquids through a combination of COSMO-SAC screening and HOMO-LUMO stability analysis.

TH-1791_136107007

3.6 Screening of potential Ionic Liquid Combination using COSMO-SAC Model

It is a well-known fact that ILs are used to generate hydrogen from EDAB at milder conditions i.e. lowering of the induction period when compared to pure EDAB. We presumed that ILs would not have gone through any structural changes. They act merely as a polar medium for the stabilization of the intermediate by lowering the activation energies of dehydrogenation. In such a context, as discussed previously the COSMO-SAC theory can be used to predict the infinite dilution activity coefficient (IDAC) and subsequent capacity ($C^{\infty} = \frac{1}{\gamma^{\infty}_{EDAB}}$). The primary criterion for selecting an IL for EDAB was higher solubility. Furthermore, selection was also considered keeping in mind the formation of acids from the ILs themselves. Hence we limited our studies to the 205 pairs of cation–anion combination, which are commercially available from Sigma-Aldrich. We divided these ILs into two sections based on the calculated IDAC (or capacity) namely: very high solubility (i.e. capacity $\geq \sim 10^5$) and medium solubility ($\sim 10^2 <$ capacity $< 10^5$). The frequency diagram for very high solubility ILs is plotted in Figure 3.8 and Table 3.5. Imidazolium, phosphonium, pyrrolidinium, pyridinium, sulfonium, ammonium and basionics types of cations are considered for the prediction of the solubility of EDAB in ILs. In Figure 3.8, ILs were grouped based on anions rather than cations. From Figure 3.9, based on the logarithmic values (γ) and anion performance, we obtained three acetate, five methyl carbonate, two hydrogen sulfate and six dibutyl phosphate based ILs in which EDAB is highly soluble. Among them, solubility of EDAB in acetate based ILs is the highest. Thus we converged to the IL having acetate anion for the dehydrogenation studies. We rejected choline acetate as it has high melting point (85°C) and is also closer to the reaction temperature.

TH-1791_136107007

Table 3.5 IDAC value and capacity of EDAB in selected IL

SL no	**Full name of the IL**	**Abbreviation**	**IDAC of EDAB**
1	1-ethyl-3-methylimidazolium Acetate	[EMIM] [AOc]	2.96×10^{-14}
2	1-butyl-3-methylimidazolium Acetate	[BMIM] [AOc]	3.16×10^{-13}
3	1-allyl,3-methylimidazolium bromide	[AMIM][Br]	2.64×10^{-10}
4	1-allyl, 3-methylimidazolium dicyanamide	[AMIM][(D(CN)$_2$]	2.07×10^{-4}
5	1-allyl,3-methylimidazolium bis (trifluoromethylsulfonyl) imide	[AMIM][Tf$_2$N]	3.36×10^{1}
6	Trihexyltetradecylphosphonium bis (2,4,4-trimethylpentyl) phosphinate	[TDTHP][Phosph]	1.77×10^{-11}
7	Trihexyltetradecylphosphonium dicyanamide	[TDTHP][DCA]	3.81×10^{-4}

TH-1791_136107007

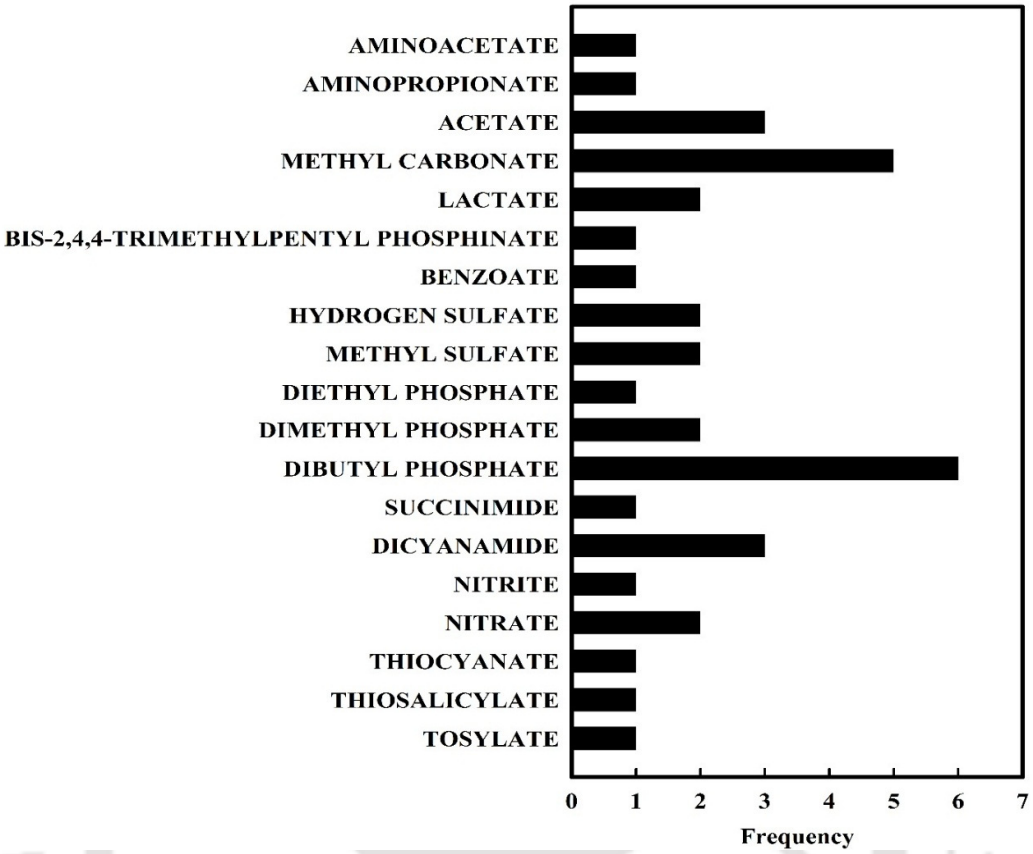

Figure 3.8 Frequency of ILs. Frequency represents the number of times an anion has shown a capacity of $\geq 10^5$.

TH-1791_136107007

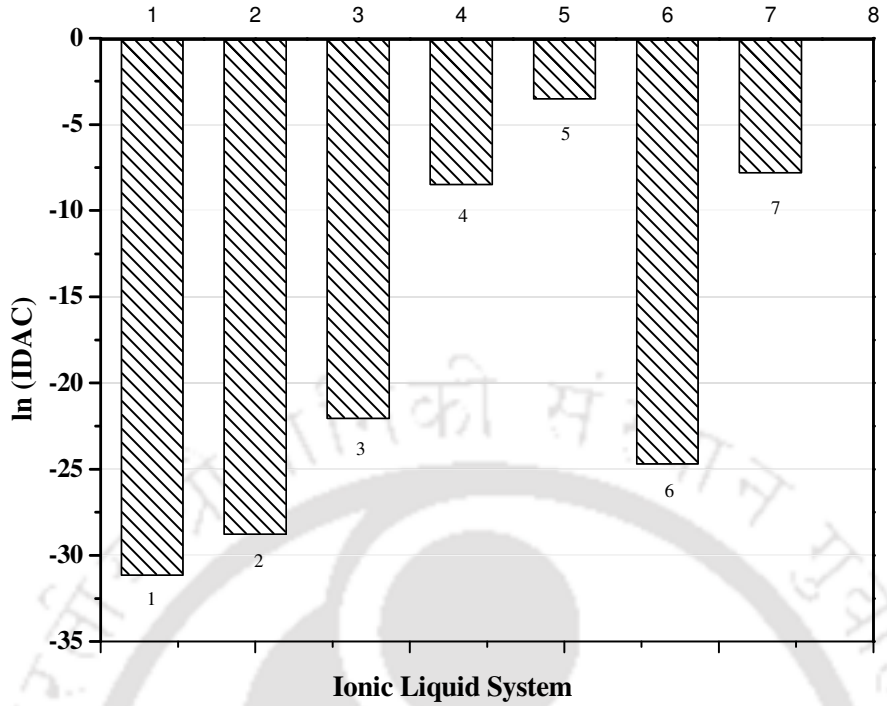

Figure 3.9 Logarithmic value of infinite dilution activity coefficient [*ln (IDAC)*] of 7 ILs. System 1: 1-ethyl-3-methylimidazolium Acetate, System 2: 1-butyl-3-methylimidazolium Acetate, System 3: 1-allyl,3-methylimidazolium bromide, System 4: 1-allyl, 3-methylimidazolium dicyanamide, System 5: 1-allyl,3-methylimidazolium bis (trifluoromethylsulfonyl) imide, System 6: Trihexyltetradecylphosphonium bis (2,4,4-trimethylpentyl) phosphinate: System 7: Trihexyltetradecylphosphonium dicyanamide

3.7 Stability Analysis using HOMO-LUMO Analysis

We shall now focus on the stability of IL-AB systems. To start with, based on the COSMO-SAC predictions the acetate based IL has been chosen. The two IL's namely [EMIM][OAc] and [BMIM][OAc] were studied for HOMO-LUMO energy gaps. The calculation were performed using 6-311+G(d) basis set at BVP86 level of density functional theory in *Gaussian09.* With the HOMO-LUMO gap, we determined the most suitable acetate IL for the dehydrogenation. LUMO is a probable location for bond formation as incoming electrons will fill in LUMO, while HOMO provides the capacity in terms of energy to make external interactions. The stability of complexes is determined by

TH-1791_136107007

higher negative values of LUMO/HOMO. The higher the negative values of LUMO or HOMO, the less stable the complex becomes and therefore the more reactive the complex. LUMO energies are more important for ILs involving complexes, as LUMO sites dominate the overlapping of incoming HOMO orbitals. Thus it becomes a prominent factor for external interaction connectivity. The HOMO-LUMO energy of pure EDAB, ILs and EDAB/IL complexes are reported in Table 3.6. Pure ILs have an almost equal LUMO energy (-0.94802 eV for [EMIM][OAc] and -0.93578 eV for [BMIM][OAc]). Thus it is not possible to determine the preference between two pure ILs. However, based on the LUMO energy of the complexes, the EDAB/[BMIM][OAc] complex has a LUMO energy of -1.44625 eV, which is lower than that of the EDAB/[EMIM][OAc] complex. This implies that EDAB/[BMIM][OAc] is less stable than EDAB/[EMIM][OAc] and thus more reactive.

Plots of the HOMO-LUMO gaps of EDAB/IL complexes are reported in Figure 3.10. For both complexes, LUMOs are located on the cationic imidazolium ring thus making it a favorable location to create transition or intermediate states with EDAB. In both cases, the HOMO lies on the anionic acetates. The lowering of the LUMO energies occurs due to formation of a donor–acceptor during dehydrogenation. Intermediate carbene formation might play a role during imidazolium IL supported dehydrogenation mechanism of EDAB [20]. In addition to possible carbene formation from imidazolium cations, which can exert a strong effect on the hydrogen yield, the basicity of anions also influences the yield. Thus we presume that the combined effect of intermediate carbine formation from the imidazolium cation coupled with the presence of a basic acetate anion lowers the LUMO energy significantly. Based on the LUMO energy, [BMIM][OAc] is more favorable than [EMIM][OAc] for hydrogen release from EDAB.

TH-1791_136107007

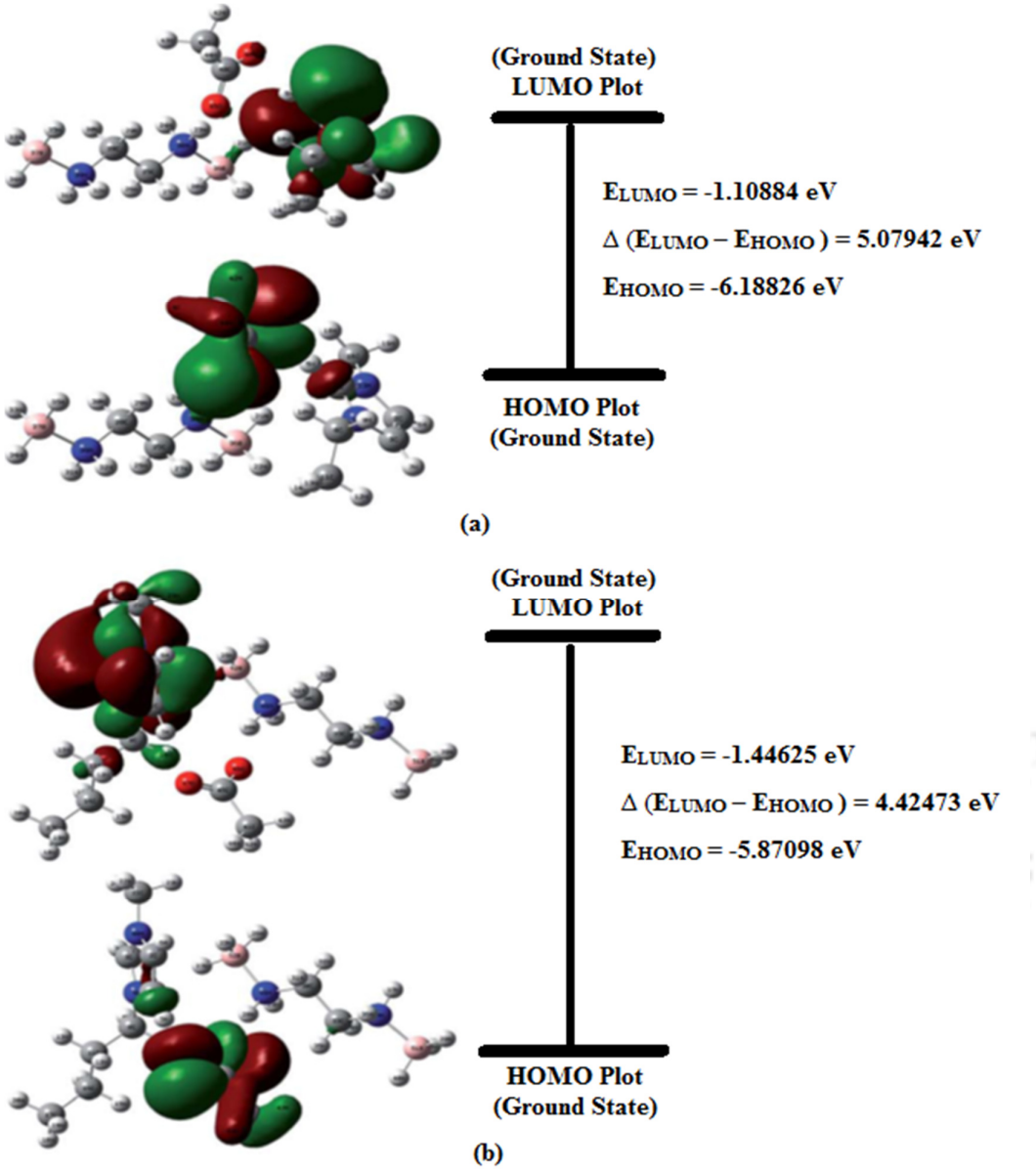

Figure 3.10 HOMO-LUMO energy gap of EDAB/IL complex.

(a) EDAB/[EMIM][OAc],

(b) EDAB/[BMIM][OAc].

TH-1791_136107007

Table 3.6 HOMO, LUMO energies and HOMO-LUMO energy gap

Name of complex	LUMO energy/eV	HOMO energy/eV	HOMO-LUMO energy gap/eV
EDAB	−1.08081	−7.95423	6.87342
[EMIM][OAc]	−0.94802	−5.32486	4.37684
[BMIM][OAc]	−0.93578	−5.32432	4.38854
EDAB/[EMIM][OAc]	−1.10884	−6.18826	5.07942
EDAB/[BMIM][OAc]	−1.44625	−5.87098	4.42473

3.8 Dehydrogenation experiments with Acetate based Ionic Liquids

3.8.1 Thermal Dehydrogenation of EDAB/[BMIM][OAc] and [EMIM][OAc]

Based on our screening results, the dehydrogenation experiment of EDAB with imidazolium cation and acetate anion was performed at 95 °C and 105 °C. The time resolved hydrogen production of the two different set of experiments are shown in Figure 3.11. The trend clearly reflects the absence of any induction period. Pure EDAB also does not show any induction period [21] and releases 2.14 equivalent of H_2 at 120 °C [22]. The rate of hydrogen desorption is nearly the same for both the systems until 50 min. After 50 min, the desorption rate of EDAB/[EMIM] [OAc] (black square) at 95 °C is lower and 2.59 equivalent of H_2 is released after 225 min of reaction. This yield is still significantly higher than 2.14 equivalent of hydrogen released by pure EDAB when heated at 120 °C. This proves the advantage of using ILs in dehydrogenation of EDAB. When the same mixture is heated at 105 °C, 3.52 equivalents of hydrogen (blue triangle) are released. The rate of desorption was found to increase during 50–80 min. The higher yield of hydrogen shows the temperature dependency in dehydrogenation. EDAB/[BMIM][OAc] releases a higher amount of equivalent hydrogen when the reaction was performed at 95 and 105 °C.

TH-1791_136107007

A total of 3.15 and 3.96 equivalents of H_2 is generated at 95 and 105 °C, respectively. The higher amount of equivalent H_2 release from EDAB/[BMIM][OAc] is also confirmed by the HOMO-LUMO calculation as the complex is found to be less stable than EDAB/[EMIM][OAc] complex. The dehydrogenation rates of EDAB/[BMIM][OAc] for both temperatures are almost similar until 80 min of operation. After 80 min, an increase of desorption rate at 105 °C suggests a delay in the effect of temperature for longer alkyl chains of imidazolium cation. Thus at 105 °C, we obtained an equivalent of hydrogen almost equal to that of theoretical prediction [23]. This fact emphasizes the catalytic role of ILs in dehydrogenation. Using vacuum, we achieved 3.96 equivalent of hydrogen release from EDAB/[BMIM][OAc] at 105 °C, which is more than the 3.81 equivalents of hydrogen at 120 °C as reported in the literature [22]. This establishes that the milder conditions of dehydrogenation can be achieved by acetate ILs. The cumulative hydrogen production at the end of the reaction is shown in Figure 3.12 and Table 3.7.

Table 3.7 Cumulative equivalent of hydrogen released by EDAB/IL complexes at two different temperatures of 95 °C and 105 °C (Acetate).

	95 °C	**105 °C**
[BMIM][OAc]	3.15	3.95
[EMIM][OAc]	2.59	3.52

TH-1791_136107007

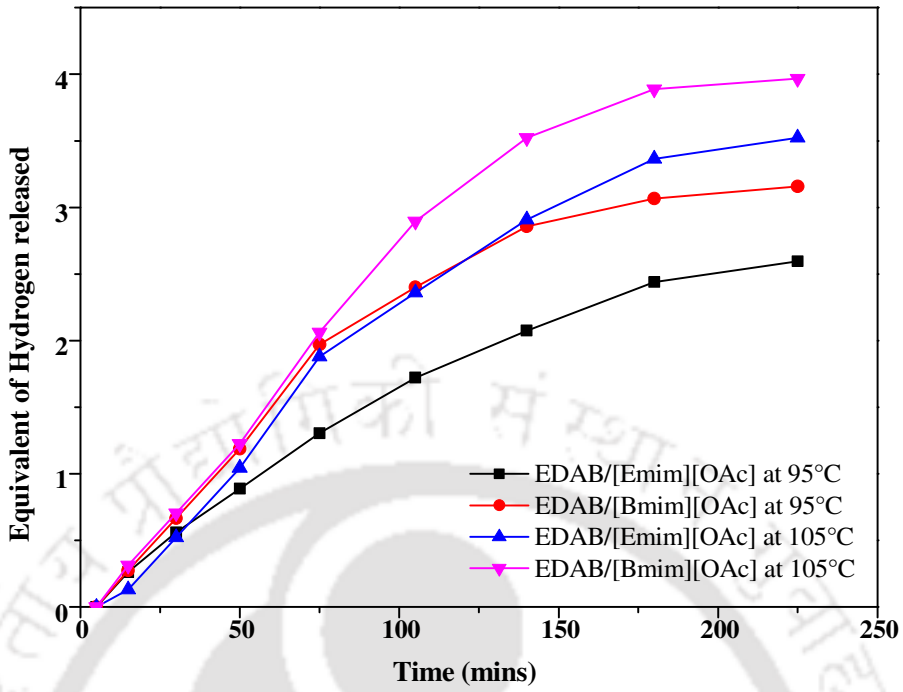

Figure 3.11 Time resolved equivalent hydrogen release from EDAB/[EMIM] [OAc] and EDAB/[BMIM][OAc] complexes at 95 °C and 105 °C. (■) EDAB/[EMIM][OAc] at 95 °C,(●) EDAB/[BMIM][OAc] at 95 °C, (▲) EDAB/[EMIM][OAc] at 105 °C, (▼) EDAB/[BMIM][OAc] at 105 °C.

TH-1791_136107007

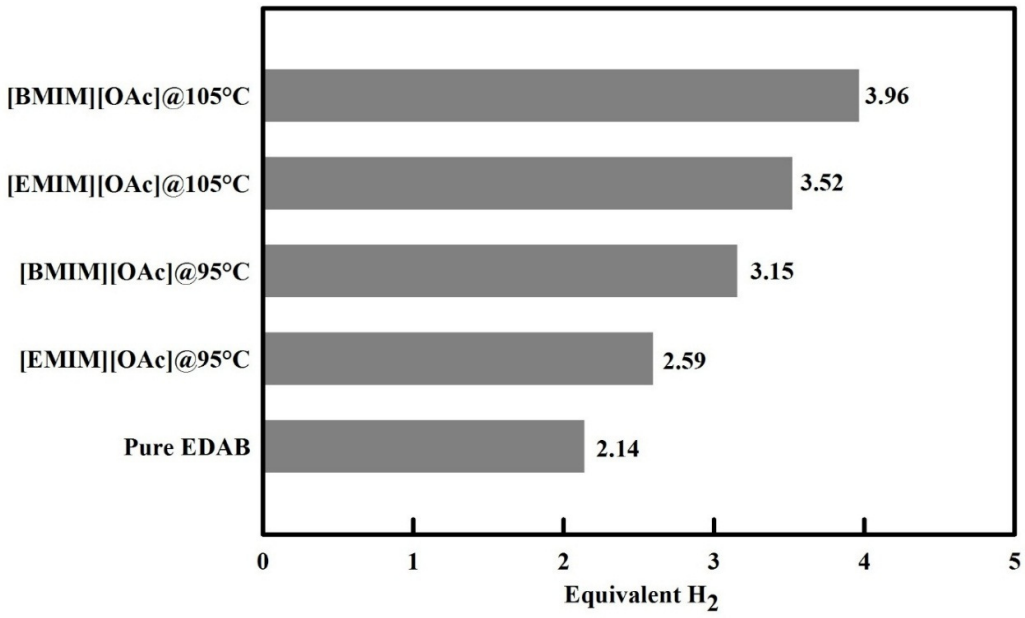

Figure 3.12 Cumulative hydrogen generation from EDAB facilitated by ILs at 95 °C and 105 °C. Hydrogen generation of pure EDAB at 120 °C is taken from the literature [22].

3.8.2 TGA profile of EDAB with acetate based Ionic Liquids

Figure 3.13 represents the TGA profiles of EDAB/[EMIM][OAc] and EDAB/[BMIM][OAc]. Two hydrogen desorption phenomena, as reported in the literature [23] are clearly visible in Figure 3.13 for both the systems. For the EDAB/[BMIM][OAc] system, the first weight loss of 16.42% occurs at 140 °C and the second major weight loss of 72.77% takes place at 250 °C. After the second major loss, there is a gradual loss of 6.31% when the sample is heated from 250 °C to 700 °C, thereby leaving a residual mass of 4.48%. For EDAB/[EMIM][OAc], the first desorption takes place at 164 °C with 6.37% mass loss and the second one at 254 °C with a corresponding weight loss of 89.09%. The concluding mass loss of 4.16% is observed from 254 °C to 700 °C. The residual mass was calculated to be 0.36%. In TGA analysis, the EDAB/[EMIM][OAc] complex requires a ~20 min longer time for its first mass loss as compared to the EDAB/[BMIM][OAc] complex. This suggests that EDAB forms a more stable complex in [EMIM][OAc] than

TH-1791_136107007

[BMIM][OAc]. This also confirms the relative stability analysis as predicted from HOMO–LUMO studies.

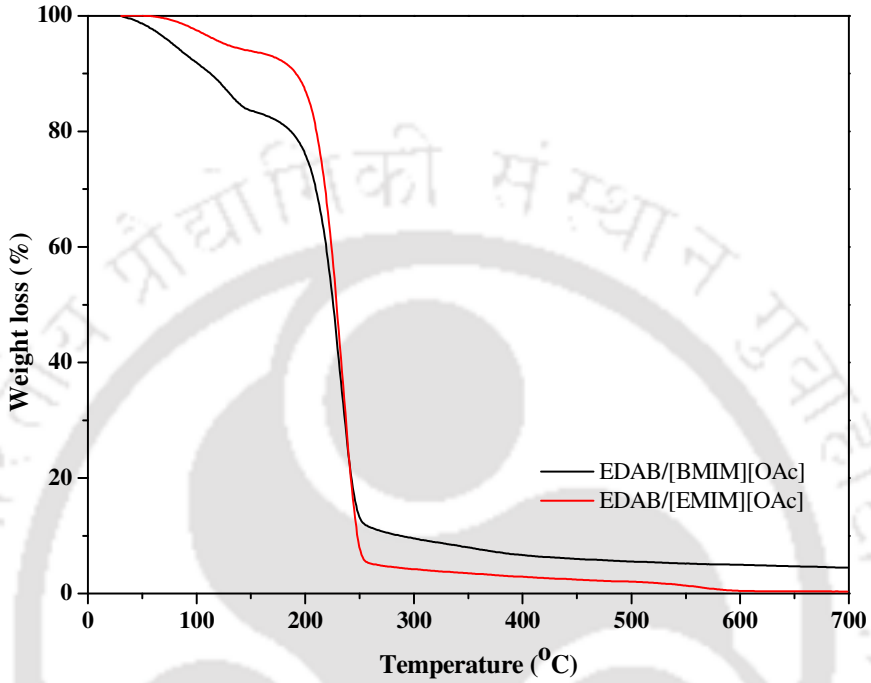

Figure 3.13 TGA profile of EDAB/[BMIM][OAc] and EDAB/[EMIM][OAc]

3.8.3 ^{1}H NMR analysis of EDAB along with acetate based Ionic Liquids

We conducted a ^{1}H NMR study to characterize pure EDAB and ILs as well as EDAB/IL complexes before and after reactions. A comparative discussion of ^{1}H NMR plots of pure EDAB, ILs and EDAB/IL complexes will determine the possible formation of any product after dehydrogenation and, furthermore, the role of IL in dehydrogenation. We adopted an approach which relates the number of hydrogens with their areas to the functional groups or attachments of EDAB and IL. We have successfully applied this approach for the determination of experimental timelines in liquid–liquid equilibria studies [24]. Here, the area of a certain peak was counted as unity and taken as the reference. The

TH-1791_136107007

area of other peaks was integrated with reference to unity. This method is particularly useful to locate peaks of compounds in mixtures and end products after reaction. ^{1}H NMR plot of EDAB is shown in Figure 3.14(a). The chemical shift for $–BH_3$ appears between 1.13–1.67 ppm, which agrees with previous work [23]. The chemical shift at 5.24 ppm is assigned to $–NH_2$ due to the presence of an electronegative atom in the vicinity of nitrogen. EDAB, having four hydrogen atoms connected to a nitrogen atom, contributes to an area of unity implying a value of 0.25 for each hydrogen. The chemical shift at 2.6 ppm assigned to $–CH_2$ (four hydrogen atoms) also has an area of unity, implying a contribution of 0.25 to each hydrogen atom. $–BH_3$ having six hydrogen atoms is located at 1.5 ppm with a peak area of 1.5. This also confirms to a contribution of 0.25 i.e., 1.5/6. Furthermore, the chemical shifts also verify the range as reported in the literature [23].

Chemical shifts of pure [EMIM][OAc] are given in Figure 3.14(b). The attached hydrogen is the acidic hydrogen atom of imidazolium core (shown as 'f') and corresponds to 9.89 ppm [24]. The other hydrogen atoms of the imidazolium ring displays chemical shift of 7.88 and 7.78 ppm. Chemical shift at 1.39–1.61 ppm are identified as methyl groups of ethyl chain of cation and acetate anion (identified as 'd' in Figure 3.14(b)). Chemical shift for hydrogen attached with $–N–CH_3$ and $–N–CH_2$ are shown to appear between 3.86–4.21 ppm. The accurate identification of peaks in the pure compound will help us to locate the peaks for functional groups in the mixture. In the mixture, a shift in the peaks may be observed but the overall trend remains the same. Figure 3.14(c) represents the ^{1}H NMR of EDAB/[EMIM][OAc] mixture before reaction. The chemical shifts of hydrogen in the imidazolium ring are identified at 9.70, 7.83 and 7.74 ppm, respectively. Hydrogens of $–N–CH_2$ and $–N–CH_3$ groups are located between 3.86 – 4.19 ppm. The hydrogen atoms in the alkyl group of cation are visible between 1.39 – 1.62 ppm. The chemical shift at 5.67 ppm is attributed to $–NH_2$ (four hydrogen atoms) with an area

TH-1791_136107007

of 1.60. Similarly the chemical shift at 2.62 ppm is due to $–CH_2$ (four hydrogen atoms) also contributing an area of ~1.60. A flat peak near 1.2 ppm can be assigned to the $–BH_3$ peak because a similar flattened peak was observed for pure EDAB (see Figure 3.14(a)). The ^1H NMR plot of EDAB/[EMIM][OAc] mixture after reaction is also reported in Figure 3.14(d). We observe that hydrogens of the imidazolium ring are present between 7.85–10.16 ppm, which is the same trend as of Figure 3.14(c). Further we observe chemical shifts for hydrogens of $–N–CH_2$ and $–N–CH_3$ in between 3.67 – 4.22 ppm. Similarly, hydrogens of the $–CH_3$ group of IL are identified between 1.39 – 1.60 ppm.

It is observed that all the peaks of [EMIM][OAc] are in the same area ratio as with its initial structure. An important observation is the absence of a peak corresponding to $–NH_2$, thus suggesting that it has reacted and all hydrogens have evolved. There is a small peak (with area of 0.02) observed at 2.62 ppm attributed to the $–CH_2$ group of EDAB. Considering that the $–CH_2$ group (four hydrogen atoms) remains unreacted in the dehydrogenation process, each hydrogen has an area of 0.005. From this, we can conclude that hydrogens are liberated from the $–NH_2$ group. A similar trend is also observed in the ^1H NMR of pure [BMIM][OAc], EDAB/[BMIM][OAc] before and after reaction as shown in Figure 3.14(e–g). With the results of ^1H NMR analysis of the two systems, it can be concluded that the release of hydrogen is mainly from the $–NH_2$ attachment of EDAB as both ILs retain their original structure. Thus ILs merely help in facilitating the dehydrogenation process at a significantly lower temperature than pure EDAB.

TH-1791_136107007

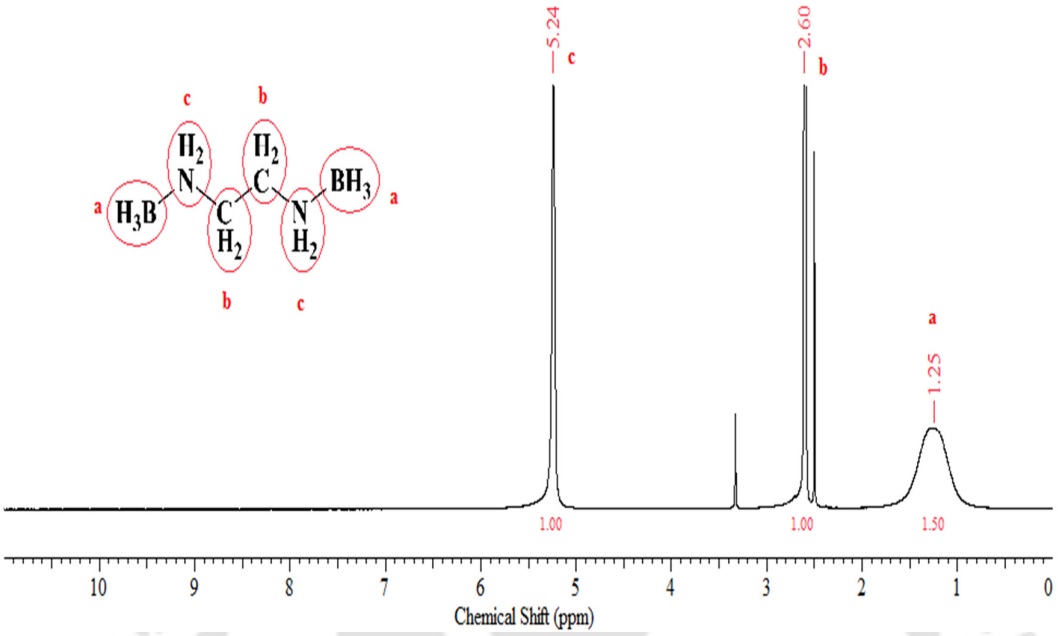

Figure 3.14 (a)

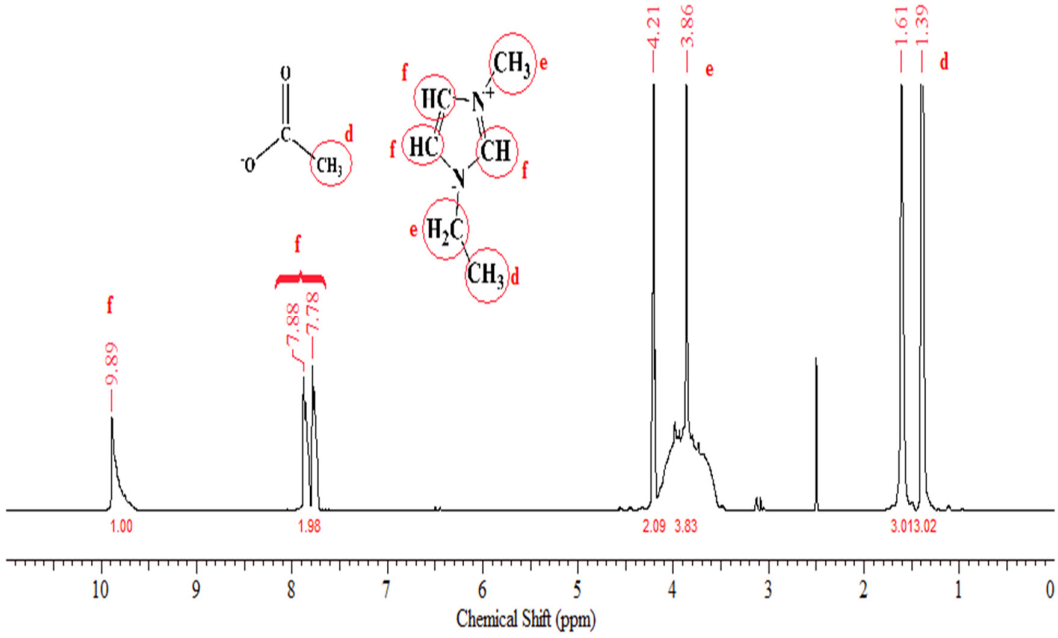

Figure 3.14 (b)

TH-1791_136107007

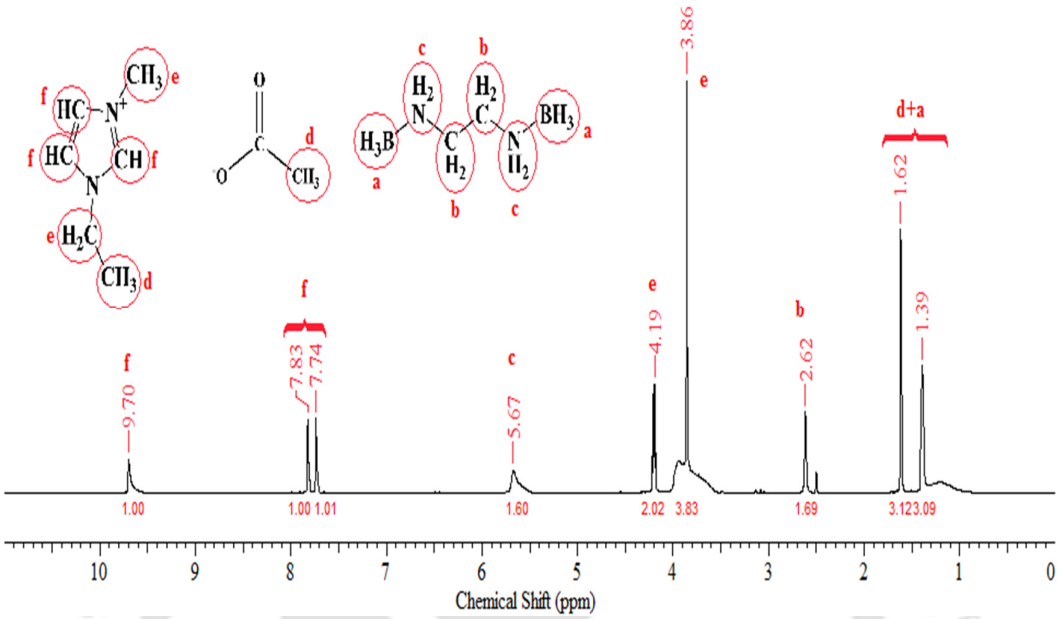

Figure 3.14 (c)

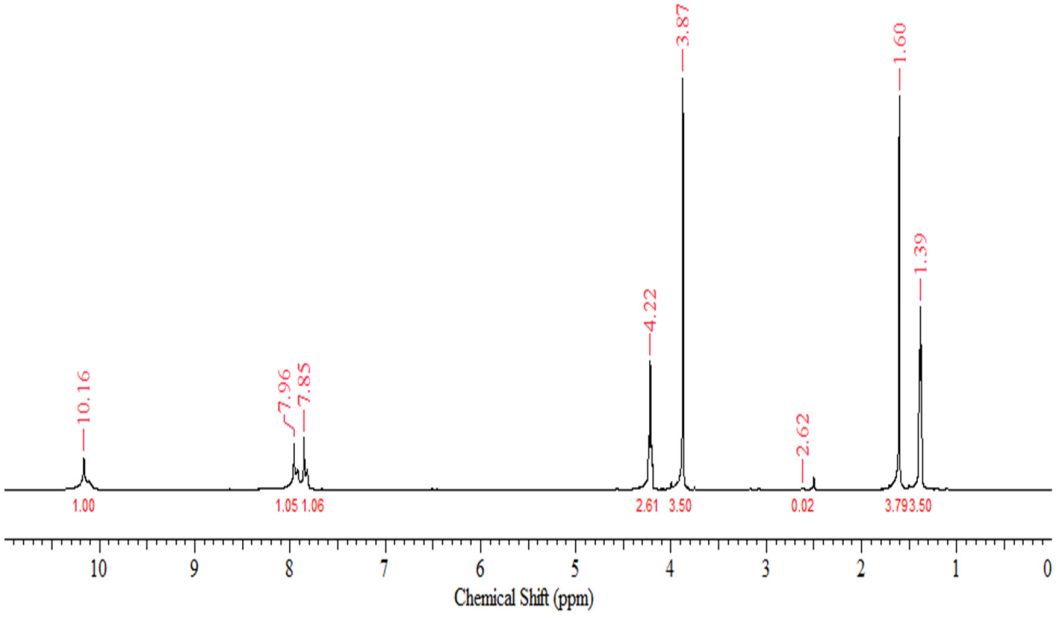

Figure 3.14 (d)

TH-1791_136107007

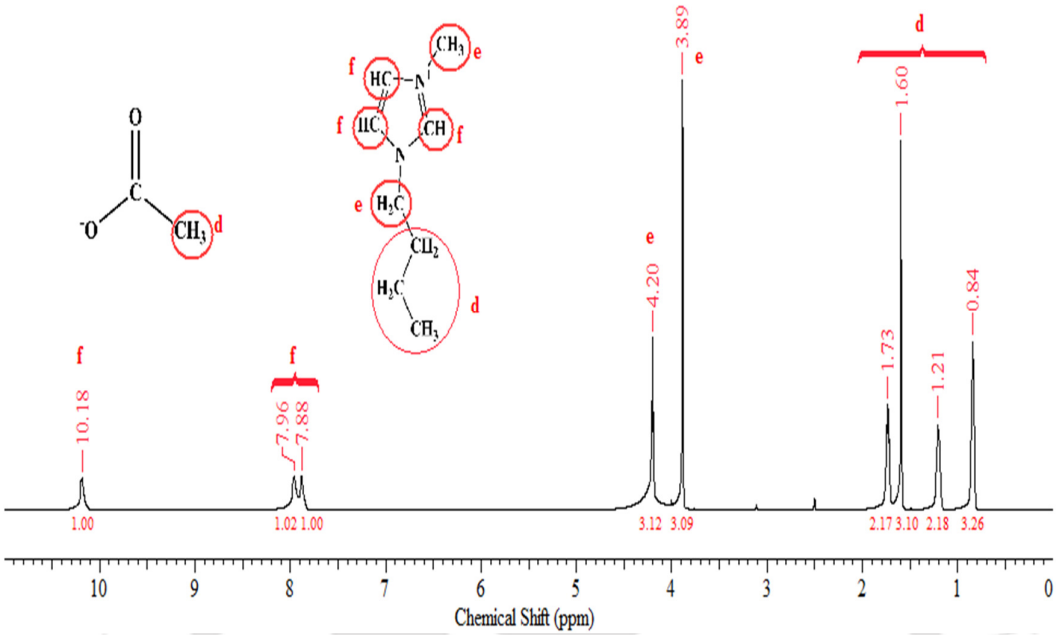

Figure 3.14 (e)

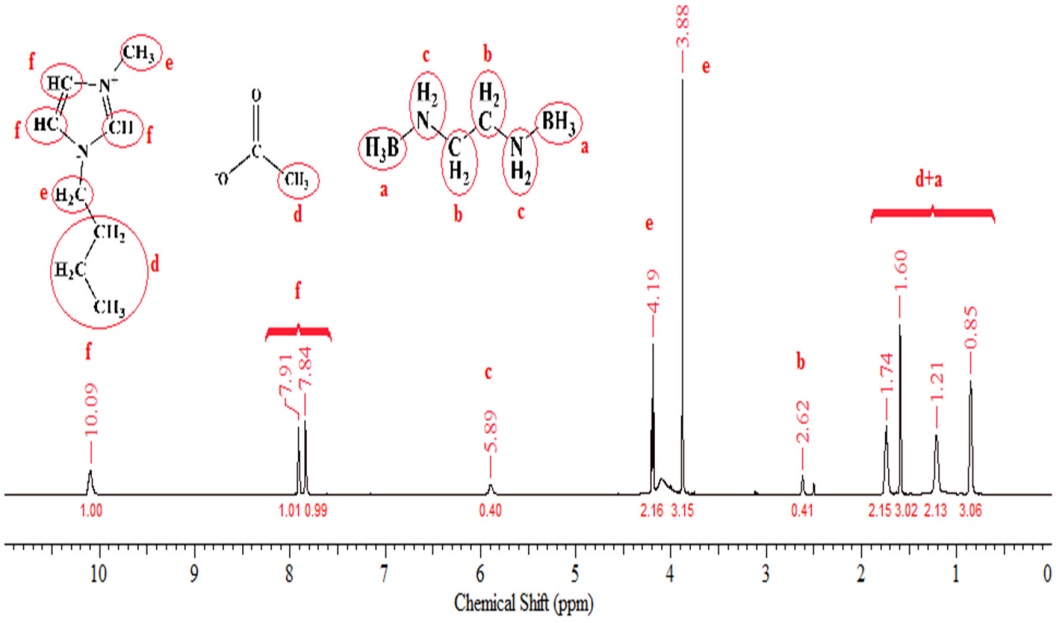

Figure 3.14 (f)

TH-1791_136107007

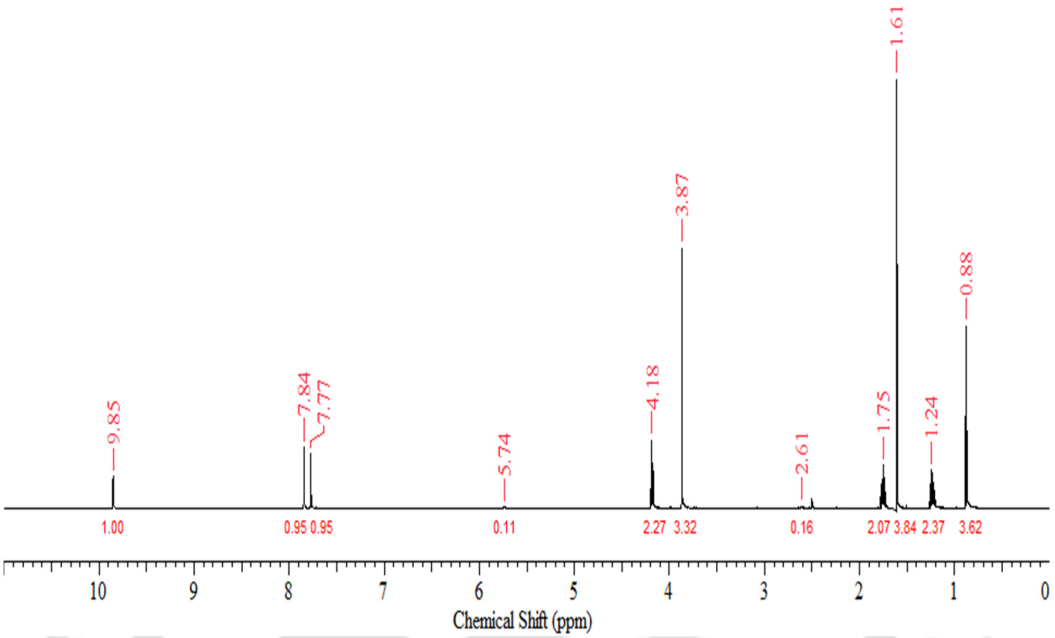

Figure 3.14 (g)

Figure 3.14 Plot for ^{1}H NMR. (a) pure EDAB, (b) pure [EMIM][OAc], (c) EDAB/[EMIM][OAc] before reaction, (d) EDAB/[EMIM][OAc] after reaction, (e) pure [BMIM][OAc], (f) EDAB / [BMIM][OAc] before reaction, (g) EDAB/[BMIM][OAc] after reaction.

3.8.4 ^{11}B NMR analysis of EDAB along with acetate based Ionic Liquids

Since [BMIM][OAc] facilitated dehydrogenation of EDAB gives a higher equivalent release of hydrogen, we conducted ^{11}B solution NMR before and after dehydrogenation samples of EDAB/[BMIM][OAc]. ^{11}B NMR analysis will give us a qualitative agreement of the boron species by comparing the respective peaks as reported in literature. As the imidazolium-acetate ILs do not possess boron species, the qualitative comparison will also reflect the possible reaction mechanism proposed in the literature [21, 23]. Figure 3.15(a) represents a ^{11}B NMR plot of EDAB/[BMIM][OAc] before

TH-1791_136107007

reaction. A chemical shift at -19.61 ppm indicates a near agreement of sp^3 BH_3 groups in EDAB as reported in the literature [21]. After the dehydrogenation (Figure 3.15(b)), the only noticeable chemical shift is at 20.52 ppm, which closely resembles the reported chemical shift of trigonal boron (sp^2) i.e. 24 ppm [21]. We consider this as a conclusive proof for the presence of a sp^2 BH_2 group in imidazolium-acetate supported dehydrogenation of EDAB. This is due to the fact that the chemical shifts for sp^3 BH and BH_3 emerge on the negative side of the scale [16]. An isolated BH_4^- group gives a sharp resonance at -39 ppm and asymmetric BH_2 resonance at -10 ppm [21]. A single peak of 20.52 ppm nullifies the possibility of having BH_4^- and asymmetric BH_2 in the end product. Thus, only trigonal boron (sp^2) is a possible presence as the end-product of dehydrogenation.

With this possibility, the possible reaction mechanism in imidazolium-acetate facilitated dehydrogenation of EDAB was deduced. As per the reported work of Neiner et al.[21] the presence of intramolecular dehydrogenation mechanism is ruled out due to the absence of BH_4^-, BH_3 and BH peaks. Neiner et al.[21] and Leardini et al.[23] proposed intermolecular reaction mechanisms which differ in their intermediate products. Both the studies identified the end species having both BH and BH_2 functional groups. In our dehydrogenation experiments, the final product has merely a moiety having the sp^2 BH_2 group. This step is depicted as the penultimate species in the reaction mechanism presented by Leardini et al. (part 3.9.4 Figure 3.21 and Scheme 3.22.3) [23].

TH-1791_136107007

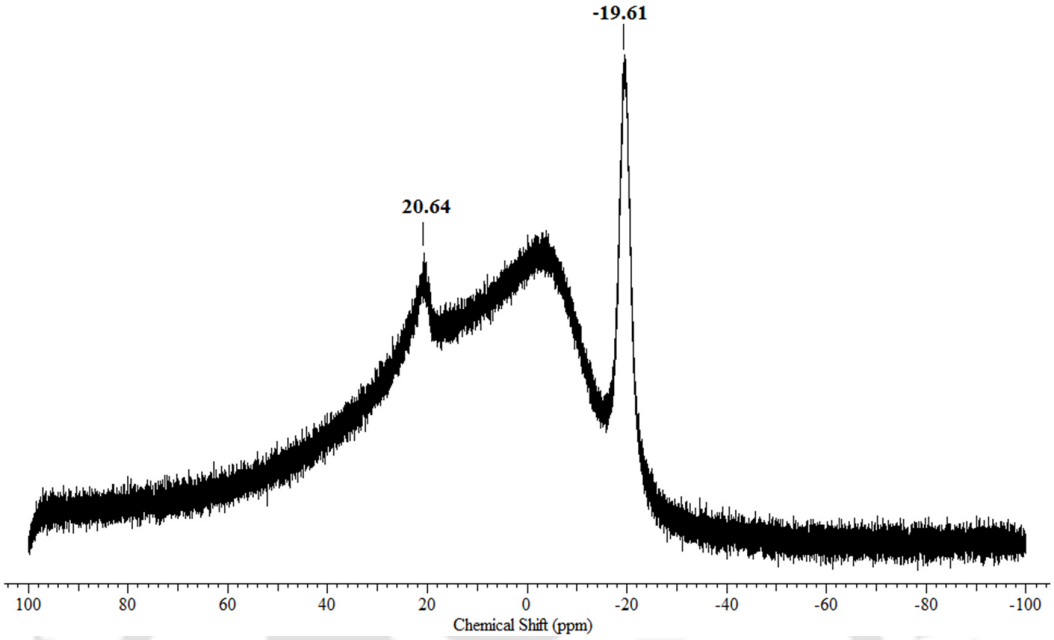

(a)

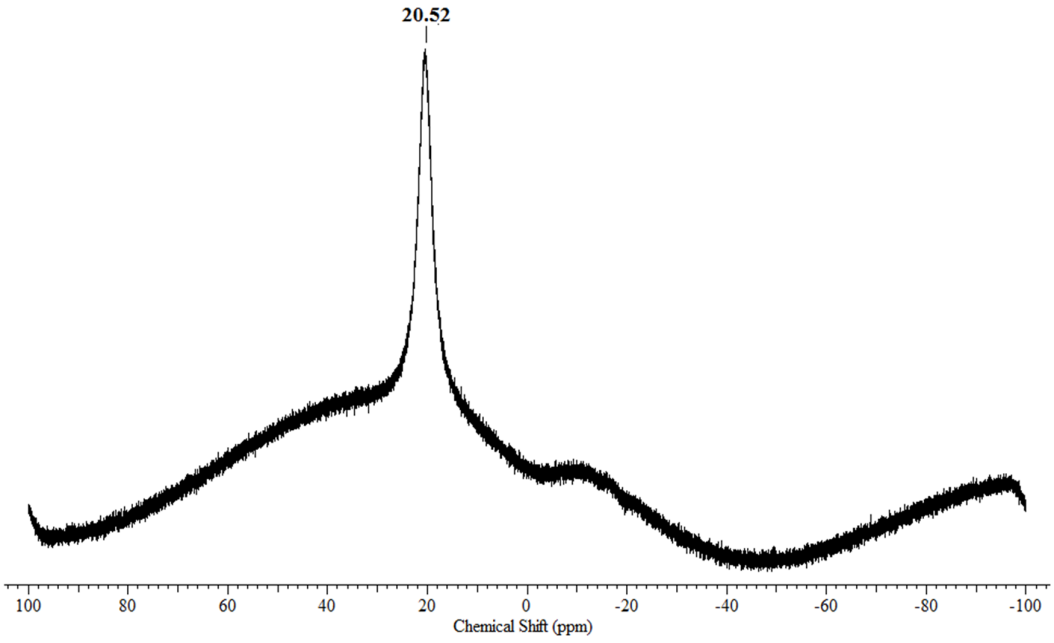

(b)

Figure 3.15 Plots for ^{11}B NMR: (a) EDAB/[BMIM][OAc] before reaction (b) EDAB/[BMIM][OAc] after reaction

TH-1791_136107007

3.8.5 HR-MS of EDAB along with acetate based Ionic Liquids

In order to confirm the ^{11}B observation on a trigonal boron (sp^2) BH_2 group, we conducted HR-MS analysis to find out the mass of the polymeric end product. It should be noted that the amount of released hydrogen cannot be explained by the degree of polymerization [20]. We conducted HR-MS analysis in the positive APCI mode and the spectra is plotted in Figure 3.16. Three distinctive peaks are observed in the +APCI scan. We assigned the peak at 139.1238 to the imidazolium cation by the mass of imidazolium cation calculated for $C_8H_{15}N_2$ (139.1230). The next two prominent peaks at 242.0734 and 339.1637 are assigned to the cyclic moiety with sp^2 BH_2. These species are given as the penultimate structures of Leardini et al. [23] (Scheme 3.22.3 Figure 3.22. e - 3.22. f). For n = 3, the exact mass of $C_8H_{44}B_8N_8$ is 340.4433 which is close to the HR-MS spectra (339.1637). For n = 2, the exact mass of $C_6H_{31}B_5N_6$ is 242.3075 which again compares well to our mass at 242.0734. Thus from the analysis of mass spectra, we obtained the penultimate species of n = 2, 3 (Scheme 3.22.3 Figure 3.22 (e-f), as proposed and presented by Leardini et al. [23]. ^1H NMR characterization of reactants and products confirms the structural integrity of ILs and highlights the catalytic role of ILs in dehydrogenation process. ^{11}B NMR confirms the presence of trigonal boron (sp^2) BH_2 as the only boron containing moiety in dehydrogenation experiments. Further analysis of high resolution mass spectra of dehydrogenated products detects the presence of EDAB having n = 2 and 3 repeat units in the end product.

TH-1791_136107007

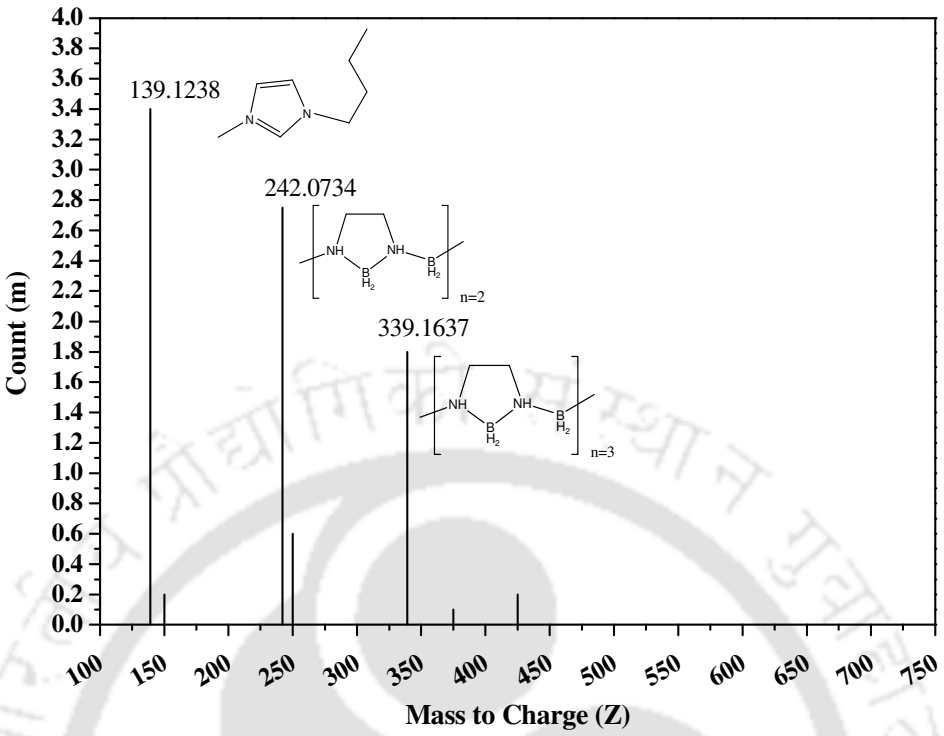

Figure 3.16 APCI-HR-MS plot of EDAB/[BMIM][OAc] after reaction.

Overall we have observed that the Amine-Borane compounds typically form dihydrogen bonds in their solid form. Hence, dehydrogenation of amine-boranes typically occurs after breaking of dihydrogen bond network. Thus an induction period is observed for AB. The solubilizing property of IL hence disrupts the dihydrogen bond network and induction period is suppressed. Thus higher the solubility of amine-borane compound in IL, easier is the hydrogen liberation.

We shall now move towards the next set of suitable Ionic Liquids which has been screened as per section 3.6 by COSMO-SAC model. The next line of Ionic Liquids here now belongs to the phosphonium based cations namely Trihexyltetradecylphosphonium bis (2,4,4-trimethylpentyl) phosphinate[TDTHP][Phosph] and Trihexyltetradecylphosphonium dicyanamide [TDTHP][DCA].The methodology and procedure shall remain exactly the same as discussed in chapter 2.

TH-1791_136107007

3.9 Dehydrogenation Experiments of EDAB/Phosphonium Ionic Liquids

The time resolved total equivalent hydrogen generation per mole of EDAB with the phosphonium IL's are given in Figure 3.17 and Table 3.8. Here temperature plays an important role in dehydrogenation and hence more equivalent of hydrogen is released at 105 °C than at 95 °C. This trend is consistent with equivalent hydrogen release from EDAB/imidazolium-acetate systems as seen in the previous section. At 105 °C, total equivalent hydrogen released from EDAB/[TDTHP][Phosph] is 3.25, which is higher than 3.04 equivalent of hydrogen as obtained from EDAB/[TDTHP][DCA]. At 95 °C, both the systems produce 2.59 and 2.45 equivalent of hydrogen. The IL facilitated hydrogen release is higher than the 2.14 equivalent hydrogen release from dehydrogenation of pure EDAB at 120 °C [22].

In all the experimental runs, the experiment time was 300 min. Figure 3.17 shows no induction period during dehydrogenation and release of equivalent hydrogen steadily increases until 60 min at all four temperatures. After 60 min the reaction slows down and after 160 min hardly any release of hydrogen is observed. The release of equivalent hydrogen facilitated by phosphonium based ILs (~3.25) is less than that of imidazolium based ILs (section 3.8). This phenomena may be due to the reaction environment provided by the ILs. Presence of acidic hydrogen in imidazolium ring provides an acidic reaction environment, which actually stabilizes the ionic intermediate when compared to the phosphonium counterpart.

TH-1791_136107007

Table 3.8 Cumulative equivalent of hydrogen released by EDAB/IL complexes at two different temperatures of 95 °C and 105 °C (Phosphonium)

	95 °C	**105 °C**
[TDTHP][Phosph]	2.59	3.25
[TDTHP][DCA]	2.45	3.04

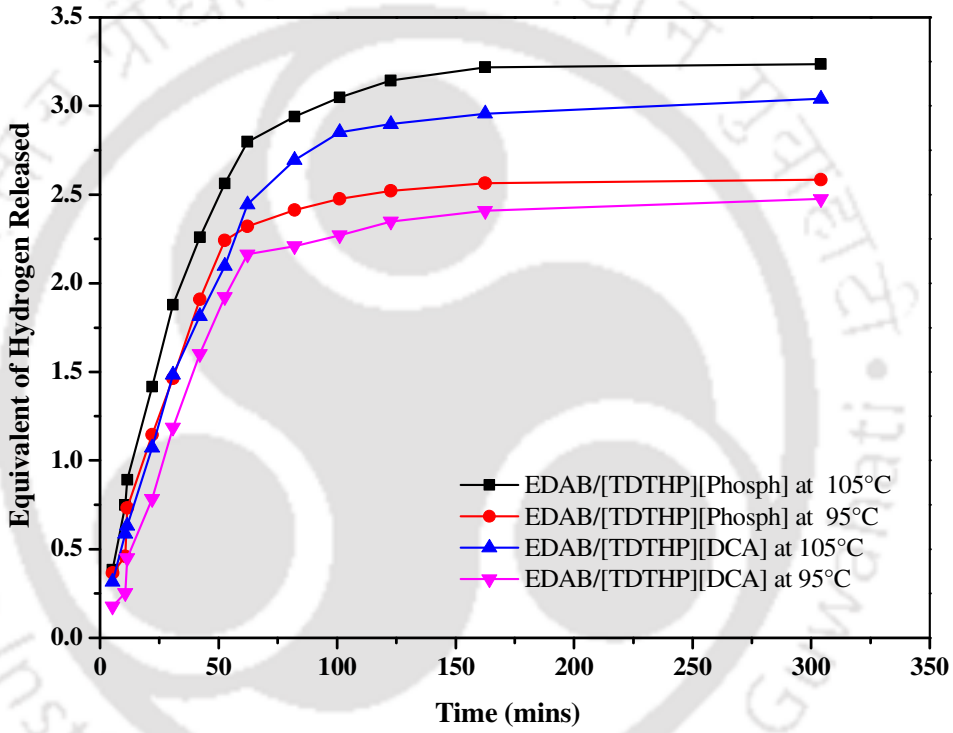

Figure 3.17 Time resolved equivalent hydrogen release from EDAB/[TDTHP][Phosph] and EDAB/[TDTHP][DCA] complexes at 95 °C and 105 °C.

(●) EDAB/[TDTHP][Phosph] at 95 °C, (▼) EDAB/[TDTHP][DCA] at 95 °C, (■) EDAB/[TDTHP][Phosph] at 105 °C, (▲) EDAB/[TDTHP][DCA] at 105 °C.

TH-1791_136107007

3.9.1 ^{1}H NMR Spectra of EDAB with Phosphonium Based Ionic Liquids

The role of ILs in dehydrogenation of EDAB was revealed by a comparative study of ^{1}H NMR spectra of pure ILs, before and after reaction mixture. These are reported in Figure 3.18 (a-f). We computed the area under the curves of each peak to relate the number of hydrogens attached to a particular moiety. ^{1}H NMR spectra of pure [TDTHP][DCA] is given in Figure 3.18(a). The peaks of this IL will solely represent [TDTHP] cation as DCA does not contain hydrogen atom. In Figure 3.18(a), the chemical shift at 0.88 ppm is assigned to the terminal $–CH_3$ of [TDTHP] cation and is represented as '*c*'. As '*c*' contains 12 hydrogens, the peak is assigned a reference area of 12.00, which gives each hydrogen an area of 1.00. With this reference area, chemical shift at 2.17 ppm has an area of 7.85, nearly equal to 8. The shift is assigned as $–CH_2$ group which is adjacent to phosphorous and is represented as '*a*' in Figure 3.18(a). Chemical shift from 1.25-1.46 ppm represents the remaining 48 hydrogens of [TDTHP] cation. Figure 3.18(b) represents ^{1}H NMR spectra of EDAB/[TDTHP][DCA] before reaction. The chemical shift for IL is located at 0.88 (m, 12H), 1.25-1.46 (m, 48H) and 2.17 (m, 8H) ppm, which is having the same area as that of pure IL. Chemical shift at 5.26 ppm is assigned to $–NH_2$ of EDAB and chemical shift at 2.61 ppm is assigned to $–CH_2$ moiety. These assignments agree well with the previous literature data [25]. Here the chemical shift of $–BH_3$ is located between 1.13-1.37 ppm, which is merged with the chemical shifts of IL. Figure 3.18(c) represent ^{1}H NMR of dehydrogenated EDAB/[TDTHP][DCA] system. Calculation of areas under the chemical shifts (0.86, 1.23-1.46, 2.16 ppm) resemble the area in pure IL (Figure 3.18(a)). Thus, it can be concluded that [TDTHP][DCA] does not degrade during dehydrogenation and it retains its original structure.

^{1}H NMR spectra of pure [TDTHP][Phosph] is given in Figure 3.18(d). We compare these spectra with Figure 3.18(a) to locate chemical shifts of phosphinate anion. There is

TH-1791_136107007

a little observable shift in peaks for [TDTHP] cation due to presence of phosphinate anion. The chemical shifts of [TDTHP] cation is obtained at 0.87 (m, 12H), 1.25-1.46 (m, 48H) and 2.19 (m, 8H) ppm. A total of 102 hydrogens of [TDTHP][Phosph] IL is found to be present within the chemical shift of 0.74-2.19 ppm, which is good agreement with literature [26]. Figure 3.18(e) represent ^{1}H NMR spectra of EDAB/[TDTHP][Phosph] before reaction. Like Figure 3.18(b), chemical shift at 5.45 ppm and 2.60 ppm are assigned for $–NH_2$ and $–CH_2$ moieties respectively. Chemical shift for IL lies between 0.72-2.19 ppm which includes the $–BH_3$ group. ^{1}H NMR spectra of dehydrogenated EDAB/[TDTHP][Phosph] is given in Figure 3.18(f). The chemical shifts closely resemble the chemical shifts of Figure 3.18(d). Thus we can conclude that [TDTHP][Phosph] has also not degraded during dehydrogenation. Even though the chemical shifts of EDAB are not visible here in both the systems, a confirmatory test needs to be carried out. In order to confirm this observation, we have recorded the HR-MS analysis for the precise identification of dehydrogenated peaks.

TH-1791_136107007

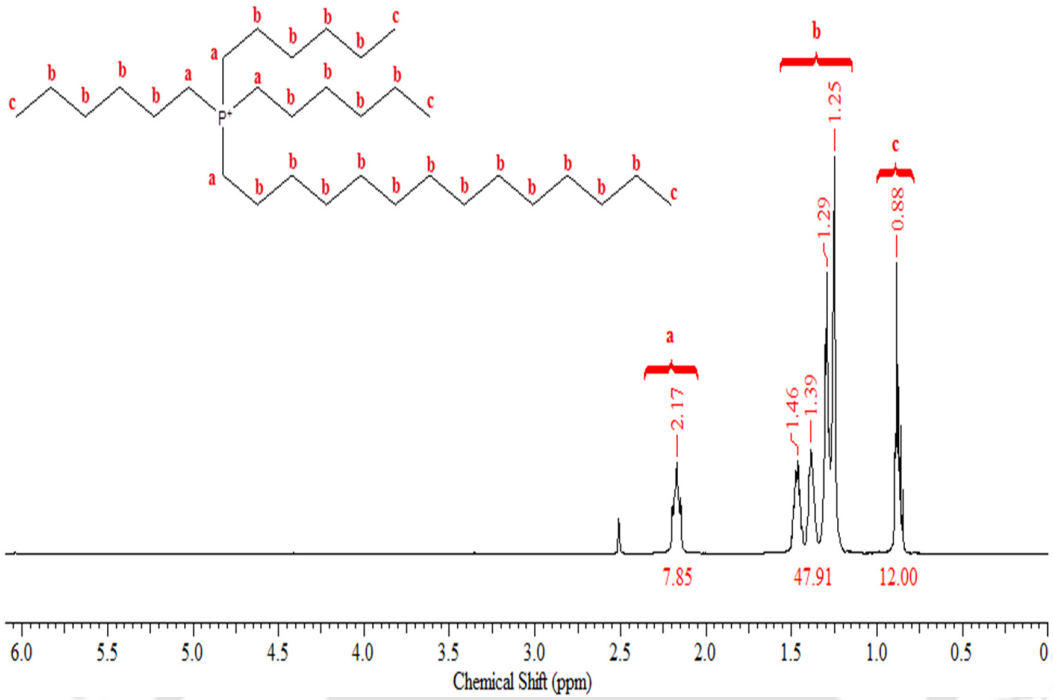

Figure 3.18 (a)

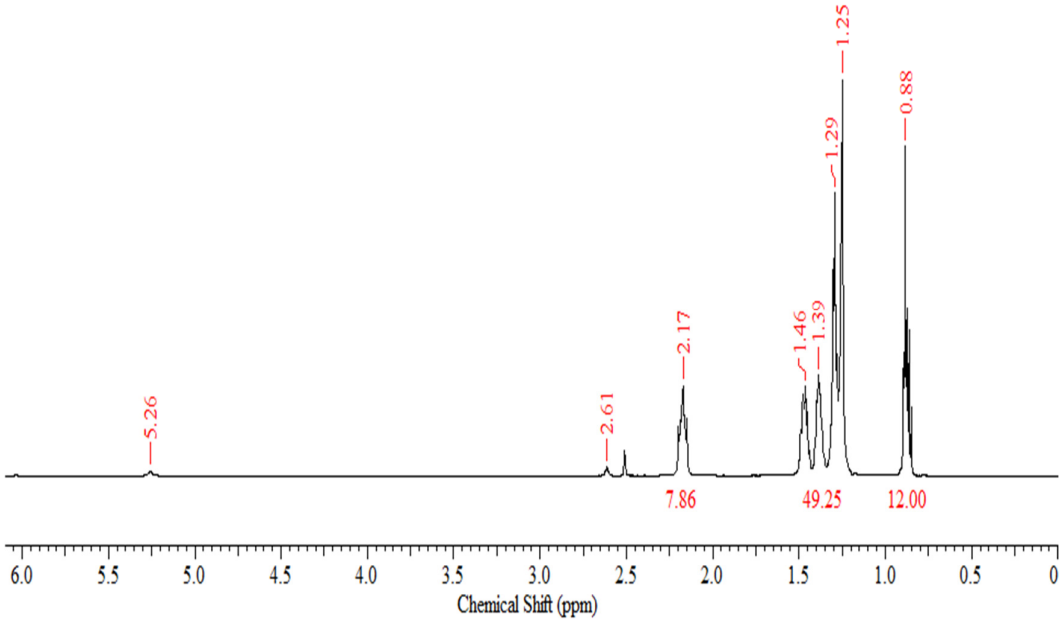

Figure 3.18 (b)

TH-1791_136107007

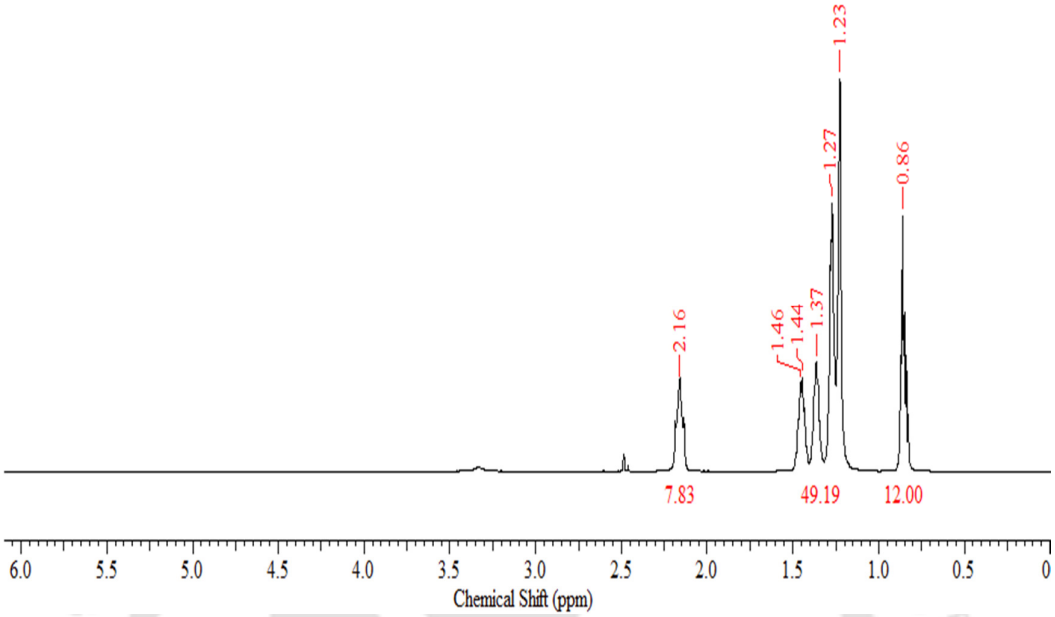

Figure 3.18 (c)

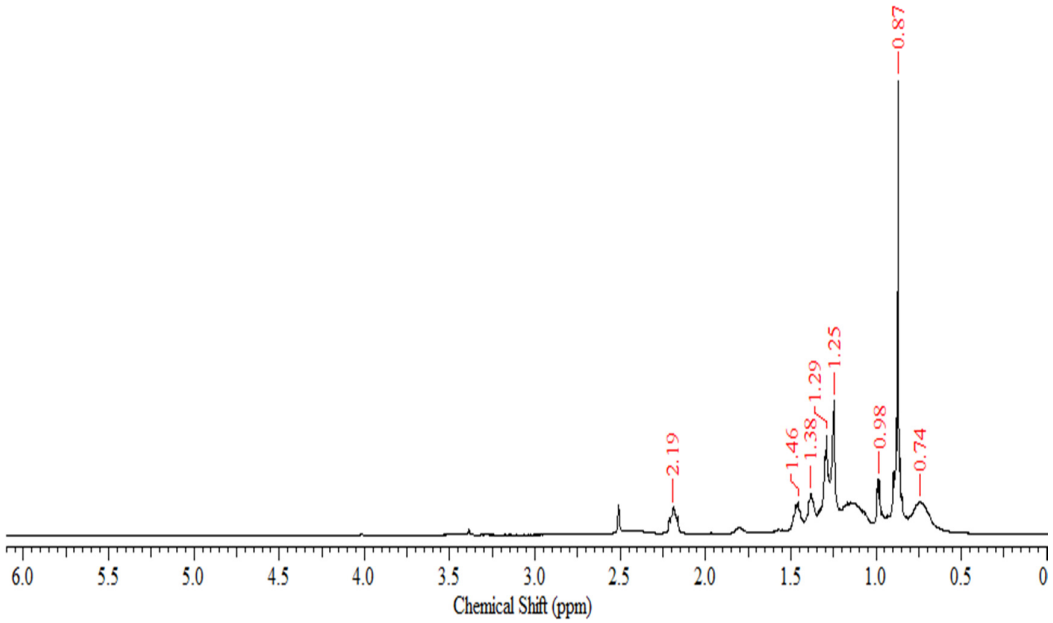

Figure 3.18 (d)

TH-1791_136107007

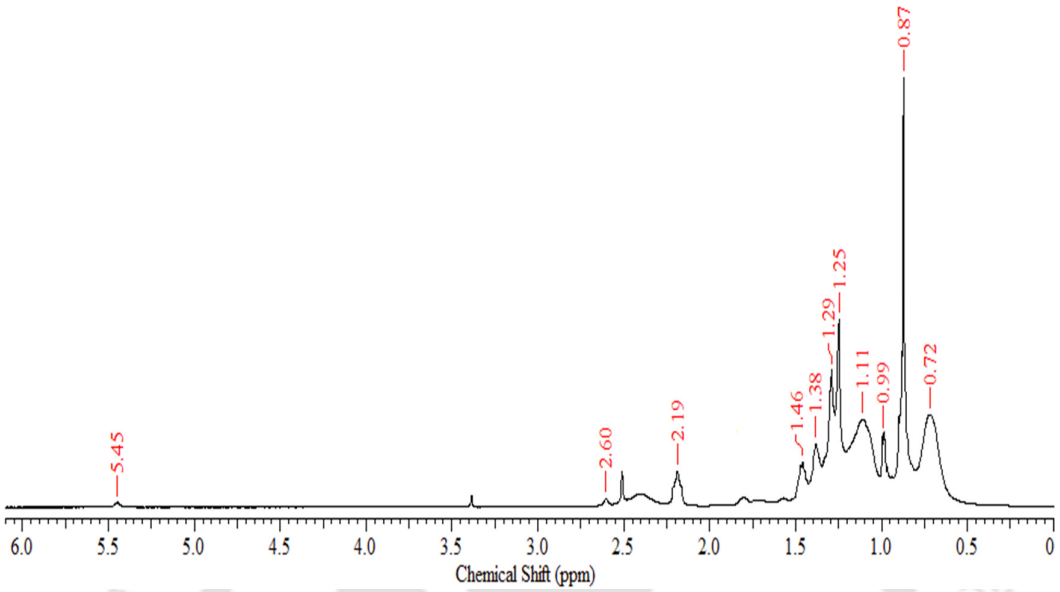

Figure 3.18 (e)

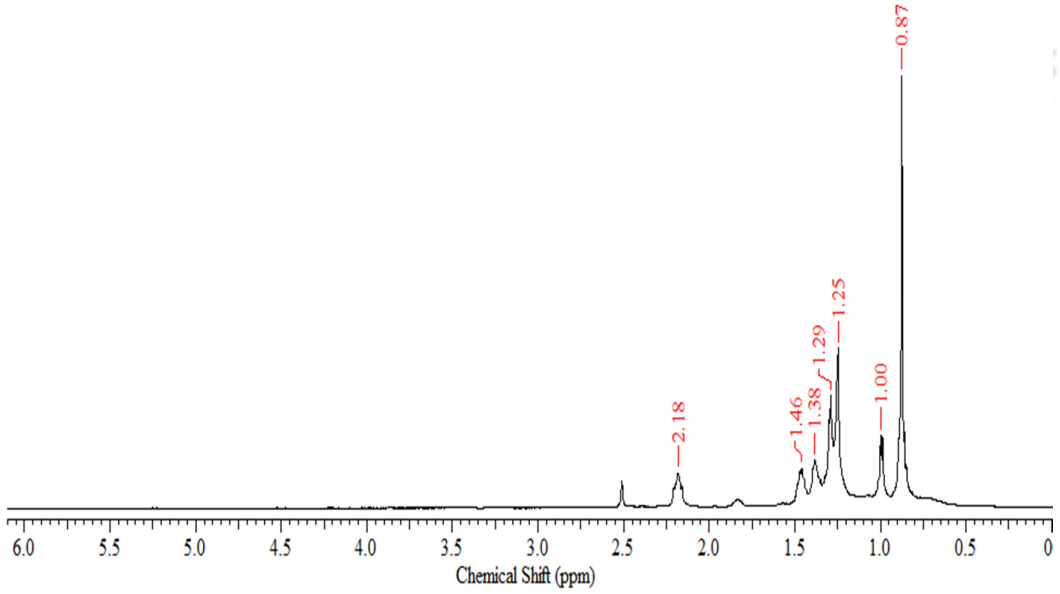

Figure 3.18 (f)

Figure 3.18 Plot for ^{1}H NMR. (a) pure [TDTHP][DCA], (b) EDAB/[TDTHP][DCA] before reaction, (c) EDAB/[TDTHP][DCA] after reaction, (d) pure [TDTHP][Phosph], (e) EDAB/[TDTHP][Phosph] before reaction, (f) EDAB/[TDTHP][Phosph] after reaction.

TH-1791_136107007

3.9.2 High Resolution-Mass Spectrometry (HR-MS) Analysis

HR-MS analysis was conducted on the dehydrogenated EDAB/phosphonium ILs systems in positive APCI mode where the mass spectra is plotted in Figure 3.20. The Structure of intermediates and residual products as obtained during and after the dehydrogenation process in represented in Figure 3.19. Four distinctive peaks are observed after dehydrogenation of EDAB/[TDTHP][Phosph] system in +APCI scan (Figure 3.20(a)). The peak at 291.24 is assigned to the phosphinate anion ($C_{16}H_{34}O_2P$) as the calculated mass of phosphinate anion is ($[M+H]^+$) 289.2302. In a similar fashion, we assigned the peak at 483.5052 for [TDTHP] cation, $C_{32}H_{68}P$ where the calculated mass of cation ($[M+H]^+$) is 483.5053. Thus HR-MS analysis of reaction mixture displayed the structural integrity of IL after dehydrogenation and confirms the role of IL as a catalytic agent. Peaks *'b'* and *'d'* of Figure 3.20(a) represent peaks for dehydrogenated EDAB oligomers. Peak *'b'* has a mass of 415.4013. The chemical formula of nearest possible dehydrogenated EDAB oligomer is $C_{10}H_{46}B_{10}N_{10}$ and the corresponding calculated mass ($[M+H]^+$) is 416.4837. In a similar fashion, peak *'d'* has a mass of 511.5061. For this peak, chemical formula of the nearest dehydrogenated EDAB oligomer is $C_{12}H_{66}B_{12}N_{12}$ with a calculated mass ($[M+H]^+$) of 510.6650. The chemical structures of peak '*b'* and '*d'* are shown in Figure 3.20. Figure 3.20(b) represents the +APCI scan of HR-MS spectra for dehydrogenated EDAB/[TDTHP][DCA] system. As the scan starts from 100, peak for dicyanamide anion is not visible. The mass of [TDTHP] cation is located at 483.5051 which is identical as Figure 3.20(a). Peak *'b'* has a mass of 415.4052 and peak *'d'* has a mass of 511.5050. Both of these are almost at a similar location as of Figure 3.20(a).

TH-1791_136107007

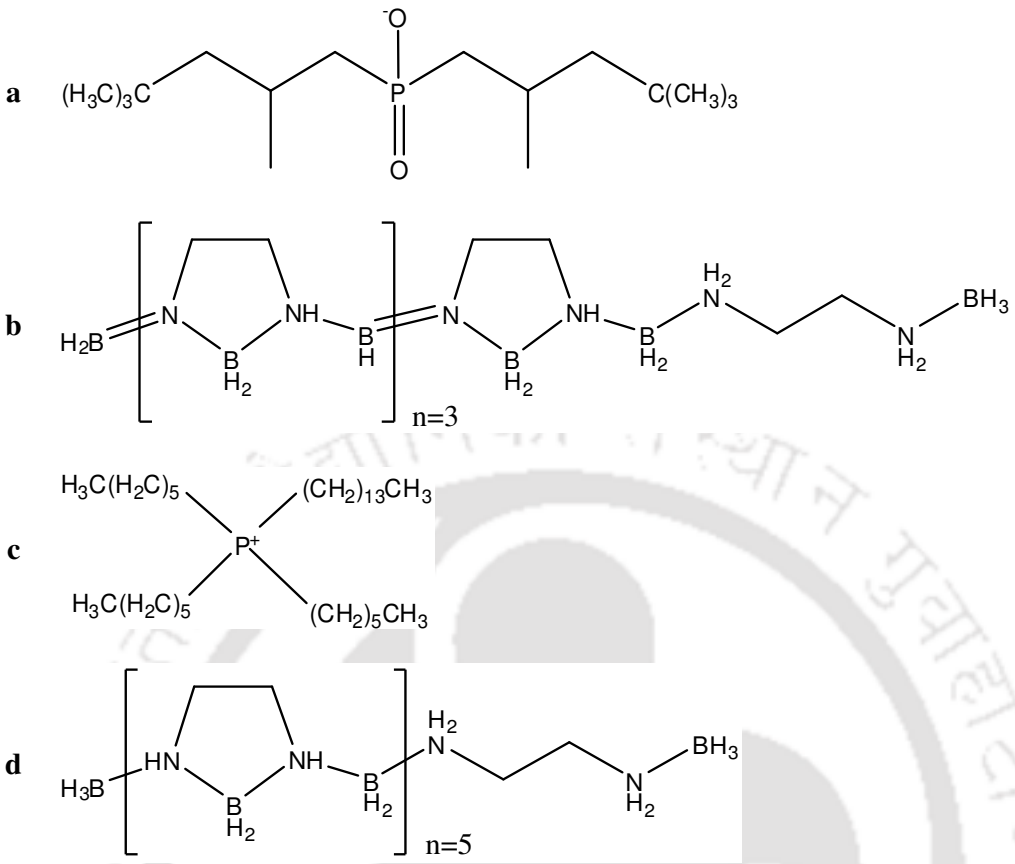

Figure 3.19 Structure of intermediates and residual products as observed in HR-MS

TH-1791_136107007

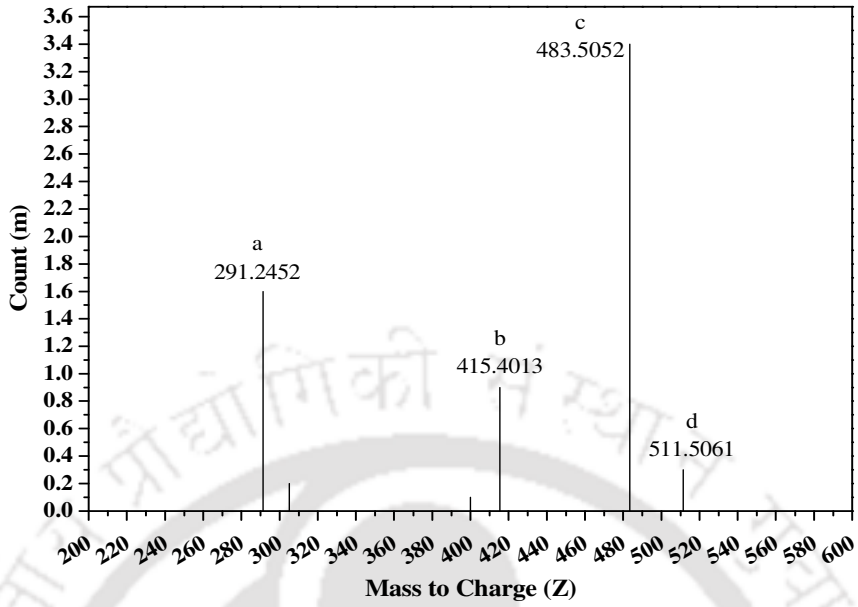

Figure 3.20(a)

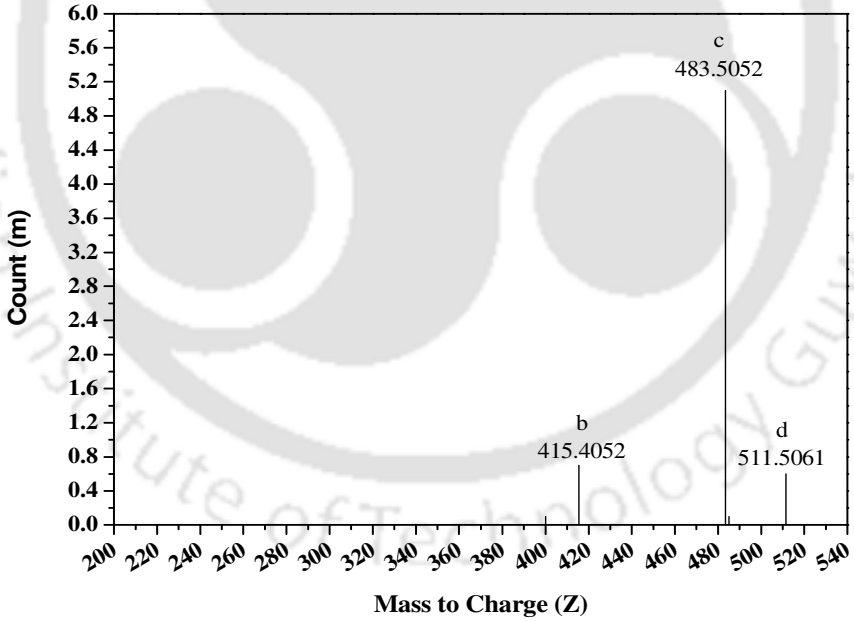

Figure 3.20(b)

Figure 3.20 APCI-HR-MS plot of EDAB/Phosphonium IL systems after reaction.

(The peaks assignment a,b,c,d represents the structures of Figure 3.19)

(a) EDAB/[TDTHP][Phosph], (b) EDAB/[TDTHP][DCA]

TH-1791_136107007

3.9.3 Experimentally Facilitated Reaction Mechanism

With the HR-MS spectra classification, we are now in a position to propose a reaction mechanism for the thermal dehydrogenation of phosphonium based IL's. Initially dehydrogenation of pure EDAB was first proposed by Neiner et al. [21] via two possible pathways; namely intramolecular and intermolecular approach. Both the processes involve formation of ionic intermediates. Intramolecular dehydrogenation does not produce oligomeric dehydrogenated EDAB structure and the reaction ends with the formation of cyclic dehydrogenated EDAB. The intermolecular dehydrogenation is initiated by the formation of EDAB dimer. This dimerization leads to the first dehydrogenation step. Larger chains are formed after subsequent polymerization of this dimer. Each repeat unit then further loses hydrogen during the formation of BH_2 cyclic groups and B=N bonds. Figure 3.21 describes the procedure as given by Leardini et al. [23]. We have now proposed a reaction mechanism based on HR-MS characterization. Here, the IL's are merely acting as a catalytic agent to facilitate dehydrogenation in milder condition, hence the proposed reaction mechanism proceeds without the inherent IL structure [6]. In this case, we consider the formation of end product with change in reaction environment and solvent i.e. IL. Hence, the selection of ILs is key for the selective dehydrogenation and extent of degree of polymerization.

TH-1791_136107007

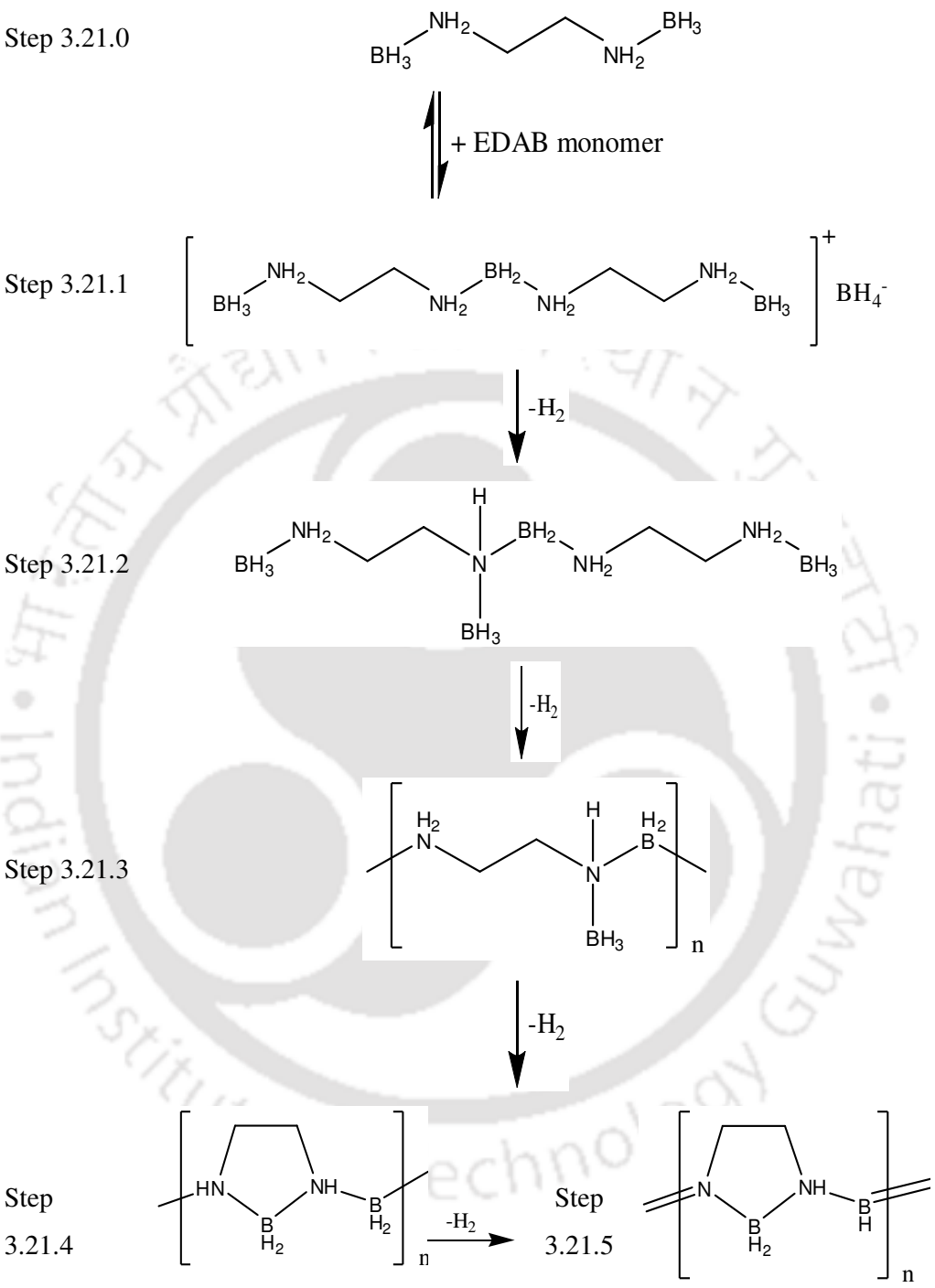

Figure 3.21 Dehydrogenation mechanism proposed by Leardini et al. [23]

TH-1791_136107007

Figure 3.22 (a-f) summarizes both the schemes of IL facilitated dehydrogenation of EDAB. Figure 3.22 is common initiation pathway of EDAB. Nature of ILs i.e. reaction environment will determine the number of EDAB monomers which can be added to the EDAB dimer and also its end time. Figure 3.22(a) and 3.22(b) explains the probable reaction intermediates of EDAB/phosphonium ILs; whereas Figure 3.22(d) and 3.22(e-f) elaborate upon the dehydrogenation mechanism of EDAB/imidazolium-acetate ILs. The dehydrogenation process initiates through the formation of ionic intermediate of EDAB dimer, which is analogous to the formation of diammoniate diborane (DADB). High level ab-initio calculations of amine-borane adducts points out to the breaking of dative B-N bond. Further this is found to be more favorable than the breaking of N-C bonds [27]. Thus with the breaking of terminal B-N bonds, the chain reaction propagates and oligomeric dehydrogenated structure is formed. It is assumed that ionic EDAB dimer is more reactive than EDAB itself. As there is no induction phase observed for dehydrogenation of EDAB, the ionic intermediate releases its first equivalent of hydrogen and reactive EDAB dimer is formed (step 3.22.0.2 of Figure 3.22). The propagation of reaction then occurs by the addition of EDAB monomer. We believe the propagation will also be through the formation of intermediate oligomer ionic EDAB species, by subsequently eliminating hydrogen from ionic intermediates.

Since, HR-MS analysis of end products identifies species *'b'* and *'d'* of Figure 3.20 as end products of both the systems, we proposed a 'propagation pathway' in Figure 3.22(a). Here three EDAB monomers will be added (step 3.22.1.1 to 3.22.1.7) with the EDAB dimer one by one through the formation of ionic intermediates. Comparison of mass spectra with various EDAB oligomers reveals that species '*b*' of Figure 3.20 have similar mass of oligomer species as shown in step 3.21.5 of Figure

TH-1791_136107007

3.21. However, other than the ring structure (step 3.21.5 of Figure 3.21), the dehydrogenated product will also have alkyl EDAB moiety as shown in step 3.22.2.a.3 of Figure 3.22(b). Figure 3.22(b), thus propagates by formation of cyclic $–BH_2$ moiety by eliminating four hydrogen molecules and later terminates the same by releasing four more equivalent of hydrogen and forming a B=N bond in end product. Thus species *'d'* of Figure 3.20 resembles step 3.21.4 of Figure 3.21. Here oligomer structure in step 3.22.1.7 of Figure 3.22(a) will add one more EDAB monomer and will terminate according to scheme 3.22(b). The end product will contain only cyclic $-BH_2$ with no presence of B=N (step 3.22.b.4 of Figure 3.22(c)). Thus phosphonium IL facilitated dehydrogenation of EDAB yields oligomer EDAB species possessing four or five repeat units.

TH-1791_136107007

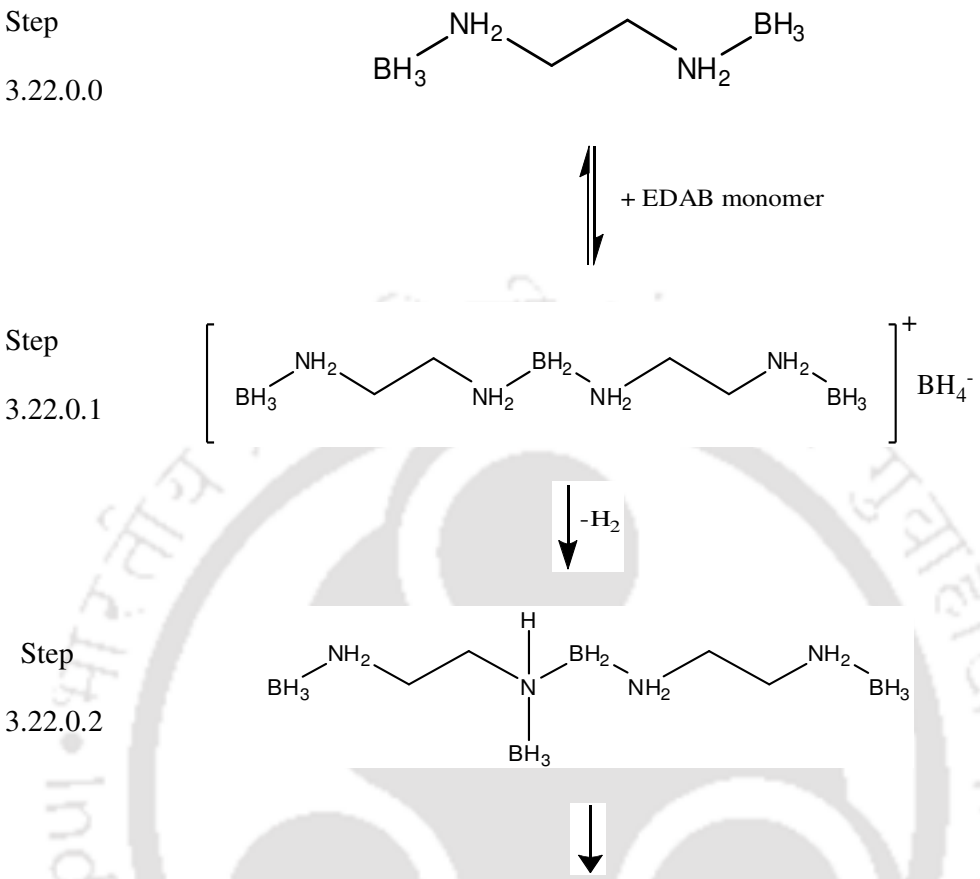

Scheme 3.22.1, 3.22.2, 3.22.3, 3.22.4

Figure 3.22 Common initiation pathways for dehydrogenation of pure EDAB

TH-1791_136107007

Step 3.22.1.1

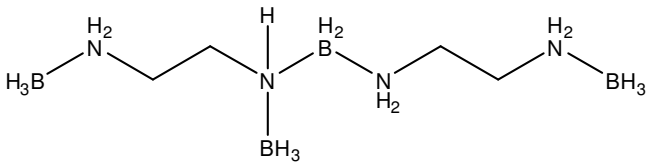

+ EDAB monomer

Step 3.22.1.2

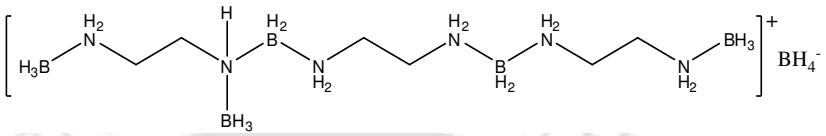

$-H_2$

Step 3.22.1.3

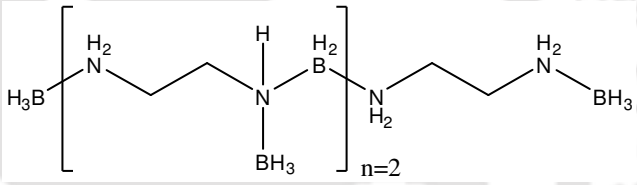

+ EDAB monomer

Step 3.22.1.4

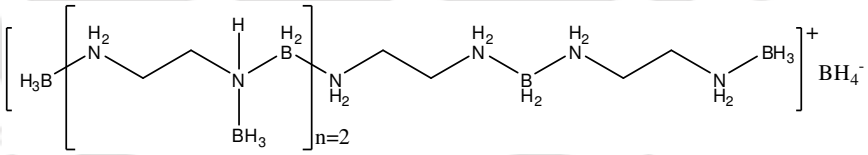

$-H_2$

Step 3.22.1.5

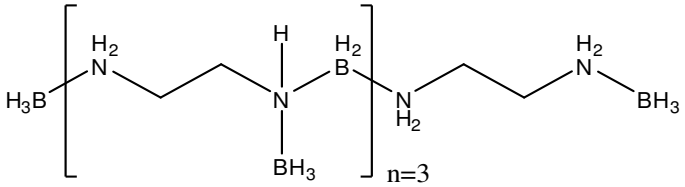

TH-1791_136107007

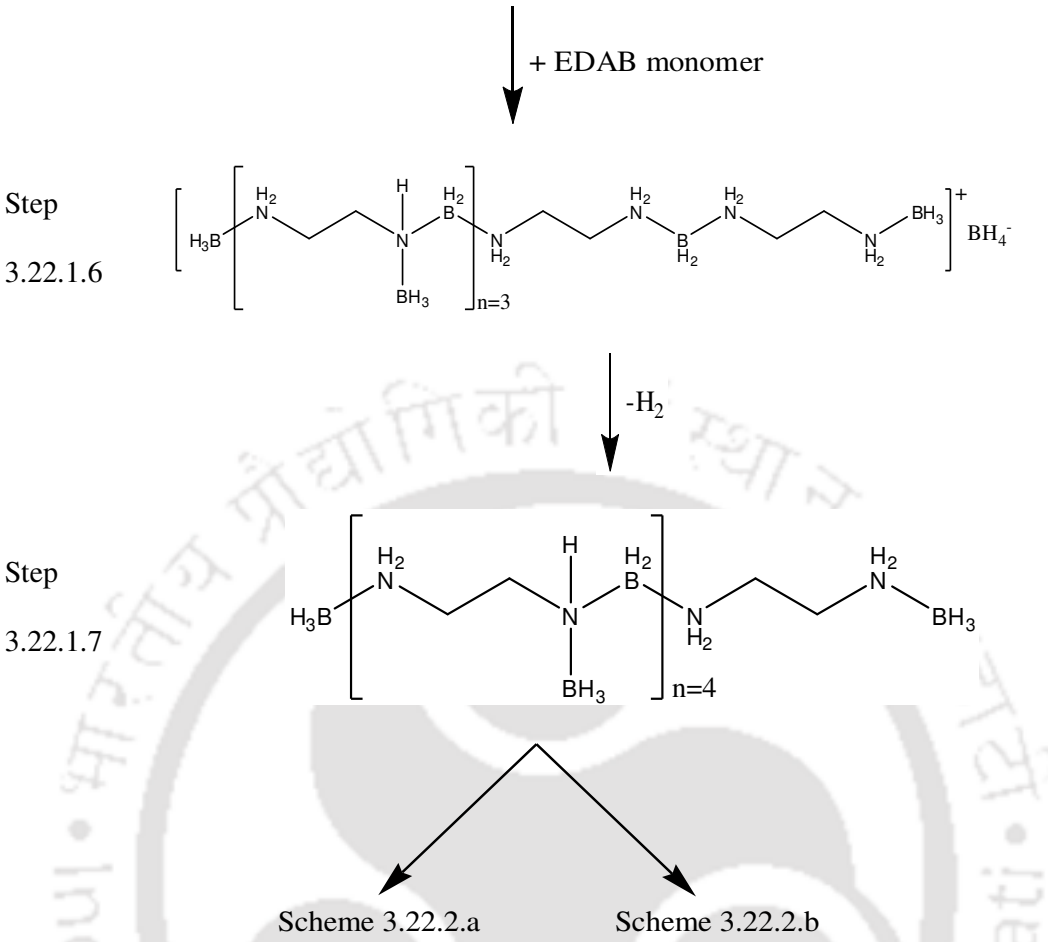

Figure 3.22(a) Scheme 3.22.1 Dehydrogenation pathway of EDAB/Phosphonium ILs

TH-1791_136107007

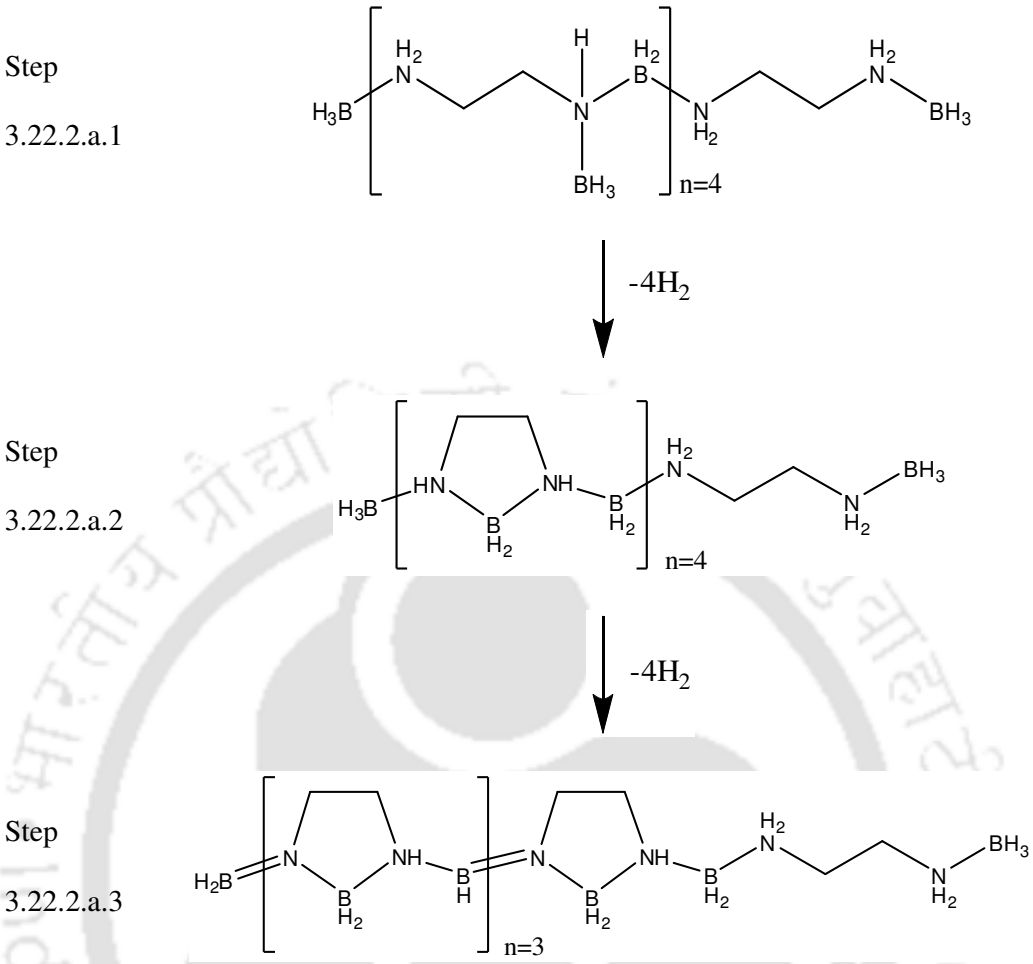

Figure 3.22(b) Scheme 3.22.2.a Dehydrogenation pathway of oligomer EDAB/Phosphonium ILs for possessing four units

TH-1791_136107007

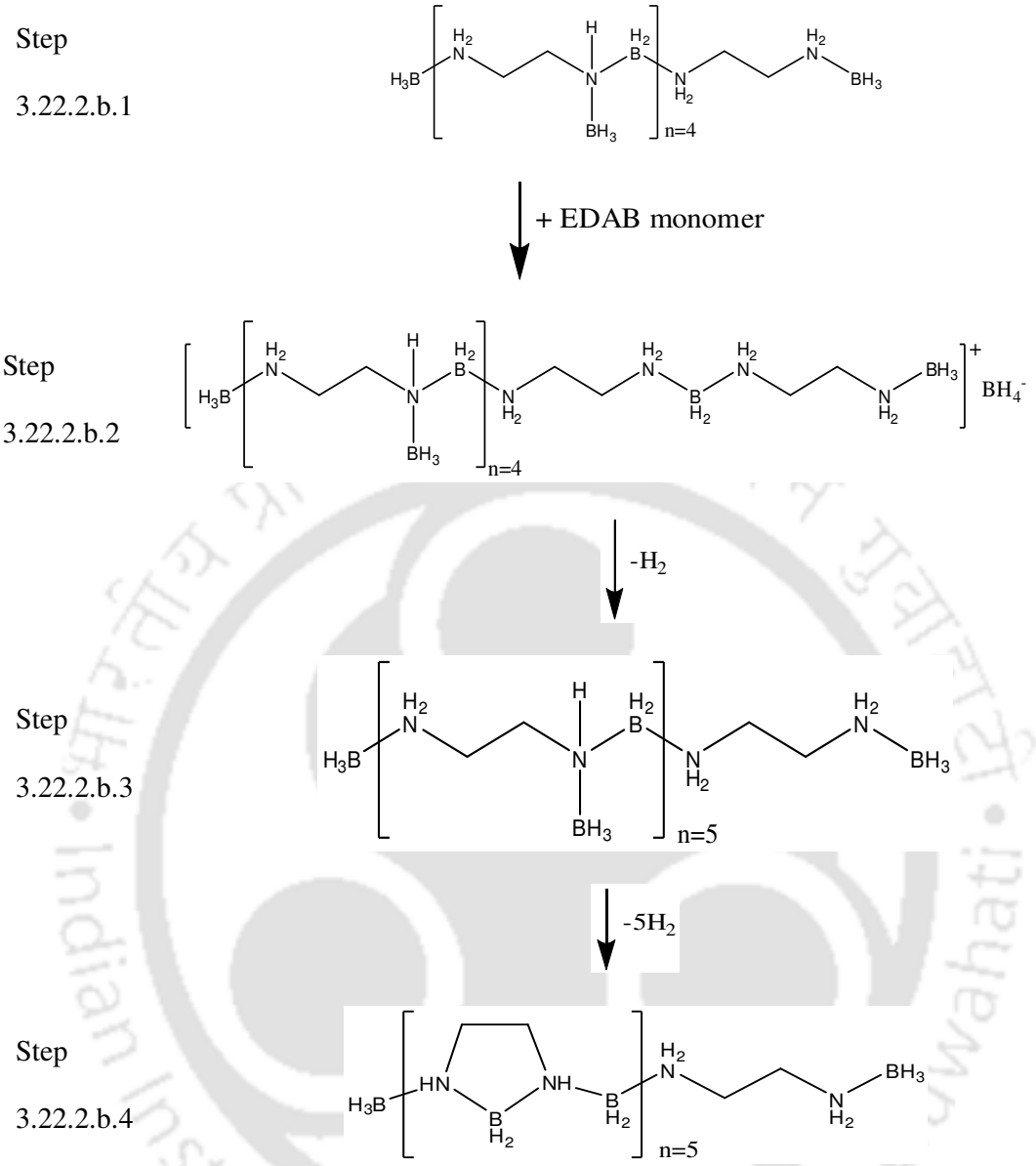

Figure 3.22(c) Scheme 3.22.2.b Dehydrogenation pathway of oligomer EDAB/Phosphonium ILs for possessing five units.

TH-1791_136107007

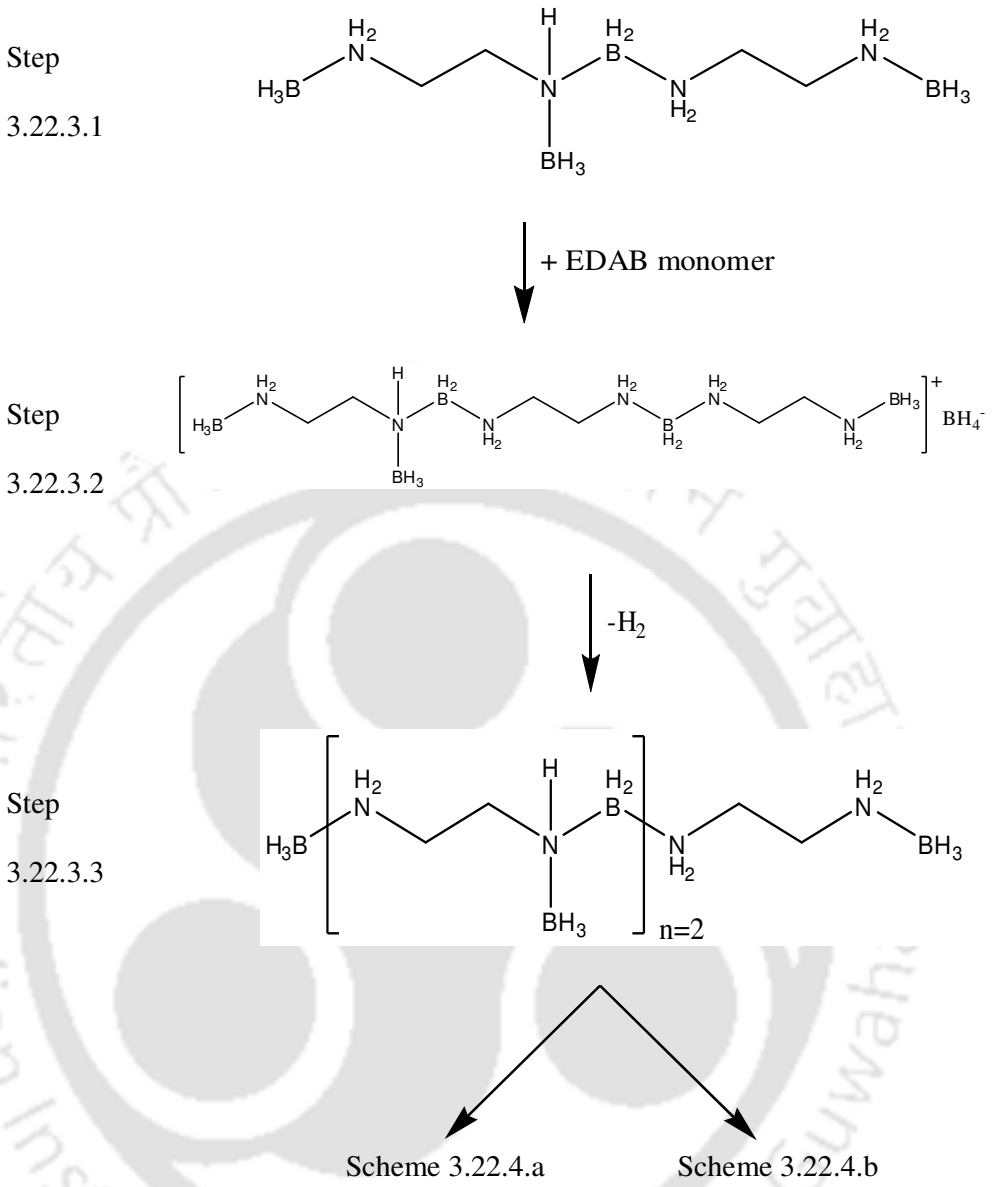

Figure 3.22(d) Scheme 3.22.3 Dehydrogenation pathway of EDAB/Imidazolium-acetate ILs

TH-1791_136107007

Step 3.22.4.a.1

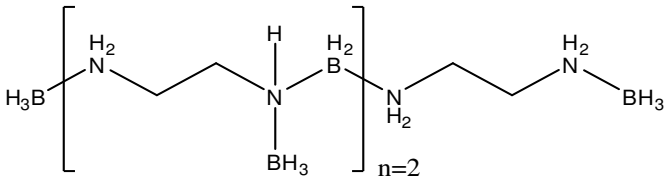

Step 3.22.4.a.2

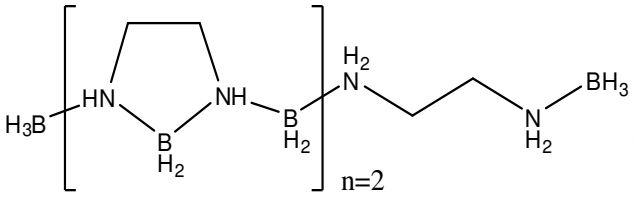

Figure 3.22 (e) Scheme 3.22.4.a Dehydrogenation pathway of oligomer EDAB/ Imidazolium-acetate ILs for possessing two units.

TH-1791_136107007

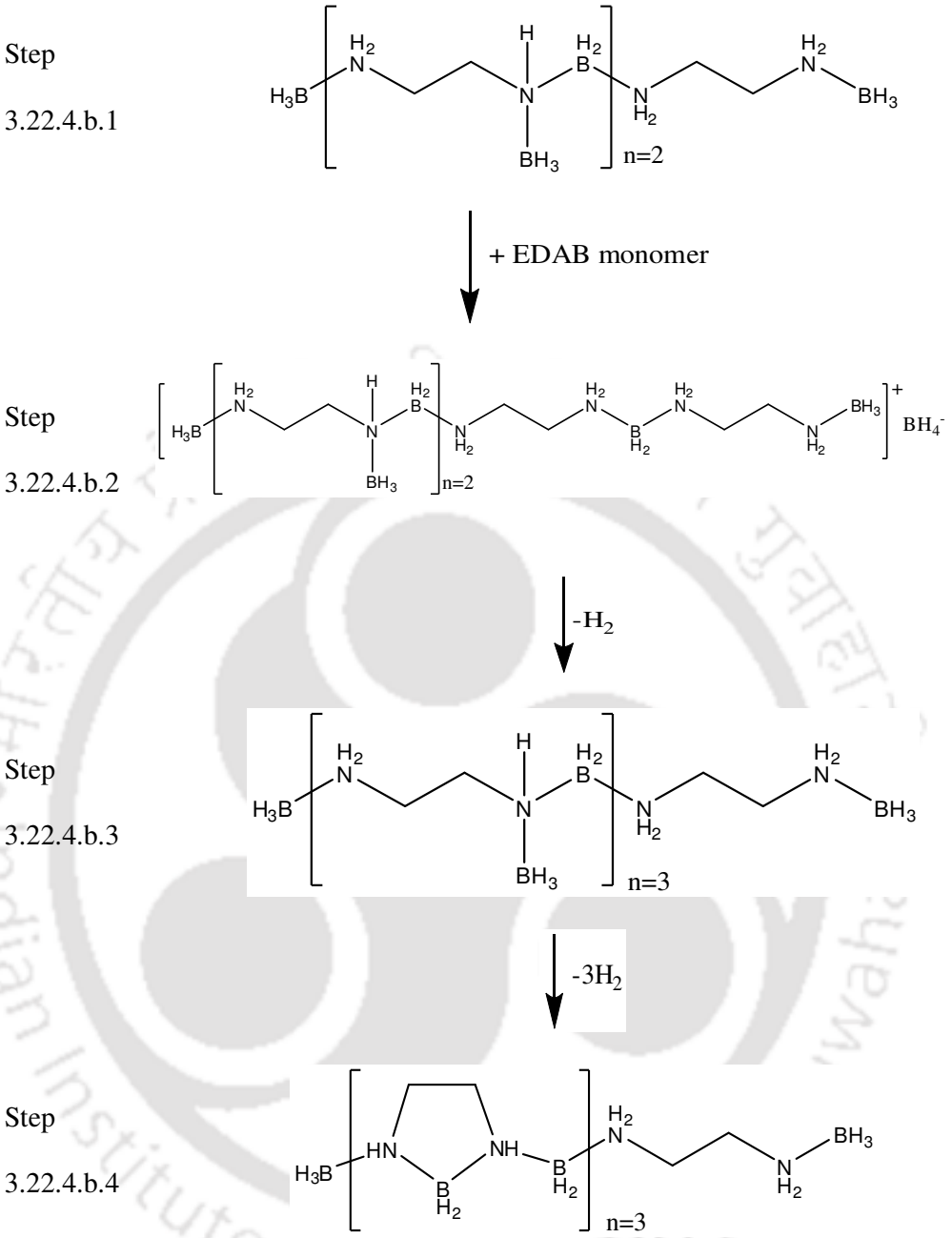

Figure 3.22(f) Scheme 3.22.4.b Dehydrogenation pathway of oligomer EDAB/ Imidazolium-acetate ILs for possessing three units

TH-1791_136107007

It should be noted that one of the two species yielding B=N containing oligomer was earlier proposed by Leardini et al. [23]. The formation of two types of oligomer in EDAB/phosphonium IL systems is a significant departure from dehydrogenation of EDAB in imidazolium-acetate ILs (section 3.8). The oligomer products formed during dehydrogenation of EDAB/imidazolium-acetate systems are identified in section 3.8 and the reaction mechanism is elaborated in Figure 3.22(d) and 3.22(e-f) Imidazolium-acetate facilitated systems do not support the formation of B=N species since only two (step 3.22.4.a.2 of Figure 3.22(c)) and three (step 3.22.4.b.4 of Figure 3.22(f)) repeat units of cyclic $–BH_2$ are formed. We believe reaction environment provided by the ILs is key in having different end products. Acidic hydrogen containing imidazolium ILs thereby restrict the dehydrogenation, which results in the formation of two to three repeat units of oligomers. The ionic intermediates containing BH_4^- anion are more stable in nucleophilic condition. Due to this reason, the acidic reaction environment restricts the propagation reaction and only few oligomers are formed. Contrary to this, phosphonium-based ILs provide more basic environment and thus promotes and stabilizes the ionic intermediates. The basic environment thus facilitates the dehydrogenation proposed by Leardini et al. [23] with the formation of longer repeat units of oligomer.

TH-1791_136107007

3.10 Dehydrogenation Experiments with 1-Allyl-3-Methylimidazolium cation based IL

Based on our COSMO-SAC screening results as reported earlier in section 3.6 and Table 3.1,we shall now test the dehydrogenation reaction with the last set of Ionic Liquids based on the allyl moiety. In this regard the IL's namely, 1-allyl-3-methylimidazolium bromide [AMIM][Br], 1-allyl- 3-methylimidazolium dicyanamide [AMIM][(D(CN)$_2$] and 1-allyl-3-methylimidazolium bis (trifluoromethylsulfonyl) imide[AMIM][Tf$_2$N] were chosen.

3.10.1 Thermal Dehydrogenation Experimental Results

The dehydrogenation experiment of EDAB and 1-allyl-3-methylimidazolium cation with anions such as bromide, bis (trifluoromethylsulfonyl) imide and dicyanamide were performed at three different temperatures (95,105 and 115 °C) (Table 3.9). Prior to the dehydrogenation experiments, all the Ionic Liquids were kept under vacuum for 24 hours at 353 K to minimize the water content and remove the impurities. The ^{1}H NMR was performed so as to validate the purity of the ILs. The ^{1}NMR spectra for pure IL are attached in Figure 3.23(a), (d) and (g). The peaks corresponding to the hydrogen atoms within the IL's are correlated and validated. An absence of excess peak suggests negligible impurity.

It should be noted that the IDAC predicted from COSMO-SAC model for only Allyl based IL is given in Table 3.5. These values are merely taken as qualitative guidelines. As a thermodynamic property, lower the IDAC values, higher the solubility of EDAB in IL and higher the capacity. This is true since the dehydrogenation proceeds with the stabilization of the intermediate product namely diammoniate of diborane (DADB), which is known to be highly stable in IL [23]. Since this step is usually the rate determining

TH-1791_136107007

step, we assume that IL assists in the stabilization of this reactive intermediate species. Hence solubility of EDAB in the IL is explored using the IDAC values.

For all the experiments, the average pressure at both the sides of the setup was maintained at 4.5 x 10^{-2} m bar. A common trend for all the IL's reflects an absence of any induction period. The total dehydrogenation time was found to be the highest for [AMIM][Br] in comparison to the other IL's. For [AMIM][Br] the complete dehydrogenation of EDAB at 95 °C took 1100 minutes (Figure 3.23(a)). However, as the temperature was increased to 105 °C and 115 °C, the EDAB/IL mixture was found to exhaust earlier at 900 minutes, thus releasing more hydrogen. It was also found that the reaction rate as well as the reaction time with [AMIM][Br] reduced as the temperature was increased from 95 °C to 115 °C.

For [AMIM][Tf_2N] (Figure 3.23(b)), the run time was 900 minutes for 95 °C; and 720 minutes for 105 °C and 115 °C. As the temperature increased we observe that the mixture exhausted faster and released higher equivalent of hydrogen. [AMIM][Tf_2N] have progressively shown an increase in the equivalent of hydrogen released with temperature. However, the lowest cumulative production of hydrogen was 2.01 equivalents at 95 °C, 2.07 at 105 °C and 2.08 at 115 °C. An interesting observation was that it did not breach the amount of equivalents released from pure EDAB i.e. 2.14 equivalent (as reported by Sahler et al. [22]).

The third and the final experiment was conducted with 1-allyl-3-methylimidazolium dicyanamide [AMIM][$N(CN)_2$] (Figure 3.23(c))**.** A run time of 910 minutes was required for the complete dehydrogenation at 95 °C (730 minutes for 105 °C and 115 °C). Unlike the other IL's whose cumulative production of hydrogen release increases with temperature, this has revealed an opposite trend. The highest amount of

TH-1791_136107007

hydrogen released was 2.74 equivalents at 95 °C whereas 1.36 and 1.32 equivalent H_2 was recorded for 105 °C and 115 °C, respectively. In comparison with pure EDAB, which also does not show any induction period [22] ; it was found to release 2.14 equivalent of H_2 at 120 °C, which is lower than the 2.74 equivalent of H_2 at 95 °C for [AMIM][$N(CN)_2$].

As already mentioned from reported literature, it is the stabilization of the reactive intermediate i.e. Diammino of Diborane (DADB) which controls the dehydrogenation process. This in turn depends on the basicity of the Ionic Liquids. This is obtained from the Kamlet-Taft parameter which quantifies the acidity and basicity of molecular solvents including IL. They are further related it to the yield of hydrogen [28]. From their measurements they computed the basicity (β) of several Ionic Liquids. It was found that IL with the Tf_2N anions are generally less polar or susceptible to be polarizable than those of the halogen anions. It is also reported that the β value is strongly controlled by the choice of anion. The average basicity of Tf_2N (0.24), $N(CN)_2$ (0.53) is way below than that of halogen such as chloride Cl (0.94). This explains a higher equivalent for [AMIM][Br]. A comparison of the IL with EDAB could not be made as the dehydrogenation with pure EDAB was conducted in the presence of air as against nitrogen in our work. The presence of air makes the quantification of hydrogen difficult owing to the other gases that may be produced due to oxidation reactions.

For all the dehydrogenation process, it was observed that two ILs, namely [AMIM][Br] and [AMIM][Tf_2N] have accelerated the catalytic effect of the dehydrogenation process. However, a contrary was observed for the remaining IL, namely [AMIM][$N(CN)_2$]. Further no induction time was observed in each of the three cases as opposed to a non-zero induction time for the neat EDAB. Also, higher reaction rates, and faster reaction time were observed, which agrees to earlier experiments [23, 29-30].

TH-1791_136107007

Table 3.9 Cumulative equivalent of hydrogen released by EDAB/IL complexes at three different temperatures of 95 °C, 105 °C and 115 °C (1-Allyl-3-Methylimidazolium).

	95 °C	**105 °C**	**115 °C**
[AMIM][Br]	2.08	2.59	3.25
[AMIM][N(CN)$_2$]	2.74	1.36	1.32
[AMIM][Tf$_2$N]	2.01	2.07	2.08

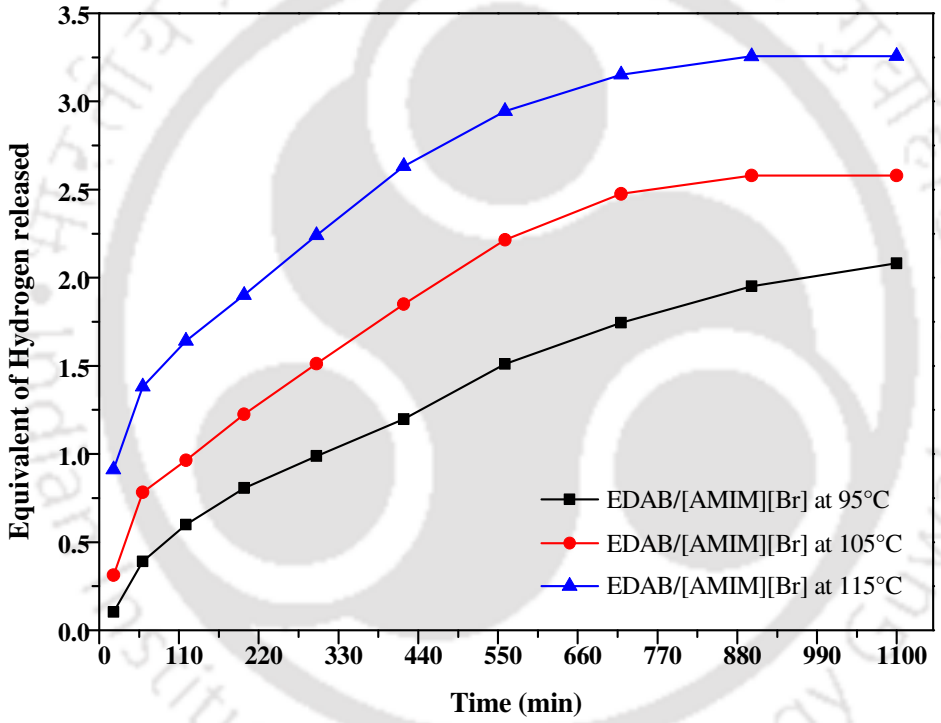

Figure 3.23(a) Equivalent release of hydrogen from EDAB/1-Allyl-3-methylimidazolium Bromide at 95 °C, 105 °C and 115 °C.

TH-1791_136107007

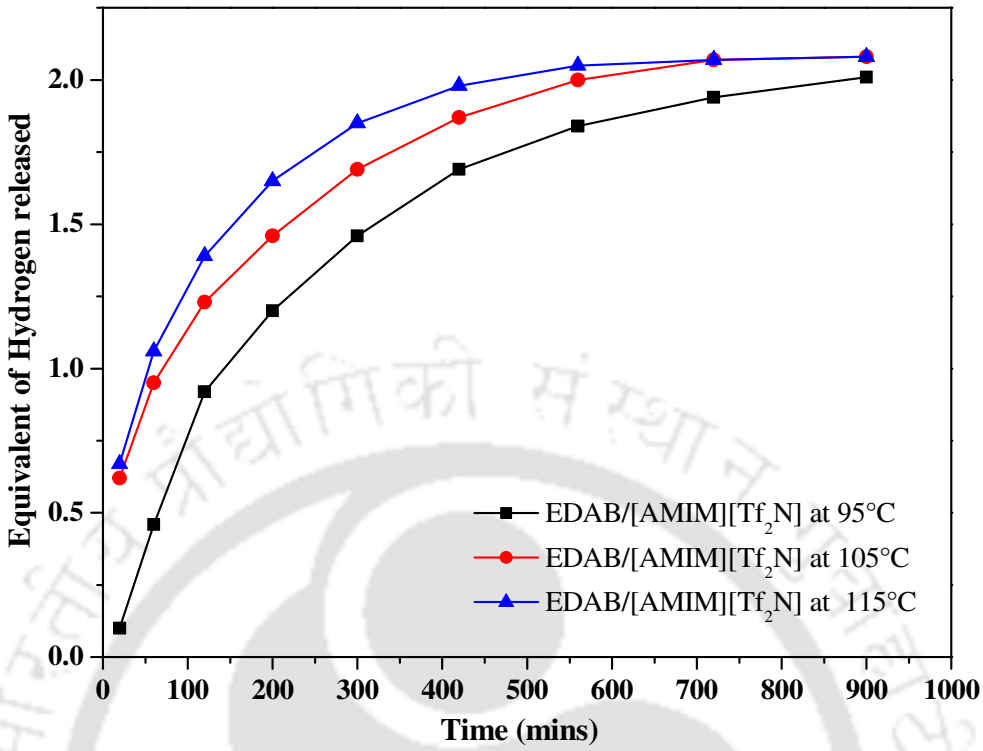

Figure 3.23(b) Equivalent release of hydrogen from EDAB/1-Allyl-3-methylimidazolium bis (trifluoromethylsulfonyl) imide at 95 °C, 105 °C and 115 °C.

TH-1791_136107007

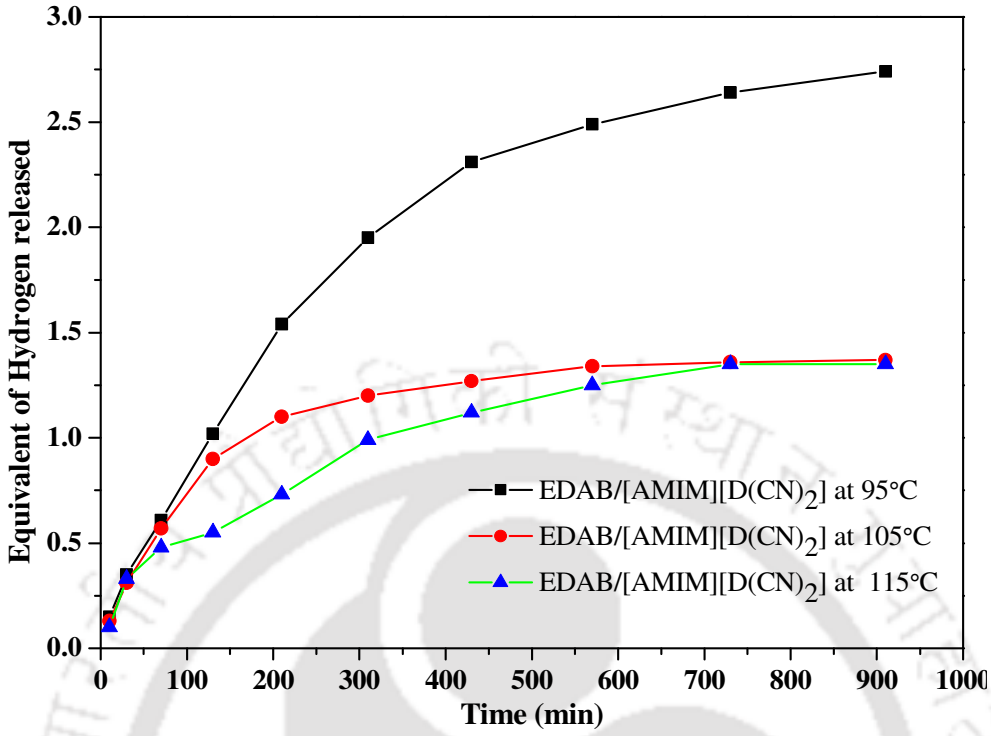

Figure 3.23(c) Equivalent release of hydrogen from EDAB/1-Allyl-3-methylimidazolium dicyanamide at 95 °C, 105 °C and 115 °C.

3.10.2 Kinetic Regression using Avrami-Erofeyev model for Allyl based Ionic Liquids

The hydrogenation was found to be due to the kinetic effect which also agrees with previous work [23]. In order to explain the effects of dehydrogenation, we regressed the experimental kinetic data using the Avrami Erofeyev model [3] in order to obtain the activation energy, rate constant and reaction order. Section 3.2 of this work demonstrates the decomposition of AB in the presence of IL which is a two-step reaction. Avrami Erofeyev model has been used since it is known to predict reaction orders of more than unity [16]. For EDAB + IL mixture, the reaction can be expressed as:

$$S_1 \rightarrow S_2 + \beta_1 H_2 \quad (3.21)$$

$$S_2 \rightarrow S_3 + \beta_2 H_2 \quad (3.22)$$

TH-1791_136107007

$$\frac{d\alpha_1}{dt} = n_1 k_1 (1-\alpha_1)[-\ln(1-\alpha_1)]^{\frac{n_1-1}{n_1}} \quad (3.23)$$

$$\frac{d\alpha_2}{dt} = n_2 k_2 (1-\alpha_2)[-\ln(1-\alpha_2)]^{\frac{n_2-1}{n_2}} \quad (3.24)$$

$$k_1 = k_{10} e^{-\frac{E_1}{RT}} \quad (3.25)$$

$$k_2 = k_{20} e^{-\frac{E_2}{RT}} \quad (3.26)$$

Here α_i is the extent of decomposition for equation 3.21 and 3.22 respectively. While S_1 stands for EDAB, S_2 stands for the intermediate DADB and S_3 for the oligomeric or the residual products. These correspond to β_1 and β_2 equivalents of hydrogen respectively. n_i and k_i represent the order and rate constant for 'i^{th}' reaction, whereas E_1 and E_2 represent the activation energies for reaction (3.21) and (3.22) respectively.

In order to regress the equations, we used the *gamultiobj* function in MATLAB. Using this function, a set of unknowns can be found out iteratively by setting bounds for each parameter. So in our case, at each iteration we computed two quantities namely: (a) cumulative hydrogen production from EDAB + IL mixtures and (b) corresponding decomposition rate per second. Adams-Bashford-Molton method was used to solve the ODE's to find out the decomposition rate per second. This data was then compared with our experimental data to find out the error. Only EDAB/[AMIM][Br] was used for the study as it gave the highest amount of hydrogen upon thermal decomposition. The error was improved by the inbuilt GA subroutine by predicting new sets of parameters or variables. The following seven variables were computed using the function: reaction orders for the two reactions (n_1 and n_2), the activation energies (E_{01} and E_{02}), the temperature independent rate constants (k_{01} and k_{02}) and the equivalents of hydrogen released (β_1/β_2). The results are compiled below (Table 3.10).

TH-1791_136107007

It can be seen that the activation energies for [AMIM][Br] for the Eq. 3.21 increases, while it is the contrary for Eq. 3.22. Hence an operation at 105 °C seems to be an optimized choice. The total equivalents also do agree with the experimental measurement (in parenthesis).Thus it is indeed a kinetic effect as the IL is seen to pronouncedly lower the activation energies for the rate determining step ($S_2 \rightarrow S_3 + \beta_2 H_2$), where S_2 is the intermediate.

Table 3.10 Rate constants for decomposition of EDAB in [AMIM][Br] using Avrami-Erofeyev model.

*( ) represents the equivalent of hydrogen obtained experimentally

T (°C)	β_1	β_2	n_1	n_2	$k_{01} \times 10^{-1}$	$k_{02} \times 10^{-17}$	E_{01} (kJ mol^{-1})	E_{02} (kJ mol^{-1})	Total H_2 Eqs.*
EDAB + 1-allyl-3-methylimidazodium bromide									
95	1.11	0.97	1.02	2.24	0.68	3.90	146.99	157.48	2.08 (2.08)
105	1.93	0.65	1.51	2.92	1.50	3.12	156.01	142.09	2.58 (2.59)
115	1.16	2.12	1.59	2.39	7.35	7.50	162.8	136.42	3.25 (3.25)

TH-1791_136107007

3.10.3 ^{1}H NMR Spectra of EDAB with 1-Allyl-3-Methylimidazolium cation based Ionic Liquids

^{1}H NMR spectra was recorded to study and characterize the pure EDAB, IL and EDAB/IL mixture before and after reactions. A comparative discussion of ^{1}H NMR plots of pure EDAB, IL , EDAB/IL complexes will determine the possible formation of any product after dehydrogenation and further elucidate the role of IL in dehydrogenation. Here the peaks from referred literature [31] were used to locate the peak of our compounds. Figure 3.24(a) shows the ^{1}H NMR study of pure [AMIM][Br] where the chemical shifts of hydrogen in imidazolium ring are identified at 9.35, 7.82 and 7.80 ppm, respectively. The hydrogen atom of N-CH_2 bond is located at 5.29 ppm and N-CH_3 at 3.87 ppm. The chemical shift at 6.01 ppm is attributed to C-H bond, while peaks at 4.90 and 4.89 ppm represent C=CH_2. Figure 3.24(b) shows the NMR spectra of EDAB/[AMIM][Br] (before reaction). From the previous ^{1}H NMR study of pure EDAB, we can identify the BH_3 peak at 1.19 ppm, CH_2 at 2.59 ppm and NH_2 at 5.29 ppm. The remaining chemical shifts of the respective hydrogen atom(s) of the IL remain the same. Figure 3.24(c) represents the NMR spectra of EDAB/[AMIM][Br] (after reaction). Here we observe that there is no change in the initial structure of IL after the dehydrogenation is completed. After the dehydrogenation study of EDAB/[AMIM][Br], it can be concluded that the liberation of hydrogen took place only from EDAB due to the disappearance of peaks of BH_3 as evident from Figure 3.24(c). From this study we can conclude that the IL merely acts as catalyst since their initial structure is retained even after reaction, whereas the absence of BH_3 peaks in EDAB indicates dehydrogenation.

In a similar manner, Figure 3.24(d) represents the ^{1}H NMR study of pure [AMIM][Tf_2N]. The structure of cation namely 1-allyl-3-methylimidazolium remains the same; hence it is the anion which causes change in the spectra. As the anion does not

TH-1791_136107007

possess hydrogen atom, hence the spectra will be similar to [AMIM][Br]. Figure 3.24(e) represents the ^{1}H NMR study of EDAB/ [AMIM][Tf_2N] (before reaction) where the hydrogen peaks of EDAB are shown along with the hydrogen peaks of IL. Figure 3.24(f) represents ^{1}H NMR study of EDAB/[AMIM][Tf_2N] (after reaction) where we can see a similar trend i.e. after the dehydrogenation, the BH_3 bond in EDAB is absent, hence concluding that EDAB takes part in the dehydrogenation process. Likewise [AMIM][$N(CN)_2$] also shows a similar spectra when compared to [AMIM][Br] and [AMIM][Tf_2N]. In a similar manner Figure 3.24(g), 3.24(h) and 3.24(i) shows ^{1}H NMR of pure [AMIM][$N(CN)_2$],^{1}H NMR of EDAB/ [AMIM][$N(CN)_2$] (before reaction) and EDAB/ [AMIM][$N(CN)_2$] (after reaction) respectively. The ^{1}H NMR spectra for the residual product gave a complete disappearance of $–BH_3$ peak for both [AMIM][Br] (Figure 3.24(c)) and [AMIM][Tf_2N] (Figure 3.24(f)). However, the same cannot be said of [AMIM][$N(CN)_2$](Figure 3.24(i)) where $–BH_3$ was visible, while $–CH_2$ peak was not present. So in such a case EDAB may tend to form a cyclic moiety based on sp^2 hybridized boron atom which cannot be isolated in a ^{1}H NMR as in Figure 3.24(i). $–NH_2$ peak is present in all the IL's but with a reduced peak area after dehydrogenation, indicating a partial release of hydrogen. . The mechanism of [AMIM][$N(CN)_2$] here needs further investigation as it might act as a regenerating catalyst because of the basicity of the dicyanamide anion [32]. The solubility trait of the dicyanamide anion tends to depends on its donor ligand property [33].

TH-1791_136107007

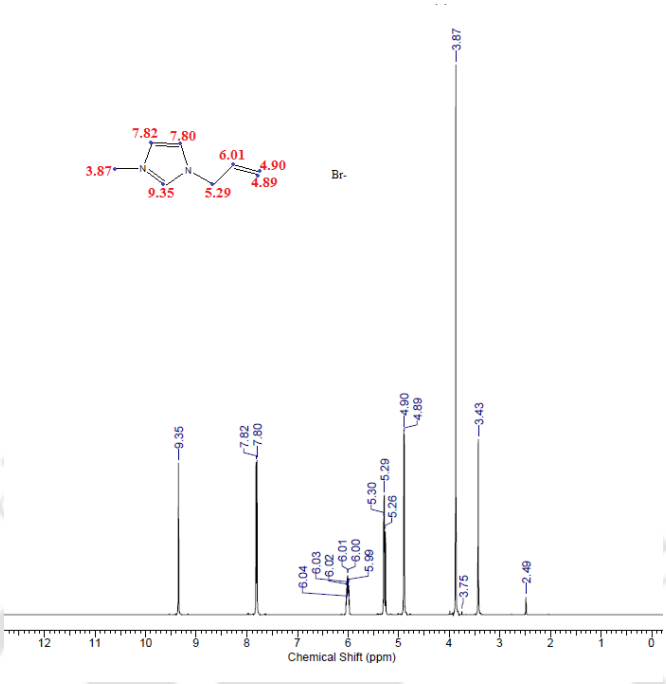

Figure 3.24(a)

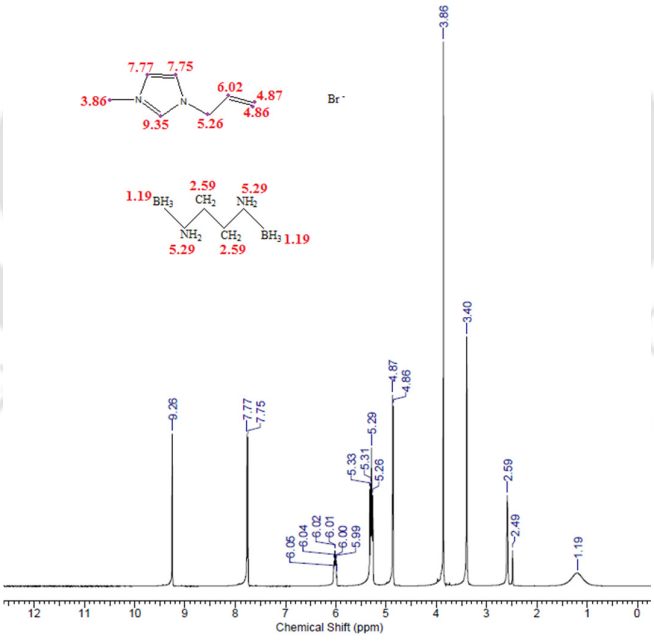

Figure 3.24 (b)

TH-1791_136107007

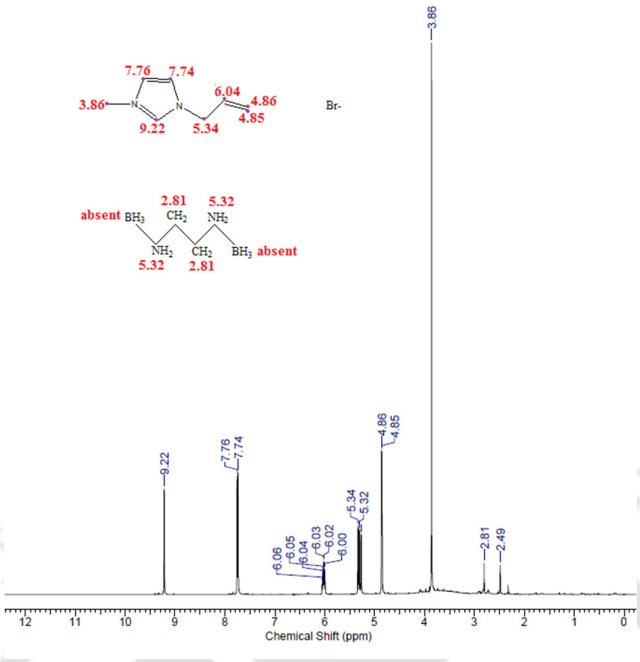

Figure 3.24 (c)

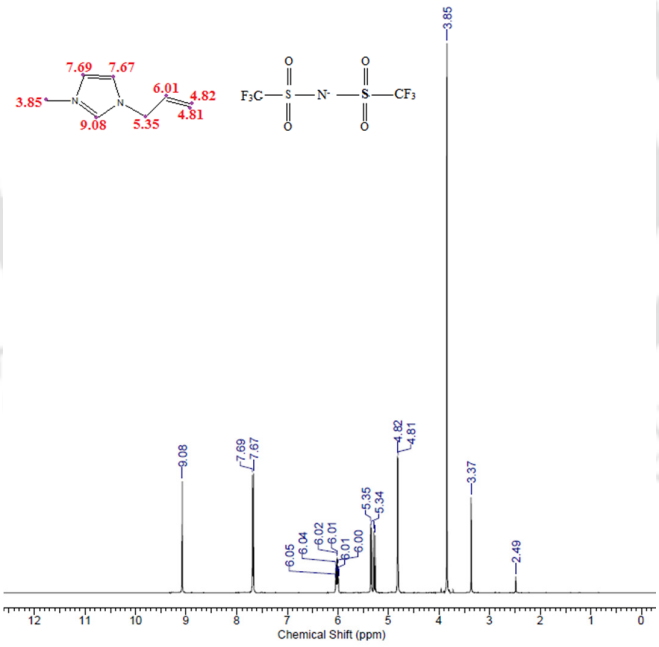

Figure 3.24 (d)

TH-1791_136107007

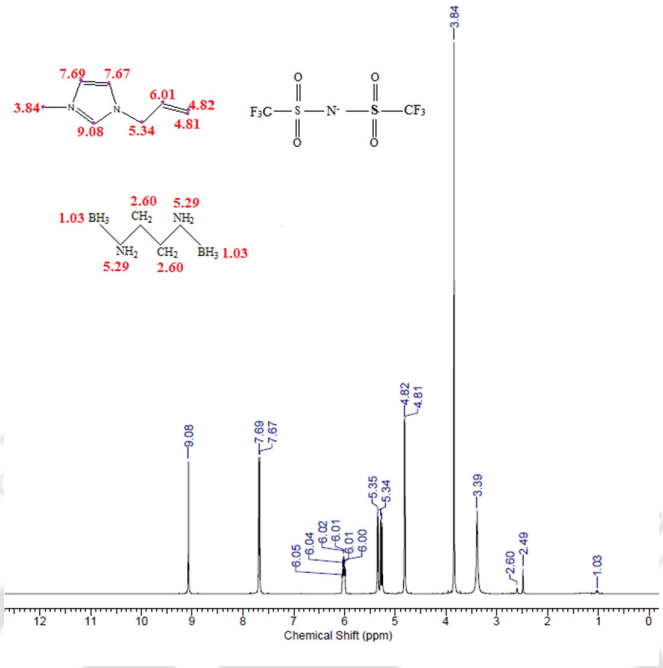

Figure 3.24 (e)

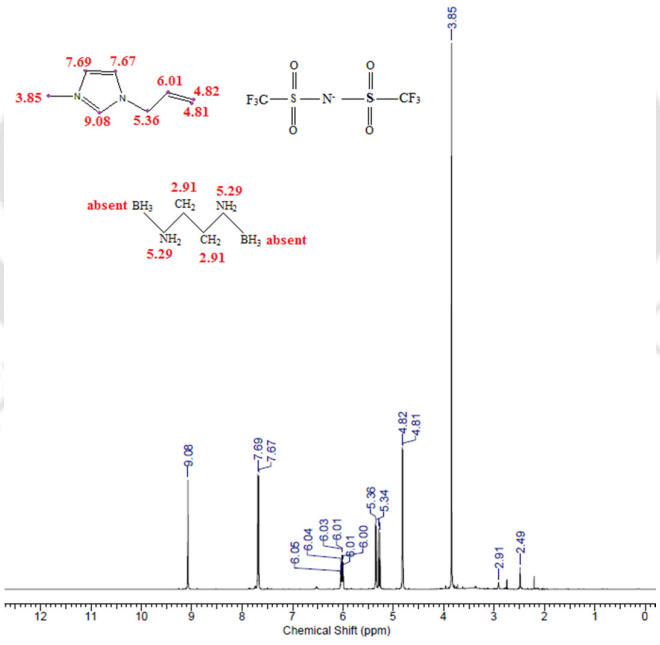

Figure 3.24 (f)

TH-1791_136107007

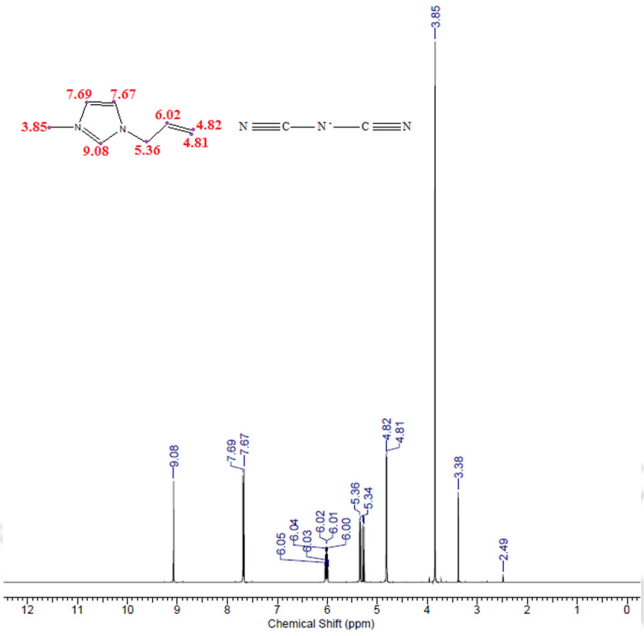

Figure 3.24 (g)

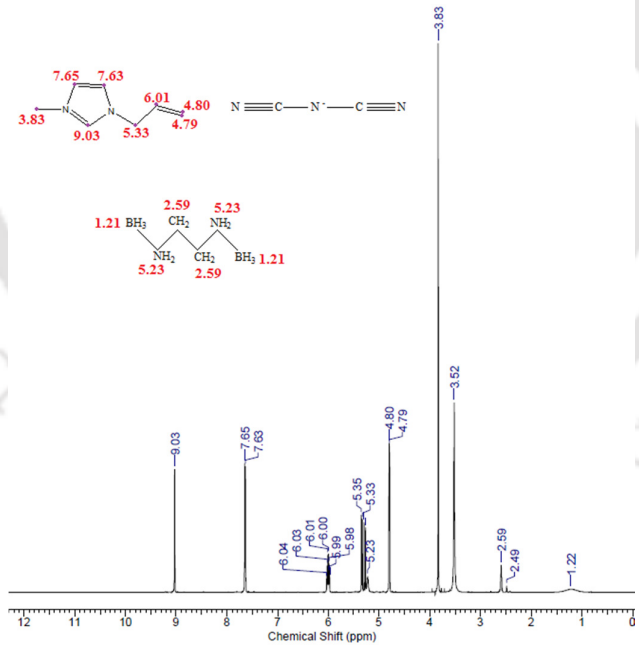

Figure 3.24 (h)

TH-1791_136107007

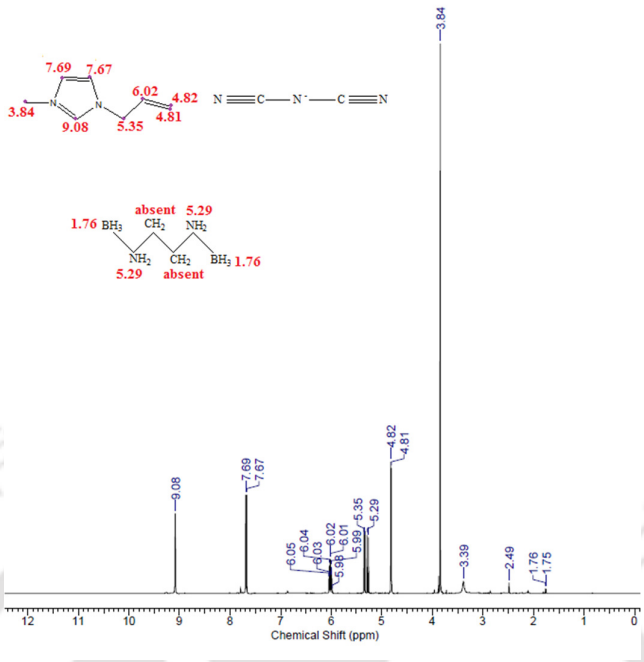

Figure 3.24 (i)

Figure 3.24 Plot for ^{1}H NMR**:**(a) pure [AMIM][Br] (b) EDAB/[AMIM][Br] (before reaction) (c) EDAB/[AMIM][Br] (after reaction),(d) pure [AMIM][Tf_2N], (e) EDAB/ [AMIM][Tf_2N] (before Reaction) and (f) EDAB/ [AMIM][Tf_2N] (after Reaction), (g) pure [AMIM][$N(CN)_2$] , (h)EDAB/ [AMIM][$N(CN)_2$] (before reaction) , (i) EDAB/ [AMIM][$N(CN)_2$] (after reaction).

3.10.4 ^{11}B NMR Spectra of EDAB with 1-Allyl-3-Methylimidazolium Bromide based Ionic Liquids

^{1}H NMR only throws insights into the shielding and deshielding effects of the hydrogen atoms in EDAB-IL complexes. Hence a need is also felt to understand the boron moieties within EDAB. ^{11}B NMR spectra were recorded on samples both before the reaction and the after reaction. This has been performed on the IL: [AMIM][Br] due to its highest hydrogen release. Further it should be noted that the 1-allyl-3-methylimidazolium cation based ILs do not possess boron species which in turn will not interfere with the

TH-1791_136107007

Boron atoms in EDAB. Figure 3.25(a) represents the ^{11}B NMR spectra EDAB/[AMIM][Br] before reaction. The sp^3 -BH_3 functional group can be assigned to the chemical shift at -19.83 ppm which agrees with literature [21]. After dehydrogenation, a chemical shift helps in the formation of sp^2 trigonal boron entity which is assigned at 20.14 ppm. It is to be noted that a negative side of the scale depicts the sp^3 BH and BH_3 attachment. For dehydrogenation experiments a peak at -39 ppm is assigned to BH_4 which is an intermediate and -10 ppm for asymmetric BH_2 resonance. However, in the residual product (Figure 3.25(b)), a chemical shift of 20.14 is seen. This can be assigned to the sp^2 trigonal boron. Similarly the peak at -1.47 ppm can be assigned to N-BN-N borons resulting from chain branched polymeric structures [4]. Hence the peaks after dehydrogenation nullify the possibility of having BH_4 and asymmetric BH_2 in the final product. This is due to the fact that the intermediate formation is a fast reaction which happens during the course of the reaction. This can be detected with in-situ measurements which is beyond the scope of this work. However, for a detailed mechanism, we shall attempt to join the observation with the ReaxFF simulations in the later section.

TH-1791_136107007

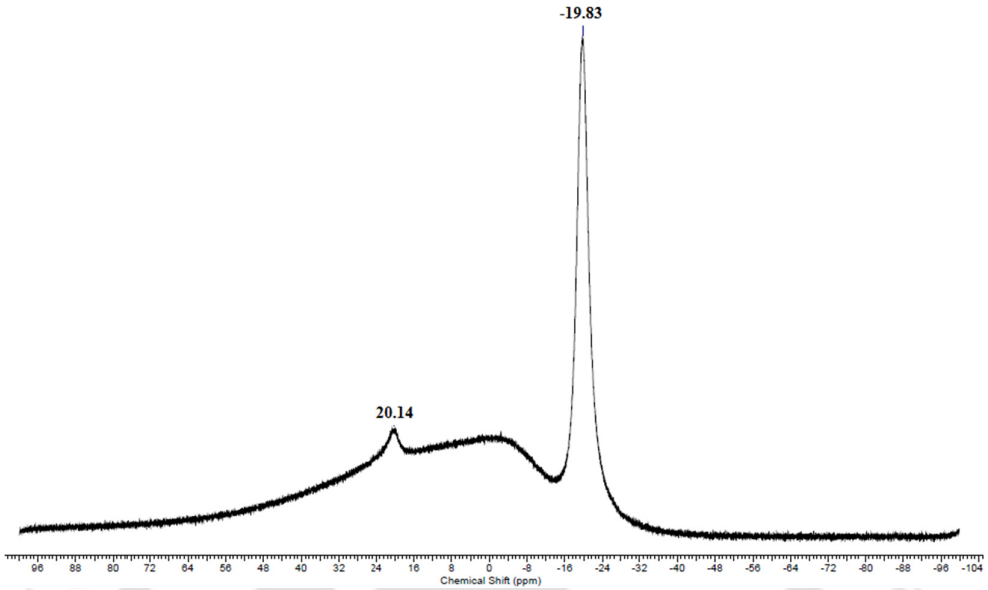

Figure 3.25(a)

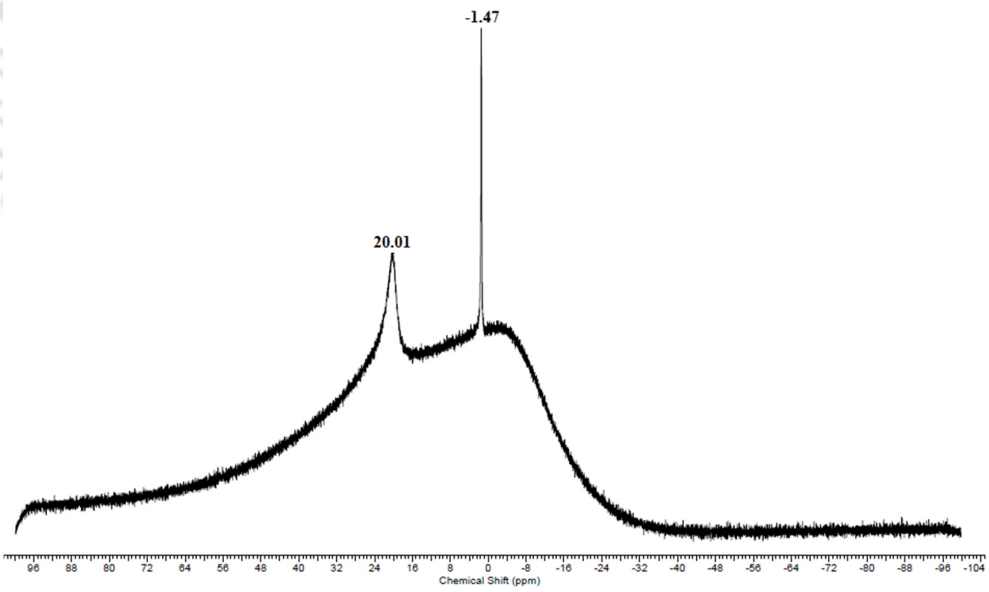

Figure 3.25(b)

Figure 3.25 Plots for ^{11}B NMR: (a) EDAB/[AMIM][Br] (before reaction), and (b) EDAB/[AMIM][Br] (after reaction)

TH-1791_136107007

3.10.5 TGA Analysis of EDAB with 1-Allyl-3-Methylimidazolium cation based IL

For confirming the thermal stability of the reacting mixture, TGA analysis was carried out on both pure EDAB as well as EDAB/IL complexes. Figure 3.26(a) represents the TGA profiles of EDAB, EDAB/[AMIM][Tf_2N] , EDAB/[AMIM][Br] and EDAB/ [AMIM][$N(CN)_2$].The black line represents EDAB, while the orange, blue and pink dotted lines represents the TGA profiles of EDAB/[AMIM][Tf_2N] , EDAB/[AMIM][Br] and EDAB/ [AMIM][$N(CN)_2$] respectively. On considering the weight loss behavior of pure EDAB, we can state that EDAB shows a negligible weight loss till 106 °C, which confirms the melting point of EDAB. EDAB is seen to depict an induction period as the weight loss remains constant. However, an intensive mass loss is being recorded from 106 °C to 150 °C where the entire EDAB is consumed. On comparison with EDAB/IL complexes, we can see that the major weight loss starts from 250 °C which is downwards (except for the EDAB/ [AMIM][$N(CN)_2$]) which proves that in the experimental studies, it is the EDAB that is going through the thermal dehydrogenation process. From the TGA profiles of EDAB and EDAB/IL complexes, the H_2 liberation with ILs is immediately observed from the slope of TGA lines with no induction period. This is suppressed by the presence of IL's.

If we now analyze the stability of the EDAB/IL complexes then we can state that, the most stable IL is [AMIM][Tf_2N] followed by EDAB/[AMIM][Br] and [AMIM][$N(CN)_2$]. When considering EDAB/[AMIM][Tf_2N] (orange dotted line) we see that the first mass loss of 12.36% was observed at 368°C and the second major mass loss of 80.52% continues from 368 °C to 465 °C. The residual mass was calculated to be 3.52%. For EDAB/ [AMIM][Br] system (blue dotted line), the first weight loss of 69.87% occurs at 235 °C and the second major weight loss of 16.96% takes place at 400 °C. After the second major loss, there is a gradual loss of around 1.96% when the sample is heated from

TH-1791_136107007

400 °C to 500 °C. For EDAB/[AMIM][Br], further minor desorption takes place at 135 °C with 4.97% mass loss and the second one at 225 °C with corresponding weight loss of 5.12%. The residual mass was calculated to be 1.12%. On observing the slope of EDAB/ [AMIM][$N(CN)_2$] (pink dotted line) we can see that the stability drops down at a higher rate as compared to other IL's. Three consecutive mass loss of 5.15%, 8.76% and 1.21% were observed at relative low temperature of 100 °C, 125 °C and 150 °C respectively. The minor losses confirms that the IL ([AMIM][$N(CN)_2$]) is unstable in comparison to the other two ILs. Further three major mass losses for the same IL were observed from 265 – 500 °C. The most significant was found to be 23.59% at 375°C.

TGA studies on EDAB and EDAB/IL mixtures were done to have an understanding about the thermal stability of the reacting mixtures, however the TGA study of pure ionic liquids were equally important as it would throw light about the thermal performance. The TGA profiles of the pure Ionic liquids were done so as to see at what temperature the IL decomposes and how it affects the dehydrogenation process of EDAB. Figure 3.26(b) represents the TGA profile of Ionic liquid [AMIM][Br] (black dash line) where a major mass loss of 83.67 % where observed between the temperature range of 260 - 375 °C with a residual mass of 9.34%. In case of [AMIM][Tf_2N] (blue dash line) we can observe the similar trend of thermal decomposition where the one and only major mass loss of 85.23% takes place at a temperature of 350 °C to 455 °C. However, like the EDAB/IL mixture, we can also observe the variant behavior of [AMIM][$N(CN)_2$] (red dash line) where the thermal stability of the IL drops quickly in comparison to other two ILs. The first major mass loss of 53.69% takes place at a temperature of 255 °C to 280 °C, followed by the last desorption of 39.90% at 425 °C with residual amount of 6.41%. TGA study furthers confirms that no hydrogen was released from the ILs as none of the above stated IL decomposed before 250 °C. The highest operating temperature for thermal

TH-1791_136107007

dehydrogenation of EDAB with 1-allyl-3-methylimidazolium cation based IL was kept at 115 °C (Figure 3.26(b)).

The experiments were conducted for a wide range of temperature (25-500 °C) as [AMIM][Tf_2N] being a highly stable IL ,goes through a weight loss till 455°C in comparison to the other two IL's. For [AMIM][Br] the range remains almost similar but when compared with EDAB/[AMIM][Br] and pure[AMIM][Br] it is seen that the hydrogen is being released earlier for EDAB/[AMIM][Br]. Thus EDAB/[AMIM][Br] was more thermally stable as a mixture. However, the comparison is only realistic within a temperature range of 25 to 120 °C, since it is these regions where the hydrogen gets evolved from EDAB. It is also a known fact that the melting point of EDAB varies from 116-120 °C. Moreover it is difficult to predict whether EDAB catalyzes the decomposition of the allyl based Ionic Liquids or vice versa at higher temperatures.

TH-1791_136107007

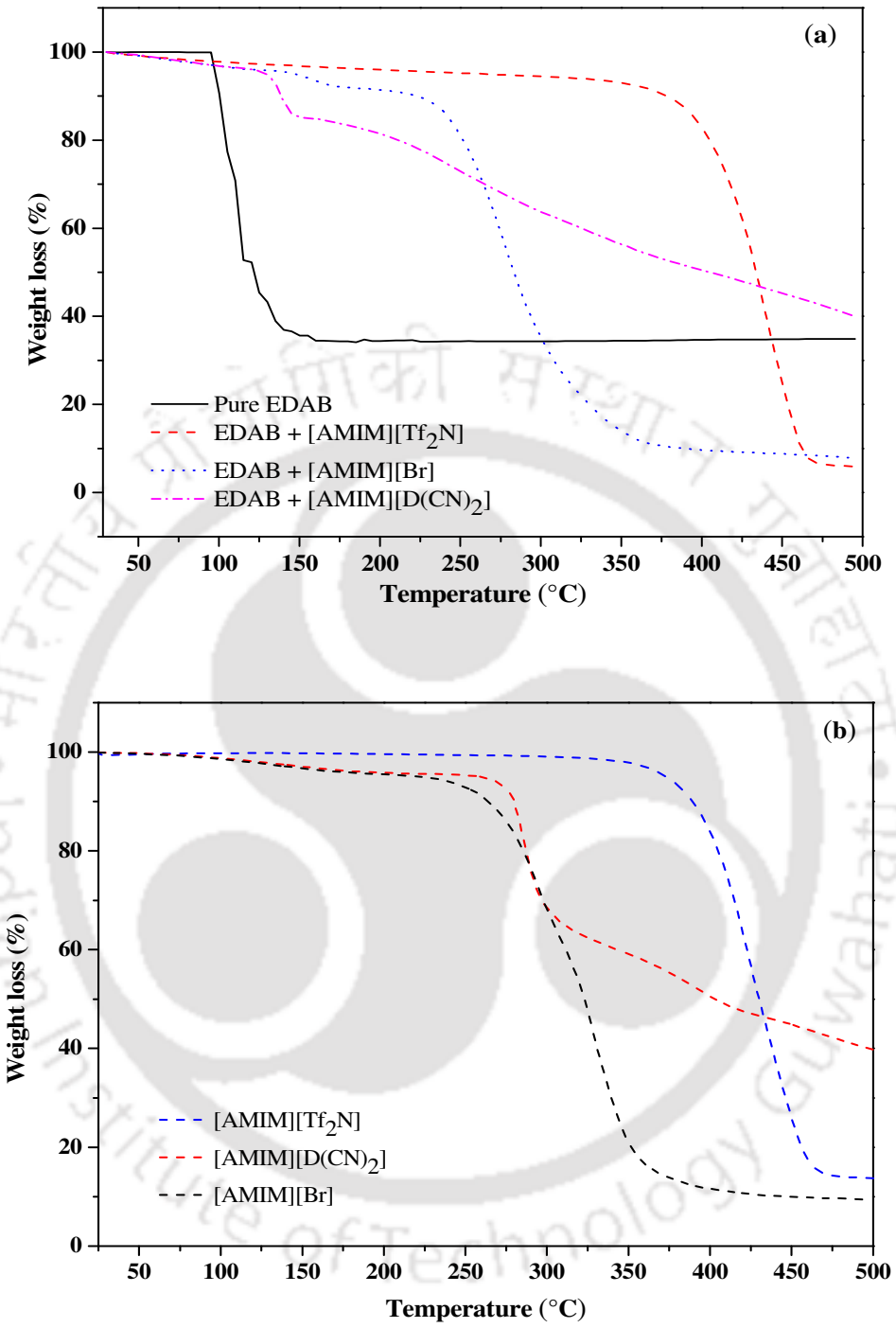

Figure 3.26 (a) TGA profile of pure EDAB, EDAB/ [AMIM][Br], EDAB/[AMIM][Tf_2N] and EDAB/ [AMIM][$N(CN)_2$], (b) TGA profile of pure ILs : [AMIM][Br], [AMIM][Tf_2N] and [AMIM][$N(CN)_2$].

TH-1791_136107007

3.11 Reactive Force Field (ReaxFF)

Recently computational technique such as molecular dynamics (MD) have evolved to evaluate the kinetic mechanisms for chemical reactions. The combination of quantum mechanics (QM) and classical mechanics model has led to the Reactive Force Field MD simulations

(ReaxFF) [34]. ReaxFF is based on the covalent formalism [35] and the bond order principle which relates the bond energy to bond lengths, valence angles, and torsion angle [36]. It is specially designed for large scale chemical system (containing more than a thousand atoms) molecular dynamic simulation. Quantum Mechanics (QM) is used for the derivation of force field parameters which are then directly applied to the system. ReaxFF is highly established on the empirically determined interatomic potentials. Here the potential energy of the system can be related to the different energies of the system equation (3.27) [34, 37].

The unique feature of ReaxFF reactive force field is that it uses "bond order" of inter atomic distance to describe bonds as a function of interatomic energy [38]. This feature allows the continuous breaking and formation of bond as the reaction proceeds. As the reaction proceeds with every iteration (as atom distance changes), the bond order is updated. Thus the sum of partial non-bonded and covalent interaction energy (equation (3.27)) [34] is the total energy of the system.

One of the notable differences between ReaxFF and classical MD is that the charges are to be iterated at every time step. Similarly to classical MD, ReaxFF also has a bonded and a non-bonded potential energy. Bond order correction can be defined as one step correction for 2-body bond order organization. Thus the removal of weak bonds of fully coordinated atoms are implied. Further the over coordination and under-coordination of valence atoms and the correction based on bond orders are used. Similarly, the non-

TH-1791_136107007

bonded van der Waals energy and Coulomb energy terms are derived from the partial charges. The total energy of the system is then the sum of the partial energy distribution terms, which are described by equation (3.27) [34],

$$E_{System} = E_{bond} + E_{over} + E_{under} + E_{val} + E_{pen} + E_{tors} + E_{conj} + E_{vdWalls} + E_{Coulombs} \quad (3.27)$$

Where,

E_{system} = potential energy of the system which describes the interaction between the particles of the systems

E_{bond} = the bond energy due to the interatomic distance between a pair of atoms.

E_{over} and E_{under} = over and under-coordinated energy

E_{val} = valence angle energy for valence angle i–j–k, where i, j, k are location for three atoms

E_{tors} = the torsion energy i.e. the position where bond order tends to zero and greater than one

E_{conj} = the conjugate effect of the molecular energy

$E_{vdWaals}$ = the non-bonded van der Waals interaction

$E_{Coulomb}$ = the coulombic interaction between all atom pairs

E_{bond} calculates the bond order between the interatomic distances, which is given by equation (3.28) [34]

$$E_{bond} = -D_e^{\sigma} BO_{ij}^{\sigma} \exp[p_{be,1}(1-(BO_{ij}^{\sigma})^{pbe,2}] - D_e^{\pi} BO_{ij}^{\pi} - D_e^{\pi\pi} BO_{ij}^{\pi\pi} \quad (3.28)$$

$BO_{ij}^{'}$ is the bond order between a pair of atoms which is obtained directly from the interatomic distances. For e.g. if a pair of atoms like carbon-hydrogen or hydrogen-hydrogen is observed, then σ-bond is accounted; while for carbon-carbon, a bond order of

TH-1791_136107007

three results in one sigma and two π-bonds. Here $p_{be,1}, p_{be,2}$, D_e^{π} and $D_e^{\pi\pi}$ are force field parameters. Hence the total bond order is given by

$$BO_{ij}^{'} = BO_{ij}^{\sigma} + BO_{ij}^{\pi} + BO_{ij}^{\pi\pi} = \exp\left[p_{bo,1}\left(\frac{r_{ij}}{r_0^{\sigma}}\right)^{p_{bo,2}}\right] + \exp\left[p_{bo,3}\left(\frac{r_{ij}}{r_0^{\pi}}\right)^{p_{bo,4}}\right] + \exp\left[p_{bo,5}\left(\frac{r_{ij}}{r_0^{\pi\pi}}\right)^{p_{bo,6}}\right] \quad (3.29)$$

Here the first, second, and third exponential terms indicate the bond orders due to a single (σ), double (π), and triple (double π) bond order contribution respectively. Each bonding parameter p and bond radii r_o have been parameterized such that atomic distances and bond strength agrees with quantum mechanically predicted values for the same species with distance r_{ij} apart. E_{over} and E_{under} represents over- and under- coordinated energy, respectively. A degree of over coordination with respect to its valency may occur after the correction of the original bond order. So to prevent this physical phenomenon of non-valence electrons get drawn into bonding, ReaxFF penalizes it in the form of E_{over} which is given below:

$$E_{over} = p_{over}\Delta_i\left(\frac{1}{1+\exp(\lambda_6\Delta_i)}\right) \quad (3.30)$$

Where, $\Delta_i^{'} = \sum_{j=1}^{nbond} BO_{ij}^{'} - Val_i$ is the degree of deviation for the sum of the uncorrected bond orders around an atomic center from its valency Val_i. In a similar manner, the under-coordination term is represented as below:

$$E_{under} = -p_{under}\frac{1-\exp(\lambda_7\Delta_i)}{1+\exp(-\lambda_8\Delta_i)}.f_6(BO_{ij,\pi},\Delta_j) \quad (3.31)$$

$$f_6(BO_{ij,\pi},\Delta_j) = \frac{1}{1+\lambda_9\exp(\lambda_9\sum_{j=1}^{neighbors(i)}\Delta_j BO_{ij,\pi})}$$

TH-1791_136107007

Other terms, including E_{val} for valence angle *i-j-k*, (*i*, *j*, *k* are location for three atoms) is given below in equation (3.32).

$$E_{val} = f_7(BO_{ij}) f_7(BO_{jk}) f_8(\Delta_j)(\mathrm{k}_a - \mathrm{k}_a \exp[-\mathrm{k}_b(\Theta_0 - \Theta_{ijk})^2]) \quad (3.32)$$

Where,

$$f_7(BO_{ij}) = 1 - \exp(\lambda_{11} BO_{ij}^{\lambda_{12}})$$

$$f_8(\Delta_j) = \frac{2 + \exp(\lambda_{13}\Delta_j)}{1 + \exp(-\lambda_{13}\Delta_j) + \exp(\mathrm{p}_{v,1}\Delta_j)} \left[\lambda_{14} - (\lambda_{14} - 1) \left(\frac{2 + \exp(\lambda_{15}\Delta_j)}{1 + \exp(-\lambda_{15}\Delta_j) + \exp(-\mathrm{p}_{v,2}\Delta_j)} \right) \right]$$

BO_{ij}, BO_{jk} are the bond orders for each of the two bonds connecting the three atoms within an angle. k_a and k_b are the harmonic force constants that determine the depth and width of the angular potential, Θ_0 and Θ_{ijk} are equilibrium and valence angle respectively. It implies that even if one of the two bonds in the angle break, the valence angle energy disappears smoothly. Thus the energy contribution from the valence angle term goes to zero as the bond orders in the valence angle goes to zero.

E_{pen} is penalty energy and it is used to stabilize the system with two double bonds sharing an atom in a valence angle. The equation is given below.

$$E_{pen} = \lambda_{19} f_9(\Delta_j) \exp[-\lambda_{20}(BO_{ij} - 2)^2] \exp[-\lambda_{20}(BO_{jk} - 2)^2] \quad (3.33)$$

Where $f_9(\Delta_j) = \dfrac{2 + \exp[-\lambda_{21}\Delta_j]}{1 + \exp[-\lambda_{21}\Delta_j] + \exp[\lambda_{22}\Delta_j]}$

E_{tor} (Equation (3.34)) represents the torsion energy i.e. the position where bond order tends to zero and is greater than one.

TH-1791_136107007

$$E_{tor} = f_{10}(BO_{ij}, \mathrm{BO}_{jk}, \mathrm{BO}_{kl}) \sin\Theta_{ijk} \sin\Theta_{jkl}$$
$$\left[\frac{1}{2}V_1\left(1+\cos\omega_{ijkl}\right)+\frac{1}{2}V_2 \exp\left[p_{tor1}(BO_{jk}-1+f_{11}(\Delta_j,\Delta_k))^2\right](1-\cos 2\omega_{ijkl})+\frac{1}{2}V_3\left(1+\cos 3\omega_{ijkl}\right)\right]$$

(3.34)

Where,

$$f_{10}(BO_{ij}, \mathrm{BO}_{jk}, \mathrm{BO}_{kl}) = (1-\exp[-\lambda_{23}BO_{ij}])(1-\exp[-\lambda_{23}BO_{jk}])(1-\exp[-\lambda_{23}BO_{kl}])$$
$$f_{11}(\Delta_j,\Delta_k) = \frac{2+\exp[-\lambda_{24}(\Delta_j+\Delta_k)]}{1+\exp[-\lambda_{24}(\Delta_j+\Delta_k)+\exp[-\lambda_{25}(\Delta_j+\Delta_k)]}$$

This contribution smoothly disappears when one of the bonds in the torsion angle breaks or the valence angle approaches π. The torsion angle is denoted as ω_{ijkl}. E_{conj} is denoted as conjugate effect of the molecular energy, especially for the aromatic molecules where successive bond have bond order values of 1.5. The conjugate energy is given by:

$$E_{conj} = f_{12}(BO_{ij}, \mathrm{BO}_{jk}, \mathrm{BO}_{kl})\lambda_{26}[1+\left(\cos^2\omega_{ijkl}-1\right)\sin\Theta_{ijkl}\sin\Theta_{jkl}] \quad (3.35)$$

Where,

$$f_{12}(BO_{ij}, \mathrm{BO}_{jk}, \mathrm{BO}_{kl}) = \exp\left[\lambda_{27}\left(BO_{ij}-1\frac{1}{2}\right)^2\right]\exp\left[\lambda_{27}\left(BO_{jk}-1\frac{1}{2}\right)^2\right]\exp\left[\lambda_{27}\left(BO_{kl}-1\frac{1}{2}\right)^2\right]$$

Next is $E_{vdWaals}$ which is the one of the penultimate term for non-bonded van der Waals interaction. This term avoids excessive high repulsion between bonded atoms or atoms sharing a valence angle. The van der Waals interaction energy is given below:

$$E_{vdWalls} = D_{ij}\left\{\exp\left[\alpha_{ij}\left(1-\frac{f_{13}(r_{ij})}{r_{vdW}}\right)\right]-2\exp\left[\frac{1}{2}\alpha_{ij}\left(1-\frac{f_{13}(r_{ij})}{r_{vdW}}\right)\right]\right\} \quad (3.36)$$

$$f_{13}(r_{ij}) = \left[r_{ij}^{\lambda_{29}}+\left(\frac{1}{r_\omega}\right)^{\lambda_{28}}\right]^{1/\lambda_{28}}$$

Here, $\alpha_{ij,\ rvdW}$ represents the van der Waals parameter.

TH-1791_136107007

$E_{Coulomb}$ represents Coulomb interaction between all atom pairs. A shielded Coulomb potential is used as adjustment for orbitals overlapping between close distances atoms.

$$E_{Coulomb} = C\frac{q_i q_j}{\left\{r_{ij}^3 + \left(\frac{1}{\gamma_{ij}}\right)^3\right\}^{1/3}} \quad (q_i,\ q_j \text{ are atomic charges}) \qquad (3.37)$$

Where γ_{ij} represents the shielded Coulomb potential which can be optimized to reproduce the charge equilibration for orbital overlap correction. Combining all the above stated expressions have led us to the formation of total energy of the system in ReaxFF force field (eq 3.27). The pictorial description is given in Figure 3.27.

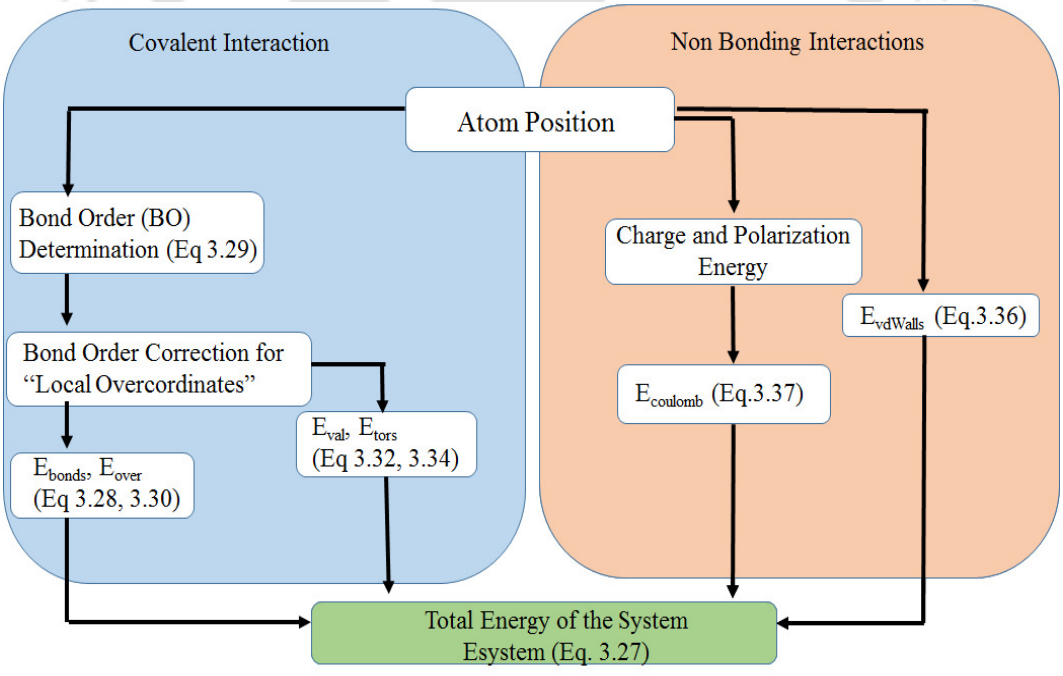

Figure 3.27 Overview of total energy of the system in ReaxFF reactive force field [37].

TH-1791_136107007

3.11.1 Pyrolysis Study of EDAB

In our study, ReaxFF was used to predict the possible intramolecular pathway of dehydrogenation of EDAB. The study will not only shed light on the pathway but also about other possible byproducts that can evolve if complete dehydrogenation of EDAB is carried out at high temperature. Since AB and EDAB is from a similar family we initiated the ReaxFF study on AB oxidation work to develop a kinetic mechanism as outlined in a previous work [39].

ReaxFF simulation were carried out in the SCM suite [40] of programs. 30 molecules of optimized EDAB molecules were placed randomly inside a periodical box size of 25 × 25 × 25 Å. The force field defined for such a reactive simulation is C/H/O/N/S/B [41-42]. The system was first minimized at 10 K at a time step of 0.25 fs. The process is a non-reactive process in which the system is validated with the intermolecular potential so as to reduce any overlap of assembly of atoms. Initially a number of NVE simulations with different time steps were performed to find the correct time step. The time step which helped in the conservation of energy were adopted for the subsequent minimization and production stages. The equilibration (non-reactive) were then carried out in a NVT ensemble for 12.5 ps with a time step of 0.1 fs. The production run then proceeds with NVT-MD simulation with a time step of 0.25 fs. The temperature of the system was maintained at 1000 K (for the reaction mechanism).However, high temperature simulations of around 2500 K- 5000 K is usually preferred so as to obtain computational affordable results with greater accuracy. Obviously this will lead to a bias with respect to high entropic reactions. However, previous results [41-42] have suggested it has no effect on the reaction mechanism but only alters the rate of the reaction. The

TH-1791_136107007

temperature here is controlled via Berendsen thermostat [43] with a damping constant was 0.5 ps. The total time kept was 250 ps to study the dehydrogenation process.

The reaction mechanism obtained via ReaxFF force field simulation have been explained in details in Figure 3.30. In this portion we shall discuss the effect of temperature on release of hydrogen. The results of hydrogen released at 1000 K is not considered, as complete dehydrogenation is not observed. This is due to the fact that the order of temperature when considered in the ReaxFF domain is not enough for observing the events such as bond breaking and bond formation. This is the reason we shall now explore the temperature range 2500-5000 K.

Figure 3.28 represents the pyrolysis studies of EDAB from 2500-5000 K. From Figure 3.28, we can see that T=2500 K is the most optimized temperature as we can see a steady growth of hydrogen liberation. We can also see the induction period of EDAB and the simultaneous liberation of hydrogen and degradation of EDAB (Figure 3.29). The probable by product gases which can be obtained from experiment have been listed in Table 3.11.

TH-1791_136107007

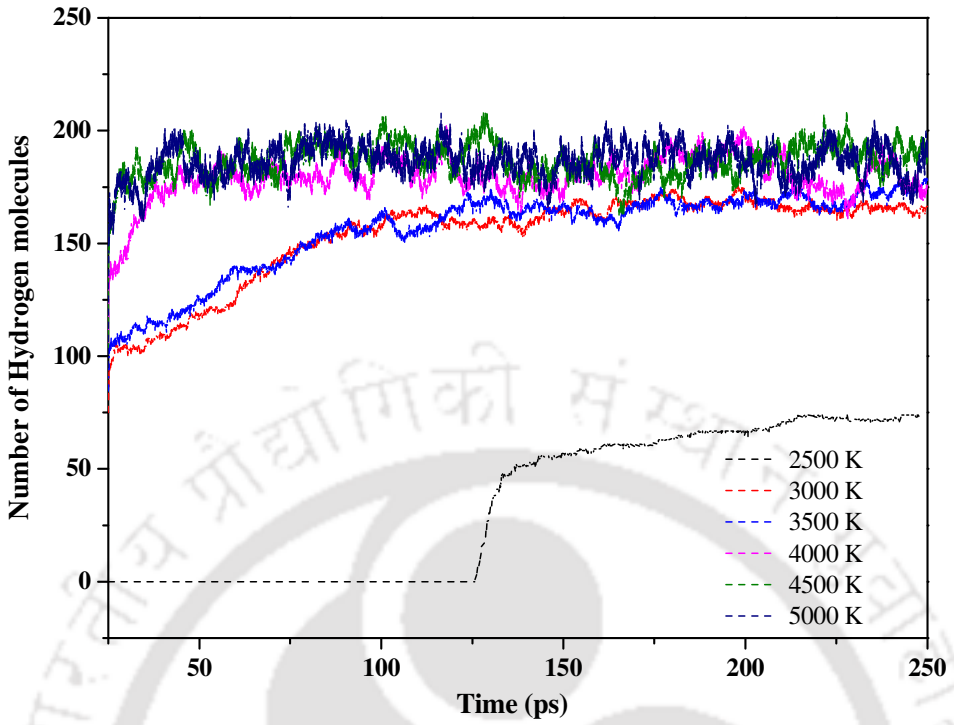

Figure 3.28 The release of H_2 at different temperature ranging from 2500 K to 5000 K

Table 3.11 Major byproduct gases released

2500K		3000K		3500K		4000K		4500K		5000K	
BH_3	16	BH_3	16	BH_3	14	BH_3	12	BH_3	9	BH_3	10
NH_3	13	NH_3	11	NH_3	16	NH_3	14	NH_3	17	NH_3	15
CH_4	4	CH_4	15	CH_4	19	CH_4	21	CH_4	21	CH_4	15

TH-1791_136107007

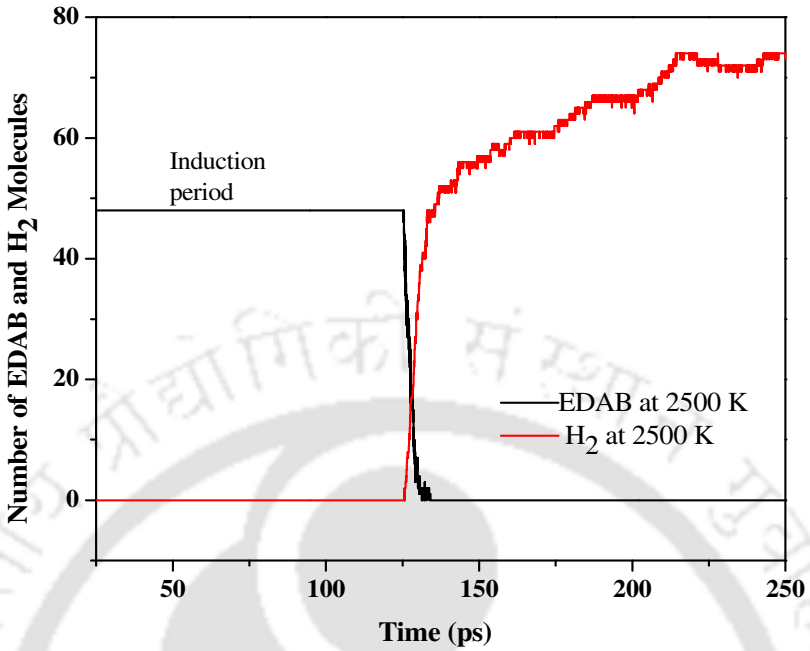

Figure 3.29 Detailed pyrolysis study of EDAB at 2500 K.

3.11.2 Reaction mechanism as proposed by using ReaxFF Force Field

Here the total time kept was at 250 ps to study the dehydrogenation process. After the simulation, the trajectory of all the molecules and intermediates were visualized within all the trajectories for EDAB dehydrogenation. It was observed that the hydrogen was found to evolve from the -BH_3 functional end of EDAB (Figure 3.30). The first abstraction in the hydrogen atom is observed at around 18.18 ps when EDAB releases its hydrogen atom(s).The hydrogen then rejoins it at the other end of -BH_3 group in EDAB. This step is crucial and supports the idea of chain branched polymerization which is also depicted by ^{11}B NMR (-1.47 ppm) (Figure 3.25.b). This step being short lived, quickly takes a form of polymeric cyclic compound which may be attributed to the sp^2 trigonal boron as per ^{11}B NMR spectra. Thereafter, the hydrogen finally detaches itself from the EDAB entity. The

TH-1791_136107007

detachment of hydrogen from rest of the EDAB cluster hence becomes the rate determining step. This mechanism partially supports the reaction mechanism as reported by Leardini et al. [23]. The reaction then goes on till 250 ps to give the residual products formed during the latter part of the experiment. The later end products are not significant because the rate of hydrogen release is highest at the start of the reaction. As observed from the reaction mechanism obtained from ReaxFF study, it can be confirmed that the release of hydrogen follows a two-step process which has been mentioned in section 3.10.2. For the decomposition of EDAB in [AMIM][Br] the following stoichiometry is proposed:

$$C_2H_{14}B_2N_2 \xrightarrow{\Delta} C_2H_{14}B_2N_2 + \beta_1 H_1 \quad (3.37)$$

$$C_2H_{14}B_2N_2 \xrightarrow{\Delta} C_2H_{12}B_2N_2 + \beta_2 H_2 \quad (3.38)$$

Where $C_2H_{14}B_2N_2$ or EDAB represents S_1; $C_2H_{14}B_2N_2$ represents S_2, and β_1 stands for equivalent hydrogen released as given in Equation 3.21. Equation 3.38 is similar to Equation 3.22 where S_3 stands for the oligomeric or the residual products.S_2 and S_3 have the same empirical formula but represents the polymeric cyclic intermediate as shown in Figure 3.30.

TH-1791_136107007

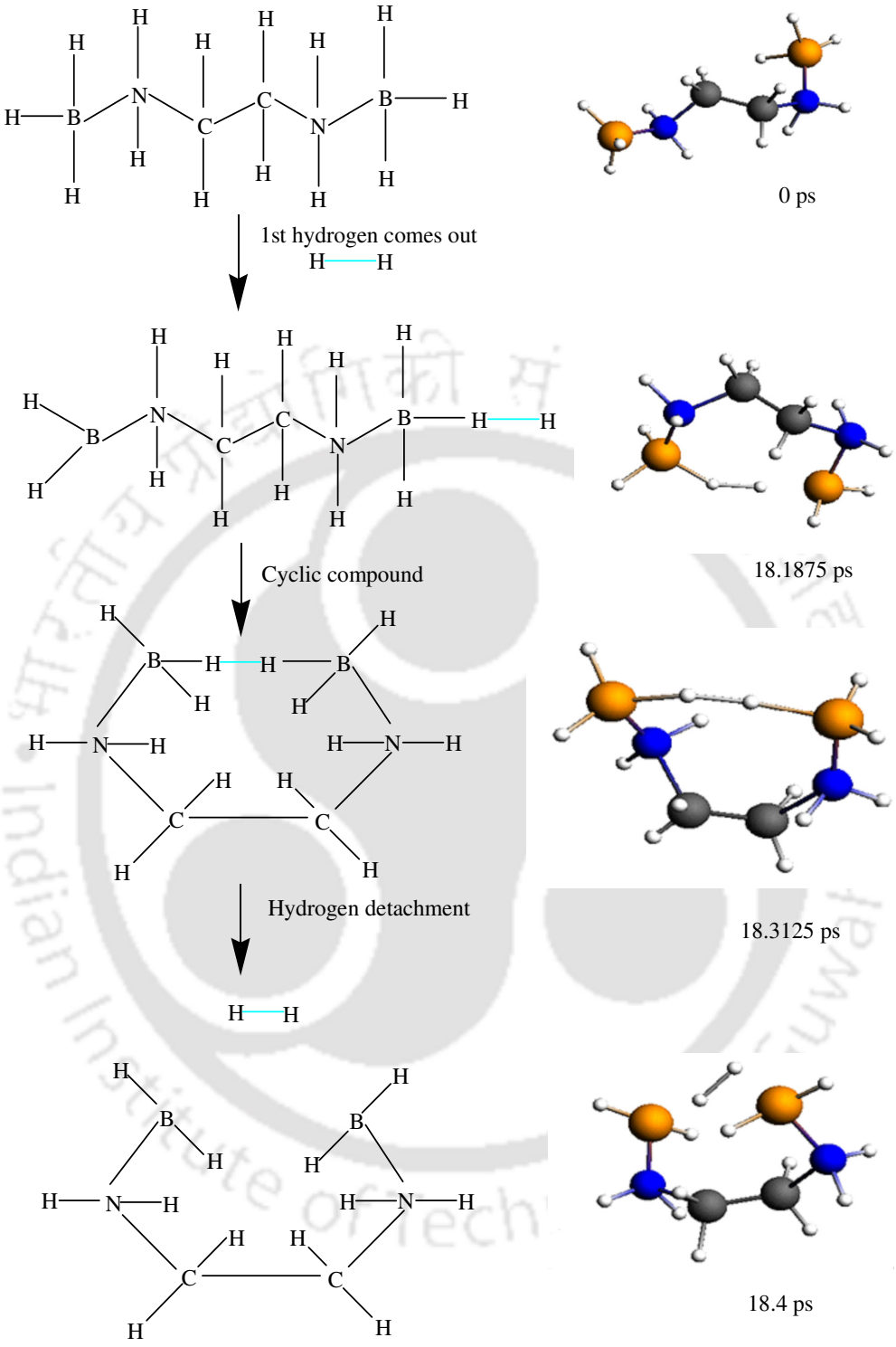

Figure 3.30 Proposed reaction mechanism of EDAB dehydrogenation using ReaxFF

TH-1791_136107007

References:

1. Himmelberger, D.W. Hydrogen Release from Ammonia Borane (Ph D thesis). US: University of Pennsylvania; **2010**. http:// repository.upenn.edu/cgi/view content.cgi/article=1135& context = edissertations [accessed 20.07.14].

2. Logistic Growth Model, https://www.math.duke.edu/education/ccp/materials/diffeq/logistic/logi1.html [accessed 05.08.14].

3. Ahluwalia, R.K.; Peng, J.K.: Hua, T.Q. Hydrogen Release from Ammonia Borane Dissolved in an Ionic Liquid. *Int. J. Hydrogen Energy*, **2011,** 36, 15689-15697.

4. Bluhm, M.E.; Bradley, M.G.: Butterick, R.,III; Kusari, U.; Sneddon, L.G. Amineborane-Based Chemical Hydrogen Storage: Enhanced Ammonia Borane Dehydrogenation in Ionic Liquids. *J.Am.Chem.Soc.* **2006**, 128, 7748-7749.

5. Khezami. L.; Burnham, A.K. Assessment of Various Kinetic Models for the Pyrolysis. *Thermochim Acta.* **2004**, 417, 79-89.

6. Himmelberger, D. W.; Alden, L. R.; Bluhm, M.E.; Sneddon, L.R. Ammonia Borane Hydrogen Release in Ionic Liquids. *Inorg. Chem.* **2009**, 48, 9883–9889.

7. Basu, S.; Zheng, Y.; Gorea, J.P. An Experimental Study of Neat and Ionic Liquid-aided Ammonia Boranethermolysis. *J Power Sour.* **2011**,196, 734-740.

8. Nakagawa, T.; Burrell, A. K.; Del Sesto, R. E.; Janicke, M. T.; Nekimken, A. L.; Purdy,; B. Paik, G. M.; Zhong, R.-Q.; Semelsberger, T. A.; Davis, B. L.; Physical, structural, and dehydrogenation properties of borane in ionic liquids. *RSC Adv*. **2014**, 4, 21681-21687.

9. Shore, S.G.; Parry, R.W. Chemical evidence for the structure of the "diammoniate of diborane." II. The preparation of ammonia-borane. *J Am Chem Soc.* **1958**, 80, 20-24.

10. Najiba, S.; Chen, J.; Drozd, V.; Durygin, A.; Sun, Y. Ammonia borane at low temperature down to 90 K and high pressure up to 15 GPa. *Int. J. Hydrogen Energy.* **2013**, 38, 4628-4635.

11. Kundu, D.; Banerjee, T. Multicomponent vapor-liquid-liquid equilibrium prediction using an a-priori segment based model. *Ind Eng Chem Res*. **2011**, 50, 14090-14096.

12. Ramalingam, A.; Banerjee, T. Quantum chemical studies on the simultaneous interaction of thiophene and pyridine with ionic liquid. *AIChE J*. **2011**, 57, 749-764.

13. Banerjee, T.; Khanna, A. Liquid liquid equilibria for ionic liquid based systems using COSMO-RS: effect of cation and anion combination. *AIChE J.* **2008**, 54, 1874-1885.

14. Schäfer, A.; Horn, H.; Ahlrichs, R. Fully optimized contracted Gaussian basis sets for atoms Li to Kr. *J. Chem. Phys.* **1992**, 97, 2571-2577.

15. Sosa, C.; Andzelm, J.; Elkin, B. C.; Wimmer, E.; Dobbs, K. D.; Dixon, D. A. A Local Density Functional Study of the Structure and Vibrational Frequencies of Molecular Transition-Metal Compounds. *J. Phys. Chem.* **1992**, 96, 6630-6636.

TH-1791_136107007

16. Klamt, A. Conductor-like Screening Model for Real Solvents: A New Approach to the Quantitative Calculation of Solvation Phenomena. *J. Phys. Chem.* **1995**, 99, 2224-2235.

17. Stephens, F.H.; Pons V.; Tom Baker, R. Ammonia–borane: the hydrogen source par excellence?. *Dalton Trans.* **2007**, 2613–2626.

18. Al-Kukhum, A.; Hwang, H.T.; Varma, A. A Comparison of Ammonia Borane Dehydrogenation Methods for Proton-Exchange-Membrane Fuel Cell Vehicles: Hydrogen Yield and Ammonia Formation and Its Removal. *Ind. Eng. Chem. Res*. **2011**, 50, 8824–8835.

19. Halseid, R.; Vie, P.J.S.; Tunold, R. Effect of ammonia on the performance of polymer electrolyte membrane fuel cells. *J Power Sour*. **2006**, 154, 343–350.

20. Sahler, S.; Sturm, S.; Kessler, M. T.; Prechtl, M. H. G. The Role of Ionic Liquids in Hydrogen Storage. *Chem Eur. J.,* **2014**, 20, 8934-8941.

21. Neiner, D.; Karkamkar, A; Bowden, M.; Choi, Y. J.; Luedtke, A.; Holladay, J.; Fisher, A.; Szymezak N.; Autrey, T. Kinetic and thermodynamic investigation of hydrogen release from ethane 1,2-di-amineborane. *Energy Environ. Sci.* **2011**, 4, 4187–4193.

22. Sahler, S.; Konnerth, H.; Knoblauch, N.; Prechtl, M.H.G. Hydrogen storage in amine boranes: Ionic liquid supported thermal dehydrogenation of Ethylene DiAmine bisBorane. *Int. J. Hydrogen Energy*, **2013**, 38, 3283-3290.

23. Leardini, F.; Valero-Pedraza, M. J.; Perez-Mayoral, E.; Cantelli, R.; Bañares, M. A. Thermolytic Decomposition of Ethane 1,2-Diamineborane Investigated by Thermoanalytical Methods and in Situ Vibrational Spectroscopy. *J. Phys. Chem. C.* **2014**, 118, 17221−17230.

24. Anantharaj, R.; Banerjee, T. Liquid–liquid equilibria for quaternary systems of imidazolium based ionic liquid+ thiophene+ pyridine+ iso-octane at 298.15 K: experiments and quantum chemical predictions *Fluid Phase Equilib.,* **2011**, 312, 20-30.

25. Banerjee, B.; Kundu, D.; Pugazhenthi, G.; Banerjee, T. Quantum chemical and experimental insights for the ionic liquid facilitated thermal dehydrogenation of Ethylene DiAmine bisBorane . *RSC. Adv.* **2015**, 5, 85280-85290.

26. Rabari, D.; Banerjee, T. Biobutanol and n-propanol recovery using a low density phosphonium based ionic liquid at T = 298.15 K and p = 1 atm. *Fluid Phase Equilib.,* **2013**, 355, 26-33.

27. Grant, D.J.; Matus, M.H.; Anderson, K.D.; Camaioni, D.M.; Neufeldt, S.R.; Lane, C.F. Thermochemistry for the dehydrogenation of methyl-substituted ammonia borane compounds. *J Phys Chem A.,* **2009**,113, 6121-6132.

28. Jessop, P. G.; Jessop, D. A.; Fu, D.; Phan, L. Solvatochromic parameters for solvents of interest in green chemistry. *Green Chem.* **2012,** *14,* 1245-1259.

29. Carpenter, J.D.; Ault, B.S. Infrared Matrix Isolation Characterization of Aminoborane and Related Compounds. *J.Phys.Chem.* **1991**, 95, 3502-3506.

TH-1791_136107007

30. Banerjee, T.; Verma, K.K.; Khanna, A. Liquid–Liquid Equilibrium for Ionic Liquid Systems Using COSMO-RS: Effect of Cation and Anion Dissociation. *AIChE J.* **2008**, 54, 1874-1885.

31. Furukawa, S.; Inoue, N.; Ishioka,T.; Furuya K.;Harata, H. Rapid Decomposition of Cellulose Dissolved in Ionic Liquid Using Gas–Liquid Interface Discharge. *Jpn. J. Appl. Phys.* **2012**, 51, 070205-1-3

32. Forsyth, S. A.; MacFarlane, D. R.; Thomson, R. J.; Itzstein M. V. Rapid, clean, and mild O-acetylation of alcohols and carbohydrates in an ionic liquid. *Chem.Comm*. **2002**, 7,714-715.

33. MacFarlane, D. R.; Golding,J,; Forsyth, S,; Forsyth, M,; Deacon, G. B. Low viscosity ionic liquids based on organic salts of the dicyanamide anion, *Chem.Comm*. **2001**, 16, 1430-1431.

34. Van Duin. A.C.T.; Dasgupta. S.; Lorant. F.; Goddard. W.A. ReaxFF: A Reactive Force Field for Hydrocarbons. *J. Phys. Chem. A.,* **2001**, 105, 9396– 9409.

35. Tersoff. J. New empirical approach for the structure and energy of covalent systems, *Phys. Rev. B.* **1988**, 37, 6991-7000

36. Brenner. D. W. Empirical potential for hydrocarbons for use in simulating the chemical vapor deposition of diamond films, *Phys. Rev. B.* **1990**, 42, 9458-9471.

37. Senftle. T. P.; Hong. S.; Islam. M. M.; Kylasa. S. B.; Zheng. Y.; Shin. Y. K.; Junkermeier. C.; Engel-Herbert. R.; Janik. M. J.; Aktulga. H. M.; Verstraelen. T.; Grama. A.; van Duin. A.C.T. The ReaxFF reactive force-field: development, applications and future directions, *npj Computational Materials*, **2016**, 2, 15011-15025.

38. Zheng. M.; Li. X.; Liu. J.; Guo. L. Initial chemical reaction simulation of coal pyrolysis via ReaxFF molecular dynamics, *Energy Fuels,* **2013,** 27, 2942-2951.

39. Weismiller. M.R.; Russo Jr. M.F.; Van Duin. A.C.T.; Yetter. R.A. Using molecular dynamics simulations with a ReaxFF reactive force field to develop a kinetic mechanism for ammonia borane oxidation. *Proceedings of the Combustion Institute.* **2013**, 32, 3489–3497

40. *Scientific Computing & Modelling (SCM). ADF; SCM, Theoretical Chemistry*, Vrije Universiteit: Amsterdam, Netherlands, **2013**,*http://www.scm.com.*

41. Weismiller, M. R.; Van Duin, A. C. T.; Lee, J.; Yetter, R. A. Reactive Force Field Development and Applications for Molecular Dynamics Simulations of Ammonia Borane Dehydrogenation and Combustion. *J. Phys. Chem. A*, **2010**, 114, 5485-5492.

42. Kamat, A.M.; Van Duin, A. C. T.; Yakovlev, A. Simulations of Laser-Induced Incandescence of Soot Using an Extended ReaxFF Reactive Force Field. *J. Phys. Chem. A.* **2010,** 114, 12561–12572.

43. Berendsen, H.J.C.; Postma, J.P.M.; van Gunsteren, W.F.; DiNola, A.; Haak, J.R. Molecular dynamics with coupling to an external bath, *J. Chem. Phys*. **1984**, 81, 3684–3690.

TH-1791_136107007

Chapter 4: Conclusions and Future Work

TH-1791_136107007

TH-1791_136107007

4.1 Conclusions

The knowledge gap from the available literature in Chapter 1 have helped us in shaping up the objectives of the thesis. Overall two strategies has been used to model the reaction kinetics namely growth propagation model and Avrami Erofeyev type model for the single and two step reaction mechanism for thermal dehydrogenation. It was found that the growth propagation model and Avrami Erofeyev type model gave the best predictions for AB and AB-IL mixture, respectively. The values of parameters of reaction kinetics for AB + IL mixtures confirm lower activation energies for AB-IL systems when compared to AB as a standalone basis. However, there was less change in the values of activation energy for various IL combinations. All the IL's gave a uniform hydrogen production in the initial 3-4 hours. From quantum chemistry, the intramolecular hydrogen bonding for the transition product namely Diammino of Diborane (DADB) indicated greater stability of the transition product. Thereafter for screening the IL combination, the activity coefficients at infinite dilution (IDAC) were predicted for AB-IL mixtures using the COSMO-SAC model. This gave the seven best ILs for dehydrogenations namely: [EMIM][OAc], [BMIM][OAc], [TDTHP][Phosph] , [TDTHP][DCA] , [AMIM][Br] , [AMIM][$N(CN)_2$] and [AMIM][Tf_2N].

The acetate based ILs promote the dehydrogenation at lower temperatures by giving higher equivalents of hydrogen. LUMO–HOMO calculations were performed to compare the relative stability of the EDAB/IL complex. EDAB in [BMIM][OAc] was proved to be less stable owing to its higher LUMO energy than [EMIM][OAc]. Furthermore, the less stable EDAB/[BMIM] [OAc] complex was found to release hydrogen earlier than EDAB/[EMIM][OAc]. This phenomenon was confirmed from the TGA characterization of both complexes. We observed a higher dehydrogenation rate with

TH-1791_136107007

both temperature and alkyl chain length of imidazolium ring. The generation of hydrogen from EDAB/ [BMIM][OAc] at 105 °C was found to be more than that of neat EDAB (2.14). Thus, we claim that the dehydrogenation process in a vacuum facilitates the creation of milder condition. ^{1}H NMR characterization of reactants and products confirms the structural integrity of ILs and highlights the catalytic role of ILs in dehydrogenation process. ^{11}B NMR confirms the presence of trigonal boron (sp^2) BH_2 as the only boron containing moiety in dehydrogenation experiments. Further analysis of high resolution mass spectra of dehydrogenated products detects the presence of EDAB having n = 2 and 3 repeat units in the end product.

In the subsequent part, the thermally stable phosphonium ILs offered a basic environment because of the absence of acidic hydrogen and thus are presumed to facilitate different product formation. No induction period was observed in dehydrogenation experiment for both IL's namely [TDTHP][Phosph] and [TDTHP][DCA]. EDAB/[TDTHP][Phosph] and EDAB/[TDTHP][DCA] released 3.25 and 3.04 equivalent of hydrogen respectively at 105 °C. ^{1}H NMR analysis of the reacting mixture revealed the structural integrity of ILs where the catalytic role of ILs is established. Analysis of HR-MS spectra in +APCI mode clearly identified the formation of four and five repeat unit containing oligomeric dehydrogenated EDAB structure. Imidazolium –acetate based ILs was found to facilitate 2-3 repeat units containing oligomeric EDAB structure. Thus with the selective nature of product formation in two different types of ILs, led us to propose two separate dehydrogenation schemes.

In the concluding part of the thesis, the next set of IL namely, 1-allyl, 3-methylimidazolium IL was studied. It was observed that the presence of IL had a catalytic effect on the thermal dehydrogenation of EDAB like in the earlier cases. No induction time was again observed as opposed to a non-zero induction time for pure EDAB. The reaction

TH-1791_136107007

rate and reaction time was also found to increase with temperature. At *T*=105 °C ,the hydrogen release from the IL-EDAB mixtures were found to decrease in the following trend: EDAB/[AMIM][Br] (2.59) EDAB/[AMIM][Tf_2N] (2.07) >EDAB/[AMIM][$N(CN)_2$] (1.36). The dehydrogenation mechanism was found to strongly depend on basicity as well as dipole moment. The only pattern worth mentioning is that the basicity of Tf_2N, $N(CN)_2$ and Br follows a decreasing trend, and so do the hydrogen equivalents. But this is true only for [AMIM][Br]. In this circumstance the unavailability of the dipole moment or the degree of polarizibility of allyl-based IL is a hindrance to explain this unusual trend. ^{1}H NMR studies for the residual compounds indicated the catalytic role of IL, which is evident in the reduction of the $–NH_2$ peak. ^{11}B NMR also helps in confirming the presence of sp^2 trigonal boron in EDAB after the dehydrogenation reaction. TGA study of EDAB, EDAB/IL and Pure IL have also confirmed the thermal stability of each group, indicating negligible mass loss from the pure IL. Reactive Force Field (ReaxFF) Molecular Dynamics simulations studies have further validated the reaction mechanism pathway for dehydrogenation of EDAB. The release of hydrogen at different temperature ranging from 2500 to 5000 K were predicted and quantified. The hydrogen liberation at 2500 K shows the presence of induction period. Further the formation of few byproduct gases were also predicted. Overall the hydrogen liberation from various cation and anion combination are summarized below in Figure 4.1.

TH-1791_136107007

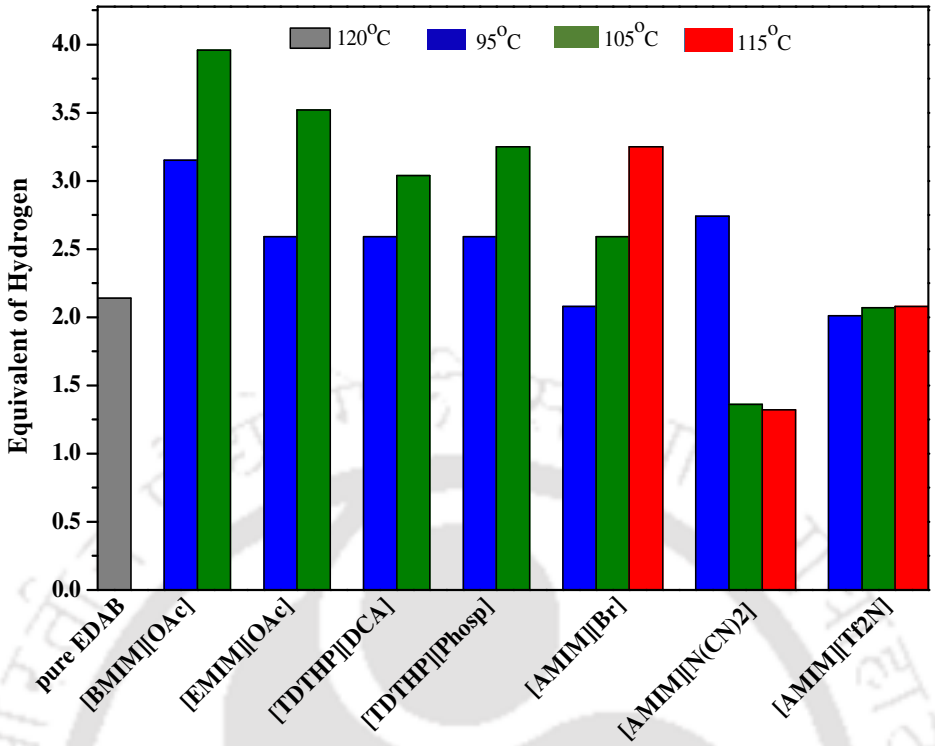

Figure 4.1 Overall thermal dehydrogenation of EDAB with selected ILs

TH-1791_136107007

4.2 Future Scope

The future work will focus on the reusability of IL by separation of oligomers of EDAB or the residual products. Involvement of liquid-liquid extraction to separate out the oligomers of EDAB particles and the solvent (IL) is another option so as to make the process sustainable. Low cost Deep Eutectic Solvents (DES) along with metallic catalyst can also recommended for thermal decomposition of EDAB. Thermal Dehydrogenation at high pressures may also be another alternative that needs to be explored in the current context. Families of other chemical hydrides such as Methyl Amine Borane (MeAB), Sec-Butyl Borane (SBAB) and Hydrazine Borane (HB) can also be studied on similar lines as EDAB. This should then be compared with respect to their capacity of releasing hydrogen equivalents with different ILs or DES at similar experimental condition.

TH-1791_136107007

TH-1791_136107007

RESEARCH OUTPUT

List of Publications

1. S. Mahato, **Basudhrity Banerjee**, G. Pugazhenthi, T. Banerjee, Optimization and Quantum Chemical Predictions for the Dehydrogenation Kinetics of Ammonia BoraneIonic Liquid Mixtures. *Int. J. Hydrogen Energy*, **2015**, 40, 10390-10400.
2. **Basudhrity Banerjee**, D. Kundu, G. Pugazhenthi and T. Banerjee, Quantum Chemical and Experimental insights for the Ionic Liquid Facilitated Thermal Dehydrogenation of Ethylene DiAmine bisBorane . *RSC Adv.,* **2015**, 5, 85280-85290.
3. D. Kundu, **Basudhrity Banerjee**, G. Pugazhenthi and T.Banerjee, Reactive Insights into the Selective Dehydrogenation of Ethylene DiAmine bisBorane Facilitated by Phosphonium Based Ionic Liquids., *Int. J. Hydrogen Energy*,**2017**,42,2756-2770.
4. **Basudhrity Banerjee**, G. Pugazhenthi and T. Banerjee Experimental Insights in the Thermal Dehydrogenation of Ethylene DiAmine bisBorane using Allyl Based Ionic Liquids. *Energy Fuels,* **2017**, 31, 5428−5440.

Conference Proceedings

1. **Basudhrity Banerjee**, G. Pugazhenthi and Tamal Banerjee, Thermal dehydrogenation studies of Ethylene DiAmine *bis*Borane complex and Ammonia Borane with Pyrrolidium based ionic liquid. CHEMFERENCE 2015, December 5-6, 2015, IIT Hyderabad, India.

2. **Basudhrity Banerjee**, G. Pugazhenthi and Tamal Banerjee, Hydrogen generation from Ethylene DiAmine *bis*Borane along with different ionic liquids. Emerging Energy Technologies Summit and Exhibition, December 5-7, 2016, Melbourne, Australia.

TH-1791_136107007